CHARACTERIZING CEREBELLIN-SHORT, A NOVEL CIRCADIAN PEPTIDE, IN THE RAT SUPRACHIASMATIC NUCLEUS

BY

JAMES L. CHU

DISSERTATION

Submitted in partial fulfillment of the requirements
for the degree of Doctor of Philosophy in Cell and Developmental Biology
in the Graduate College of the
University of Illinois at Urbana-Champaign, 2018

Urbana, Illinois

Doctoral Committee:

Associate Professor Stephanie S. Ceman, Chair
Professor Martha U. Gillette, Advisor
Professor Lisa J. Stubbs
Professor Jonathan V. Sweedler

ABSTRACT

Circadian rhythms in mammals, such as metabolism, hormone release, and the sleep/wake cycle, are orchestrated by the suprachiasmatic nucleus (SCN) located in the hypothalamus. Mass spectrometry peptidomics of the SCN identified the small peptide cerebellin-short (SGSAKBSAIRSTN) consisting of 15 amino acids, which is released from the SCN in circadian fashion. Cerebellin-short is the C-terminus truncated form of the 16 amino acid cerebellin peptide highly enriched in the cerebellum. The distribution of cerebellin-short in the SCN and the functional implications of its circadian release, however, are unknown. Here we showed that the precursor of cerebellin-short, Cbln1, is expressed in the SCN with daily oscillations in mRNA level. The level of Cbln1 process intermediate also oscillates around the day. Immunofluorescence revealed that a portion of both AVP- and VIP- positive cells in the SCN are also positive for cerebellin-short. Cbln1 on the other hand localized immediately dorsal to the SCN along the 3rd ventricle. Cbln1 also showed strong localization to the paraventricular nucleus (PVN), the supraoptic nucleus (SON) and the median eminence. No Cbln1 or process intermediate were observed in GFAP-positive astrocytes. Crude synaptosome fractionations of the SCN revealed that the processing intermediate, but not Cbln1, is enriched at the synapse. Exogenous application of cerebellin-short at midday and early night phase advance the spontaneous firing rhythm of SCN neurons. These results suggest that Cbln1 is actively processed into cerebellin-short at the synapses throughout the SCN, and is likely involved in the intrinsic circadian time keeping mechanism.

To My Mother

ACKNOWLEDGEMENTS

I would like to thank my mother for her enormous support through the long years of pursing my Ph.D. degree. It takes so much to raise a child, then send me to school and nurturing me to be a good person. My achievement would not have been possible without my mother's selfless love. I would like to thank my advisor Dr. Martha Gillette, who is the nicest and most supportive professor I've met. She cared for my wellbeing and provided so much beyond advising my research. I am blessed to have her as my advisor. Dr. Jennifer Mitchell and Karen Weis took me under their wings and taught me essentially all the techniques and experiments I've done in the lab. Ann Benefiel made sure our lab supplies are always stocked and knows all the ins and outs when it comes to animal care and usage. They answered all my weird questions and never hesitated to offer their assistance. I also had the pleasure to work with my great lab mates and friends, Chris, Sam, Mia, Harry, Ghazal, Collin, Olivia and Raj. Whether it was the furious debates during lab meetings about each other's data, or the ridiculously inappropriate conversations about dumb things, every moment spent with these characters were great and memorable.

I would also like to thank Dr. Jonathan Sweedler, who is a great collaborator and a tremendously knowledgeable member of my committee. Jonathan always asked the clever questions, which often caught me by surprise, but turned out to be critical for my investigation. Dr. Stephanie Ceman and Dr. Lisa Stubbs of my thesis committee also helped tremendously in guiding my thesis and making important suggestions. Dr. Qian Wu who worked with me on the CNLM project taught me a lot about MS and how to approach analytical chemistry. Elizabeth Good was a fantastic course coordinator that I had the pleasure to work for. She made sure that the four years I spent teaching MCB 253 were as smooth and as rewarding as possible. The animal care staff were always there, making sure that our animals were healthy and made my investigations possible. I would like to give a shout out to my cat Sesame, who kept me company for the better part of my graduate career.

The works presented in my thesis were supported by funding from NSF IOS 1354913, NIH HL086870 and 392 Abbott CNLM 2015-06958 Antc grants. I greatly appreciate all the people that helped me along the way in my graduate journey. Thanks to you all, it has truly been a blast.

TABLE OF CONTENTS

LIST OF ABBREVIATIONS

AA	Arachidonic Acid
ACSF	Artificial Cerebral Spinal Fluid
AMPAR	AMPA Receptor
ARC	Arcuate Nucleus
AVP	Arginine Vasopressin
BBB	Blood-Brain Barrier
C1q	Complement Component 1q
Cbln	Cerebellin
CK	Creatine Kinase
CK1δ	Casein Kinase 1δ
CNS	Central Nervous System
CP	Cocoa Powder
Cr	Creatine
CT	Circadian Time
DA	Dopamine
DAB	3.3'-Diaminobenzidine
DAG	Diacylglycerol
DAPI	4',6-Diamidio-2-Phenylindole
DCV	Dense Core Vesicle
DHA	Docosahexaenoic Acid
EBSS	Earle's Balanced Salt Solution
fEPSP	Field Excitatory Postsynaptic Potential
FO	Fish Oil
FTICR	Fourier Transform Ion Cyclotron Resonance
GABA	Gamma-Aminobutyric Acid
$GABA_AR$	$GABA_A$ Receptor
GAPDH	Glyceraldehyde-3-Phosphate Dehydrogenase
GFAP	Glial Fibrillary Acidic Protein

GLU	Glutamate
GluRD1	Glutamate Receptor δ1
GluRD2	Glutamate Receptor δ2
GPCR	G Protein-Coupled Receptor
GRP	Gastrin Releasing Peptide
HFS	High Frequency Stimulation
HPLC	High Performance Liquid Chromatography
HRP	Horse Radish Peroxidase
IGL	Intergeniculate Leaflet
IR	Immunoreactivity
KO	Knock-Out
LC-MS	Liquid Chromatography-Mass Spectrometry
LTD	Long Term Depression
LTP	Long Term Potentiation
MALDI	Matrix-Assisted Laser Desorption/Ionization
MSI	Mass Spectrometry Imaging
MW	Molecular Weight
NMDAR	NMDA Receptor
NPY	Neuropeptide Y
OPLS	Orthogonal Partial Least Squares
PACAP	Pituitary Adenylate Cyclase-Activating Peptide
PAF	lyso-Platelet-Activating Factor
PBS	Phosphate Buffer Saline
PC	Phosphatidylcholine
PC	Purkinje Cell
PCA	Principle Component Analysis
PCr	Phosphocreatine
PE	Phosphoethanolamine
PER2::LUC	Period2::Luciferase
PF	Parallel Fiber

PFA	Paraformaldehyde
PI	Phosphatidylcholine
PKA	Protein Kinase A
PKG	Protein Kinase G
PLA2	Phospholipase A2
PRC	Phase-Response Curve
PUFA	Polyunsaturated Fatty Acid
PVN	Paraventricular Nucleus
qRT-PCR	Quantitative Reverse Transcription Polymerase Chain Reaction
RHT	Retinohypothalamic Tract
ROI	Region of Interest
SCN	Suprachiasmatic Nucleus
SON	Supraoptic Nucleus
SUA	Single-Unit Activity
TACE	Tumor Necrosis Factor α Converting Enzyme
TOF-SIMS	Time-of-Flight Secondary-Ion Mass Spectrometry
TTFL	Transcription-Translation Feedback Loop
VIP	Vasoactive Intestinal Peptide
VPAC2	Vasoactive Intestinal Peptide Receptor 2
ZT	Zeitgeber Time

CHAPTER ONE: INTRODUCTION

1.1 CIRCADIAN RHYTHM AND THE SCN

The suprachiasmatic nucleus (SCN) in the mammalian hypothalamus orchestrates the organism's circadian rhythms, such as the daily sleep/wake cycle, metabolism, and hormone release [1]. The SCN is a pair of bilateral nuclei positioned above the optic chiasm, with each nucleus consisting of approximately 10,000 cells. The SCN can adjust the body's circadian rhythms so they align to the external environment in response to temporal cues such as light and temperature, contributing to the optimal health and survival of the organism [2]. Ablation of the SCN in rodents leads to the loss of rhythms in behavior such as wheel running and physiology such as body temperature fluctuations. To function as a time keeper, cells within the SCN must synchronize with one another to generate a coherent rhythm, which can then be communicated to other parts of the hypothalamus as well as the rest of the body [3].

1.2 CORE CLOCK PROTEINS

At the core of circadian time keeping is the transcription-translation feedback loop (TTFL). The TTFL is present in all cells in the body, and provides the basis for the rhythmicity in expression of additional genes and cellular functions [4]. In mammals, the positive feedback loop includes CLOCK and BMAL1, which heterodimerize and induce the expression of the clock genes *Period* (*Per1*, *Per2* and *Per3*) and *Cryptochrome* (*Cry1* and *Cry2*). The negative feedback loop consists of PERIOD and CRY proteins, which heterodimerize to re-enter the nucleus and suppress the activities

of CLOCK and BMAL1. CLOCK and BMAL1 also induce the expression of retinoic acid-related orphan nuclear receptors REV-ERBα and RORα. REV-ERBα re-enters the nucleus and inhibits the expression of *Bmal1*, while RORα induces the expression of *Bmal1*. Together, the positive and negative elements of the feedback loop cycle on a period of around 24 h, thus setting the basis of the circadian clock [4]. Transgenic mice expressing PERIOD2::LUCIFERASE (PER2::LUC) fusion protein enable bioluminescence imaging of PER2 to directly monitor the phase of the TTFL [5].

1.3 HUMORAL ENTRAINMENT IN THE SCN

Previous experiments demonstrated that fetal SCN grafts encapsulated in membrane impermeable to neuronal processes can restore behavior and physiological circadian rhythmicity in hamsters with electrically ablated SCNs [6]. This result suggests that humoral signaling is a part of the SCN output to the hypothalamus and the rest of the organism. The inability of the graft to restore circadian endocrine rhythms of hormones released via the pituitary suggests that physical contact such as synaptic communication is also an important part of the SCN output.

The SCN expresses a rich, heterogeneous collection of neuronal subtypes with region-specific expression of peptides [7], number of which are implicated in circadian function. The SCN is conventionally divided into the ventrolateral and the dorsomedial sub-regions, designated by the peptides released and specific circadian network properties [7]. The cells of the ventrolateral SCN receive direct photic inputs via the retinohypothalamic tract (RHT) and release vasoactive intestinal peptide (VIP) in

response to light to synchronize the SCN [8–10]. The central sub-region in the ventrolateral SCN receives input from the RHT and secretes gastrin-releasing peptide (GRP) and little-SAAS [11,12]. The ventrolateral region relays signals to the dorsomedial SCN, which contains arginine vasopressin (AVP) neurons and is responsible for communicating the rhythm to the rest of the hypothalamus [7,13,14]. Dorsomedial SCN is also believed to be the location of the true circadian clock [14]. Knockout of VIP can result in loss of behavior rhythms and disrupted coordination among SCN neurons in mouse, suggesting a role in cell-cell synchronization. Exogenous VIP, GRP, and little-SAAS can alter the phase of rat SCN, each with a specific window of action [12,15,16]. Like the clock proteins in the TTFL, circadian peptides exhibit diurnal rhythms in expression and release. For example, mRNA level of AVP in the mouse SCN is high at dusk and low at dawn. VIP and GRP on the other hand, have mRNA levels that peak in the day and trough in the night [17]. Some of these rhythms are species-specific. For instance, GRP expression has no clear rhythm in the rat [17].

1.4 DIFFERENT RHYTHMS AND PHASE-SHIFTING IN THE SCN

Clock proteins and circadian peptides are not the only oscillating elements in the SCN. Daily rhythms in Ca^{2+} are also observed in the SCN [18,19]. Neurons and astrocytes in the SCN demonstrate Ca^{2+} rhythms that are in anti-phase [20]. SCN neurons fire spontaneously and the frequency of the firing peaks during the midday (ZT 7) [21]. The overall redox state of the SCN also oscillates daily, being more oxidized during the day and more reduced during the night [22]. Ca^{2+}, spontaneous firing, and PER2

protein rhythms have strict phase relationships [19,20]. All three oscillations mentioned above are intrinsic to the SCN, and can be recorded for prolonged periods of time in organotypic SCN slice cultures *ex vivo* as in the PER2::LUC rhythm [20,22,23].

The hallmarks of a biological clock are: A) in constant conditions the period of the oscillation is close but equal to 24 h, B) the free-running rhythm is temperature-compensated, and C) the rhythm can entrain to external cues, such as the light/dark cycle [24]. The ability to phase-shift allows the SCN to adjust phase in reaction to external temporal cues. One example is the response to light and glutamate (GLU). GLU is the excitatory neurotransmitter that conveys photic cues from the RHT to the SCN. When applied to the SCN *in vitro* during the subjective day, GLU does not alter the phase of the SCN. In the early night GLU induces phase delay and in the late night induces phase advance. A phase-response curve (PRC) can be generated based on how the SCN reacts to GLU at different points of the phase. Light exposure in intact animals have similar phase-shifting effects [25]. The temporal difference in response to light and GLU enables entrainment of the SCN to changes in the light/dark cycle. In addition to GLU, the SCN is also known to phase-shifts in response to a number peptides and compounds. For example, peptides like VIP, NPY and little-SAAS can induce phase-shifts with different PRCs [12,26,27]. Compounds like melatonin, caffeine and serotonin can also alter the circadian clock [25,28–31].

1.5 CBLN1, CEREBELLIN AND CEREBELLIN-SHORT

Investigations of peptides in the SCN was advanced significantly when direct high-resolution mass spectrometry-based peptidomics studies revealed 102 endogenous SCN peptides, 33 of which had been previously unidentified [32]. Several unexpected small peptides are found to be released in circadian fashion [33]. One such peptide is the 15 amino acid cerebellin-short, a C-terminus histidine truncated form of the full length 16 amino acid cerebellin peptide known to be richly expressed in the cerebellum [33,34]. There exists an alternative form of truncated cerebellin. Instead of the C-terminus histidine, the N-terminus serine is removed. The N-terminus serine-truncated cerebellin is expressed in the cerebellum in comparable amounts to the full-length peptide [34]. To avoid confusion, from this point forward cerebellin-short will always refer to the C-terminus truncated form while cerebellin refers to the full-length peptide. Although all three forms of cerebellin are present in the SCN [32,35], only cerebellin-short is released in a circadian pattern from the SCN in *in vitro* brain slices. Release of cerebellin-short showed a peak 4 h into the subjective night (CT 16) [33]. Cerebellin and cerebellin-short are proteolytic products of the full-length precursor protein, Cerebellin 1 (Cbln1), which has been found to be highly expressed in the cerebellum, and to lesser degrees in the forebrain and the spinal cord [36–39].

Cbln1 is a member of the C1q family and is one of four Cbln proteins (Cbln1 to Cbln4), all of which contain C1q domain at the C-terminus [36]. The C1q domain is present in many secreted proteins and allows Cbln to form 3-fold symmetric homotrimers. Two conserved cysteine residues near the N-terminus enable

homotrimers of different Cbln to cross-interact and dimerize into a collection of hexamer complexes [40,41]. The combination of different Cbln homotrimers in the hexamer determines its downstream binding partners and function [42–45]. Cbln1 is the best studied Cbln protein, and is the only one out of the four known to be extensively processed into specific cerebellin peptide forms on top of its regular synapse forming functions.

Cbln1 is known to bind to glutamate receptor δ 1 and 2 (GluRD1 and GluRD2) and several subtypes of neurexin β receptors [40,45–47]. GluRD1 and GluRD2 are orphan receptors that are identified through sequence homologies to other ionotropic glutamate receptor subunits but do not form functional ion channels [47,48]. GluRD2 is highly expressed in the Purkinje cell of the cerebellum [49]. GluRD2-KO animals share similar synaptic and behavioral phenotypes with Cbln1 KO mice, an observation that later led to the discovery of the interaction between Cbln1 and GluRD2 [47]. GluRD1 is highly expressed in the adult hippocampus and inner ear, but its function is not well understood [49]. Mutation or deletion of GluRD1 is associated with loss of high-frequency hearing as well as cognitive deficits and mental health disorders, such as schizophrenia [50–52].

Cbln1 has well studied synaptic functions. Cbln1 protein is crucial for the formation and maintenance of excitatory synapses between the Purkinje cells (PC) and the parallel fibers (PF) in the cerebellum by interacting with presynaptic neurexin β and postsynaptic GluRD2 receptors [41,47]. Cbln1-KO animals are ataxic and have

significantly decreased number of PC-PF synapses. Injection of recombinant Cbln1 in-KO animals rapidly restores PC-PF synapses and rescues the ataxic phenotype. This rescue is not permanent, demonstrating the dynamic nature of the role of Cbln1 in maintaining PC-PF synapses [53]. In cultured cortical neurons, Cbln1 contributes to the formation of inhibitory synapses [54]. In the forebrain Cbln1 likely contributes to the formation of both excitatory and inhibitory synapses in different regions. GluRD1 is expressed in the hippocampus while Cbln1 is expressed in entorhinal cortical neurons that project to the hippocampus. Cultured entorhinal cortical neurons can form both excitatory and inhibitory axonal terminals on HEK cells expressing GluRD1, while cultured hippocampal neurons require the addition of recombinant Cbln1 to achieve the same effect [55]. These results suggest Cbln1 might contribute to synapse formation in the hippocampus through interaction with GluRD1.

Cerebellin peptide has been reported to have diverse regulatory functions in the nervous system, although the mechanisms are not elucidated. Synthetic cerebellin has been shown to induce catecholamine release from human adrenal cells *in vitro* and norepinephrine release from rat adrenal gland *in vivo* [56,57]. Intracerebroventricular injection of synthetic cerebellin increases feeding behavior in rats, possibly by acting through one or more hypothalamic nuclei [58]. Spinal injection of the N-terminus serine-truncated cerebellin leads to mechanical hypersensitivity in mouse [38].

Unlike Cbln1, cerebellin peptides have no known receptors. The lack of critical cysteine residues and the intact C1q domain preclude interaction with known Cbln1

binding partners [36,40,59]. Compared to Cbln1, studies on cerebellin are scarce possibly due to several reasons. Traditional antibody-based detection methods such as immunohistochemistry cannot effectively distinguish cerebellin from its precursor Cbln1 due to overlap in amino acid sequences. The existence of multiple processing intermediates further complicates the analysis. At approximately 1.5 kDa, endogenous concentration of cerebellin cannot be resolved on a Western blot. All of these issues make Cbln1 the more attractive choice of study. Nevertheless, Cbln1 and cerebellin present an intriguing case where the precursor and the processed peptide have very different functions. The possible involvement of cerebellin-short in circadian time keeping adds another dimension to this curious dichotomy. Full-length cerebellin and the two forms of truncated cerebellin are all endogenous to the rat SCN as shown by mass spectrometry analysis [35]. However, whether Cbln1, cerebellin or cerebellin-short are involved in SCN timekeeping has been unknown.

1.6 STATEMENT OF PROBLEMS AND SIGNIFICANCE

The goal of this investigation is to characterize the expression, localization, and circadian function of cerebellin-short in the rat SCN. Based on the circadian release of cerebellin-short from the rat SCN, I hypothesize that cerebellin-short undergoes cell type-specific circadian expression in sub-regions of the rat SCN and exerts a circadian function through mechanism different from Cbln1. In this study, I examined the expression profiles of cerebellin-short and the precursor Cbln1 in the SCN. I investigated the circadian functions of cerebellin-short in phase-shifting the SCN spontaneous neuronal firing rhythm. I also characterized the region-specific

localizations of cerebellin-short processing intermediate and the precursor Cbln1 within the SCN.

1.7 REFERENCES

1. Nishino H, Koizumi K, Brooks CMCCM. The role of suprachiasmatic nuclei of the hypothalamus in the production of circadian rhythm. Brain Res. 1976;112: 45–59.

2. Roenneberg T, Wirz-Justice A, Merrow M. Life between Clocks: Daily Temporal Patterns of Human Chronotypes. J Biol Rhythms. 2003;18: 80–90.

3. Gillette MU, Sejnowski TJ. Physiology. Biological clocks coordinately keep life on time. Science. 2005;309: 1196–8.

4. Ko CH, Takahashi JS. Molecular components of the mammalian circadian clock. Hum Mol Genet. 2006;15: R271–R277.

5. Yoo SH, Yamazaki S, Lowrey PL, Shimomura K, Ko CH, Buhr ED, et al. PERIOD2::LUCIFERASE real-time reporting of circadian dynamics reveals persistent circadian oscillations in mouse peripheral tissues. Proc Natl Acad Sci U S A. United States; 2004;101: 5339–5346.

6. Silver R, LeSauter J, Tresco P. A diffusible coupling signal from the transplanted suprachiasmatic nucleus controlling circadian locomotor rhythms. Nature. 1996;382: 810–813.

7. Moore RY, Speh JC, Leak RK. Suprachiasmatic nucleus organization. Cell Tissue Res. 2002;309: 89–98.

8. Dibner C, Schibler U, Albrecht U. The mammalian circadian timing system: organization and coordination of central and peripheral clocks. Annu Rev Physiol. 2010/02/13. 2010;72: 517–549.

9. Gillette MU, Reppert SM. The hypothalamic suprachiasmatic nuclei: circadian patterns of vasopressin secretion and neuronal activity in vitro. Brain Res Bull. Elsevier; 1987;19: 135–139.

10. Francl J, Kaur G, Glass J. Regulation of vasoactive intestinal polypeptide release in the suprachiasmatic nucleus circadian clock. Neuroreport. 2010;21: 1055–1059.

11. Romijn H, Sluiter A, Pool C. Differences in colocalization between Fos and PHI, GRP, VIP and VP in neurons of the rat suprachiasmatic nucleus after a light stimulus during the phase delay versus. J Comp Neurol. 1996;372: 1–8.

12. Atkins Jr. N, Mitchell JW, Romanova E V, Morgan DJ, Cominski TP, Ecker JL, et al. Circadian integration of glutamatergic signals by little SAAS in novel suprachiasmatic circuits. PLoS One. United States; 2010;5: e12612.

13. Moga MM, Moore RY. Organization of neural inputs to the suprachiasmatic nucleus in the rat. J Comp Neurol. 1997;389: 508–34.

14. Yan L, Karatsoreos I, LeSauter J, Welsh DK, Kay S, Foley D, et al. Exploring spatiotemporal organization of SCN circuits. Cold Spring Harb Symp Quant Biol. 2007;72: 527–541.

15. Colwell CS, Michel S, Itri J, Rodriguez W, Tam J, Lelievre V, et al. Disrupted circadian rhythms in VIP- and PHI-deficient mice. Am J Physiol Regul Integr Comp Physiol. 2003;285: R939-49.

16. Maywood ES, Reddy AB, Wong GK, O'Neill JS, O'Brien JA, McMahon DG, et al. Synchronization and maintenance of timekeeping in suprachiasmatic circadian clock cells by neuropeptidergic signaling. Curr Biol. 2006/03/21. 2006;16: 599–605.

17. Dardente H, Menet JS, Challet E, Tournier BB, Pevet P, Masson-Pevet M. Daily and circadian expression of neuropeptides in the suprachiasmatic nuclei of nocturnal and diurnal rodents. Brain Res Mol Brain Res. 2004/05/12. 2004;124: 143–151.

18. Brancaccio M, Maywood ES, Chesham JE, Loudon ASI, Hastings MH. A Gq-Ca(2+) Axis Controls Circuit-Level Encoding of Circadian Time in the Suprachiasmatic Nucleus. Neuron. Elsevier Inc.; 2013;78: 714–728.

19. Enoki R, Ono D, Kuroda S, Honma S, Honma K. Dual origins of the intracellular circadian calcium rhythm in the suprachiasmatic nucleus. Sci Rep. Nature Publishing Group; 2017;7: 41733.

20. Brancaccio M, Patton AP, Chesham JE, Maywood ES, Hastings MH. Astrocytes Control Circadian Timekeeping in the Suprachiasmatic Nucleus via Glutamatergic Signaling. Neuron. 2017; 1–16.

21. Prosser RA, McArthur AJ, Gillette MU. cGMP induces phase shifts of a mammalian circadian pacemaker at night, in antiphase to cAMP effects. Proc Natl Acad Sci. National Acad Sciences; 1989;86: 6812.

22. Wang TA, Yu Y V, Govindaiah G, Ye X, Coleman TP, Sweedler J V, et al. Circadian Rhythm of Redox State Regulates Excitability in Suprachiasmatic Nucleus Neurons. Science. 2012;337: 839–842.

23. Enoki R, Ono D, Kuroda S, Honma S, Honma K. Dual origins of the intracellular circadian calcium rhythm in the suprachiasmatic nucleus. Sci Rep. 2017;7: 41733.

24. Golombek DA, Rosenstein RE. Physiology of circadian entrainment. Physiol Rev. United States; 2010;90: 1063–1102.

25. Ding JM, Buchanan GF, Tischkau S a, Chen D, Kuriashkina L, Faiman LE, et al. A neuronal ryanodine receptor mediates light-induced phase delays of the circadian clock. Nature. 1998;394: 381–4.

26. Harmar AJ. An essential role for peptidergic signalling in the control of circadian rhythms in the suprachiasmatic nuclei. J Neuroendocr. 2003/03/08. 2003;15: 335–338.

27. Besing RC, Hablitz LM, Paul JR, Johnson RL, Rebecca A, Gamble KL, et al. NPY-Induced Phase Shifts of PER2::LUC Rhythms are Mediated by Long-Term Suppression of Neuronal Excitability in a Phase-Specific Manner. Chronobiol Int. 2013;29: 91–102.

28. Medanic M, Gillette MU. Serotonin regulates the phase of the rat suprachiasmatic circadian pacemaker in vitro only during the subjective day. J Physiol. 1992;450: 629–42.

29. McArthur AJ, Gillette MU, Prosser RA. Melatonin directly resets the rat suprachiasmatic circadian clock in vitro. Brain Res. 1991;565: 158–61.

30. Vincent M C, Chesworth J M, Armstrong Maxwell S. Dose-dependent entrainment of rat circadian rhythms by daily injection of melatonin. J Biol Rhythms. 1986;1: 219–229.

31. Emens J, Lewy AJ, Laurie AL, Songer JB. Rest-activity cycle and melatonin rhythm in blind free-runners have similar periods. J Biol Rhythms. 2010;25: 381–4.

32. Lee JE, Atkins Jr. N, Hatcher NG, Zamdborg L, Gillette MU, Sweedler J V, et al. Endogenous peptide discovery of the rat circadian clock: a focused study of the suprachiasmatic nucleus by ultrahigh performance tandem mass spectrometry. Mol Cell Proteomics. United States; 2010;9: 285–297.

33. Hatcher NG, Atkins Jr. N, Annangudi SP, Forbes AJ, Kelleher NL, Gillette MU, et al. Mass spectrometry-based discovery of circadian peptides. Proc Natl Acad Sci U S A. United States; 2008;105: 12527–12532.

34. Slemmon JR, Blacher R, Danho W, Hempstead JL, Morgan JI. Isolation and sequencing of two cerebellum-specific peptides. Proc Natl Acad Sci U S A. 1984;81: 6866–70.

35. Lee JE, Zamdborg L, Southey BR, Atkins N, Mitchell JW, Li M, et al. Quantitative peptidomics for discovery of circadian-related peptides from the rat suprachiasmatic nucleus. J Proteome Res. 2013;12: 585–93.

36. Bao D, Pang Z, Morgan JI. The structure and proteolytic processing of Cbln1 complexes. J Neurochem. England; 2005;95: 618–629.

37. Wei P, Smeyne RJ, Bao D, Parris J, Morgan JI. Mapping of Cbln1-like immunoreactivity in adult and developing mouse brain and its localization to the endolysosomal compartment of neurons. Eur J Neurosci. France; 2007;26: 2962–2978.

38. Su J, Sandor K, Sköld K, Hökfelt T, Svensson CI, Kultima K. Identification and quantification of neuropeptides in naïve mouse spinal cord using mass spectrometry reveals [des-Ser1]-cerebellin as a novel modulator of nociception. J Neurochem. 2014;130: 199–214.

39. Cagle MC, Honig MG. Parcellation of Cblns 1, 2, and 4 among different subpopulations of dorsal horn neurons in mouse spinal cord. The Journal of comparative neurology. 2013.

40. Elegheert J, Kakegawa W, Clay JE, Shanks NF, Behiels E, Matsuda K, et al. Structural basis for integration of GluD receptors within synaptic organizer complexes. 2016;353.

41. Matsuda K, Yuzaki M. Cbln1 and the Delta2 Glutamate Receptor-An Orphan Ligand and an Orphan Receptor Find Their Partners. Cerebellum. 2010;11: 78–84.

42. Bao D, Pang Z, Morgan M a, Parris J, Rong Y, Li L, et al. Cbln1 is essential for interaction-dependent secretion of Cbln3. Mol Cell Biol. 2006;26: 9327–37.

43. Miura E, Matsuda K, Morgan JI, Yuzaki M, Watanabe M. Cbln1 accumulates and colocalizes with Cbln3 and GluRdelta2 at parallel fiber-Purkinje cell synapses in the mouse cerebellum. Eur J Neurosci. 2009/03/03. 2009;29: 693–706.

44. Rong Y, Wei P, Parris J, Guo H, Pattarini R, Correia K, et al. Comparison of Cbln1 and Cbln2 functions using transgenic and knockout mice. J Neurochem. 2011/11/29. 2012;120: 528–540.

45. Yuzaki M. Cbln1 and its family proteins in synapse formation and maintenance. Curr Opin Neurobiol. England: Elsevier Ltd; 2011;21: 215–220.

46. Uemura T, Lee SJ, Yasumura M, Takeuchi T, Yoshida T, Ra M, et al. Trans-synaptic interaction of GluRdelta2 and Neurexin through Cbln1 mediates synapse formation in the cerebellum. Cell. United States: Elsevier Inc; 2010;141: 1068–1079.

47. Matsuda K, Miura E, Miyazaki T, Kakegawa W, Emi K, Narumi S, et al. Cbln1 is a ligand for an orphan glutamate receptor delta2, a bidirectional synapse organizer. Science. United States; 2010;328: 363–368.

48. Yuzaki M. The delta2 glutamate receptor: 10 years later. Neurosci Res. Ireland; 2003;46: 11–22.

49. Hepp R, Hay YA, Aguado C, Lujan R, Dauphinot L, Potier MC, et al. Glutamate receptors of the delta family are widely expressed in the adult brain. Brain Struct Funct. 2014;220: 2797–2815.

50. Livide G, Patriarchi T, Amenduni M, Amabile S, Yasui D, Calcagno E, et al. GluD1 is a common altered player in neuronal differentiation from both MECP2-mutated and CDKL5-mutated iPS cells. Eur J Hum Genet. Nature Publishing Group; 2015;23: 195–201.

51. Yadav R, Hillman BG, Gupta SC, Suryavanshi P, Bhatt JM, Pavuluri R, et al. Deletion of Glutamate Delta-1 Receptor in Mouse Leads to Enhanced Working Memory and Deficit in Fear Conditioning. PLoS One. 2013;8: 1–12.

52. Gao J, Maison SF, Wu X, Hirose K, Jones SM, Bayazitov I, et al. Orphan Glutamate Receptor 1 Subunit Required for High-Frequency Hearing. Mol Cell Biol. 2007;27: 4500–4512.

53. Ito-Ishida A, Miura E, Emi K, Matsuda K, Iijima T, Kondo T, et al. Cbln1 regulates rapid formation and maintenance of excitatory synapses in mature cerebellar Purkinje cells in vitro and in vivo. J Neurosci. United States; 2008;28: 5920–5930.

54. Yasumura M, Yoshida T, Lee SJ, Uemura T, Joo JY, Mishina M. Glutamate receptor δ 1 induces preferentially inhibitory presynaptic differentiation of cortical neurons by interacting with neurexins through cerebellin precursor protein subtypes. J Neurochem. 2012;121: 705–716.

55. Ryu K, Yokoyama M, Yamashita M, Hirano T. Induction of excitatory and inhibitory presynaptic differentiation by GluD1. Biochem Biophys Res Commun. Elsevier Inc.; 2012;417: 157–161.

56. Mazzocchi G, Andreis PG, De Caro R, Aragona F, Gottardo L, Nussdorfer GG. Cerebellin enhances in vitro secretory activity of human adrenal gland. J Clin Endocrinol Metab. 1999;84: 632–5.

57. Albertin G, Malendowicz LK, Macchi C, Markowska A, Nussdorfer GG. Cerebellin stimulates the secretory activity of the rat adrenal gland: in vitro and in vivo studies. Neuropeptides. 2000;34: 7–11.

58. Gardiner J V, Beale KE, Roy D, Boughton CK, Bataveljic A, Campbell DC, et al. Cerebellin1 is a novel orexigenic peptide. Diabetes Obes Metab. England: Blackwell Publishing Ltd; 2010;12: 883–890.

59. Kuroyanagi T, Hirano T. Flap loop of GluD2 binds to Cbln1 and induces presynaptic differentiation. Biochem Biophys Res Commun. United States: Elsevier Inc; 2010;398: 537–541.

CHAPTER TWO: CHARACTERIZING CEREBELLIN-SHORT, A NOVEL CIRCADIAN PEPTIDE, IN THE RAT SUPRACHIASMATIC NUCLEUS

2.1 ABSTRACT

The suprachiasmatic nucleus (SCN), the central circadian clock in mammals, contains a number of peptides important for synchronizing the intrinsic rhythm and conveying it to other parts of the brain. Cerebellin-short (SGSAKVAFSAIRSTN) is a small peptide consisting of 15 amino acids identified in mass spectrometry proteomics secreted from the SCN in circadian fashion. Cerebellin-short is the C-terminus histidine- truncated form of 16 amino acid full-length cerebellin, a peptide enriched in cerebellum. The distribution and function of cerebellin-short in the SCN, however, are unknown. Here we show that Cbln1, the precursor for cerebellin, is expressed in the SCN with daily oscillations in mRNA and peptide processing intermediates. Immunoreactivity in the SCN of anti-cerebellin-short showed different localization patterns compared to precursor Cbln1. Exogenous cerebellin-short applied at midday and early night phase advance the spontaneous firing rhythm of SCN neurons. These results suggest that endogenous cerebellin-short contributes a circadian regulatory function. Cerebellin-short, therefore, is likely involved in the intrinsic circadian time-keeping of the SCN.

2.2 INTRODUCTION

The suprachiasmatic nucleus (SCN) in the mammalian hypothalamus orchestrates the organism's circadian rhythms, such as the daily sleep/wake cycle, metabolism, and hormone release [1]. The SCN is able to adjust the body's circadian rhythms so as to align to the external environment in response to temporal cues such as light from the day/night cycle, contributing to the health and survival of the organism [2]. To function as a timekeeper, cells within the SCN must synchronize with one another to generate a coherent rhythm, which can then be communicated to the rest of the hypothalamus [3]. The SCN expresses a rich, heterogeneous collection of neuronal subtypes with region-specific expression of peptides [4], a number of which have been shown to be involved in circadian timekeeping. The cells of the ventrolateral SCN receive photic inputs via the retinohypothalamic tract (RHT) and release vasoactive intestinal peptide (VIP) in response to light to synchronize the SCN [5–7]. The central sub-region in the ventrolateral SCN receives input from RHT and secretes gastrin-releasing peptide (GRP) and little SAAS [8,9]. Knockout of VIP can result in loss of behavior rhythms in the mouse, suggesting a role in cell-cell synchronization. VIP, GRP, and little SAAS can alter the circadian timing of rat SCN, each with a specific window of action [9–11].

Investigation of peptides in the SCN was advanced significantly when direct high-resolution mass spectrometry-based peptidomic studies revealed 102 endogenous SCN peptides, 33 of which had been previously unidentified [12]. A number of unexpected

small peptides were also found to be released in a circadian fashion [13]. One such small peptide is the 15 amino acid cerebellin-short (SGSAKVAFSAIRSTN), a C-terminus histidine truncated form of the 16 amino acid cerebellin peptide (SGSAKVAFSAIRSTNH) known to be richly expressed in the cerebellum [13,14]. Cerebellin-short was released in a circadian pattern from the SCN brain slice; peak release was 4 h into the subjective night of the SCN *in vitro*. Cerebellin and cerebellin-short are proteolytic products of Cerebellin 1 (Cbln1) (Fig. 2.1), which has been found to be expressed in both the forebrain and the cerebellum [15,16]. Cbln1 and full-length cerebellin peptide have been reported to have diverse regulatory functions in neurons. Cbln1 protein is crucial for the formation and maintenance of excitatory synapses between the Purkinje cells and the parallel fibers in the cerebellum [17,18]. In cultured cortical neurons, Cbln1 contributes to the formation of inhibitory synapses [19]. Synthetic full-length cerebellin peptide has been shown to induce catecholamine release from human adrenal cells *in vitro* and norepinephrine release from rat adrenal gland *in vivo* [20,21]. Intracerebroventricular injections of full-length cerebellin peptide increases feeding behavior in rats [22]. However, whether Cbln1, cerebellin, or cerebellin-short are involved in SCN timekeeping remains unknown. In this study we examined temporal and spatial patterns of Cbln1 within the SCN. Further, we investigated the functional effects of cerebellin-short on SCN timekeeping.

2.3 MATERIALS AND METHODS

Animal

Long Evans/BluGill rats of both genders (University of Illinois, Urbana, IL) between the ages of 7 to 13 weeks were used for adult rat experiments. The colony is inbred, and genomic scan revealed one allele at each locus examined. Rats are housed under 12h:12h light-dark cycle with constant temperature, humidity, and food and water *ad libtium*. *Zeitgeber time* (ZT), standardized to the environmental light cycle, is designated ZT 0 when the light turns on and ZT 12 when the light goes off.

Tissue acquisition

For Western blot and quantitative RT-PCR analysis, unanesthetized animals were decapitated by guillotine at designated ZT times and the brain quickly extracted. The hypothalamus was surgically reduced and a 500 μm thick coronal slice containing the SCN, the third ventricle, and the optic chiasm was prepared using fresh razor blades and a mechanical tissue chopper. A tissue puncher (r = 1.5 mm) was used to isolate the SCN from the slice, followed by flash freezing over dried ice. Cerebellum punch (r = 1.5 mm, 500 μm thick) were collected from the same brain and flash frozen over dried ice.

For fixed tissue collection, animals were euthanized with 1 ml Euthasol (Virbac, Fort Worth, TX) at designated ZT times and perfused through the heart with 300 ml of

0.9% saline, followed by 300 ml of 4% paraformaldehyde (PFA) in 0.1 M PBS. The brain was removed and fixed in 4% paraformaldehyde overnight at 4 °C, then transferred to 30% sucrose solution in PBS for 72 hrs at 4 °C for cryo-protection. Coronal brain sections (40 μm) were obtained by cryostat (Microm).

Real-time qRT-PCR

Total RNA was extracted with TRIzol reagent (Invitrogen) followed by ethanol precipitation. RNA quantity and purity were assessed by 260 nm/280 nm absorbance. Reverse transcription of 500 ng total RNA with random hexamer primers was performed with SuperScript III Reverse Transcriptase (Invitrogen) in duplicates at 50 °C for 1 h, then terminated at 70 °C for 10 min. Quantitative PCR was performed with iQ SYBR Green Supermix (Bio-Rad) with 300 nM primers in MicroAmp 96-well plates (Life Technologies) on StepOne Real-Time PCR System (Life Technologies). Denaturation was performed at 95 °C for 10 min, followed by 40 cycles of 94 °C for 15 s and 60 °C for 1 min. A melting curve was constructed at the end of the last cycle. Triplicates of identical reactions were set up for the real-time PCR to control for pipetting errors. Data was analyzed in StepOne Software (Life Technologies). Results were presented as relative expression levels compared to a stably expressed housekeeping ribosomal protein transcript (*acidic ribosomal protein*, NM022402) [23], and normalized to ZT 16. Primer sets span across intron gaps to avoid amplification of genomic DNA. Cbln1 primers were adopted from a previous publication [24].

Primers

Cbln1 (NM001109127)

Forward 5’- CCAGGTACTAGTGAACATCGGG -3’

Reverse 5’- TCAGAGGGGAAACACGAGGAATC -3’

GFAP (NM017009)

Forward 5’- ATGGCATCACCATTCCTGTAC -3’

Reverse 5’- TGGCCTTCTGACACCGATTT -3’

Acidic ribosomal protein (NM022402)

Forward 5’- CGTGATGCCCAGGGAAGA -3’

Reverse 5’- TCCACAATGAAGCATTTTGG -3’

Synthetic peptide and antiserum

Cerebellin, cerebellin-short, and scrambled cerebellin-short peptides were synthesized by GenScript or the Carver Biotechnology Center (University of Illinois). Synthesized cerebellin-short peptide was used as the epitope to generate rabbit anti-cerebellin-short antisera (UIUC Immunological Resource Center). The anti-sera was affinity purified with the EpiMAX Affinity Purification Kit (Abcam) using synthetic cerebellin peptide as antigen. Specificity for cerebellin-short was confirmed by reactivity against synthetic cerebellin-short, but not scrambled peptide. A single band at ~15 kDa is

detected by the affinity purified anti-sera from rat brain tissue lysates, corresponding to the predicted molecular weight of the C-terminus portion of Cbln1 when cleaved at the beginning of the cerebellin sequence (Fig. 2.1B). Strong punctate staining near the Purkinje cell layer of the cerebellum further confirms the specificity of the anti-sera.

Western blot

Total protein (15 μg) was resolved on 12% SDS-PAGE and transferred to polyvinvldifluoride (PVDF) membrane (Bio-Rad, Hercules, CA). Cbln1 and cleavage products were detected with either 1:1,000 dilution of rabbit polyclonal anti-precerebellin antibody (PA5-20159, Thermo Fisher) or 1:1,000 cerebellin-short antisera, followed by 1:2,500 dilution of HRP-conjugated goat anti-rabbit antibody (Invitrogen), and visualized with SuperSignal West Femto Maximum Sensitivity Substrate (Thermo Fisher). The membrane was then subjected to 1:10,000 dilution of rabbit anti-GAPDH antibody (G-9545, Sigma-Aldrich), followed by 1:2,500 HRP-conjugated goat anti-rabbit antibody (Invitrogen) and visualized. Protein levels were quantified by band intensities relative to GAPDH and normalized to the levels at ZT 16.

Immunohistochemistry

To localize Cbln1/cerebellin-short in the SCN, 40 μm coronal brain sections were antigen retrieved for 30 min at 75 °C in 10 mM sodium citrate (pH 9) then blocked in

0.3% Triton X-100 PBS with 5% normal goat serum (Vector Labs) or normal donkey serum (Jackson ImmunoResearch) at room temperature for 1 h. Tissue was exposed to either 1:1,000 rabbit anti-Cbln1 (ab92526, Abcam) or 1:2,000 affinity-purified rabbit anti-cerebellin-short anti-sera in 0.3% Triton X-100 PBS with 2% normal goat serum or normal donkey serum for 48 h at 4 °C. Sections were washed with PBS and stained for 1 h at room temperature in 0.3% Triton X-100 PBS with 2% normal goat serum or donkey serum containing appropriate 1:1,000 Alexa Fluor dyes that emit at 488, 568 or 594 (Life Technologies). To visualize the nuclei, sections were stained with diamidinophenylindole (DAPI), washed in PBS and mounted on gelatin-coated Superfrost microscope slides. Once dried, slides were coverslipped with Prolong Gold Antifade (Life Technologies).

Image acquisition

Immunofluorescence images were captured on a LSM-710 confocal microscope (Zeiss, Oberkochen, Germany). Image acquisition parameters (gain, offset, scan properties and laser power) were optimized for each objective lens and kept constant across samples examined. Captured images were compiled in Zen2 and Adobe Photoshop CC software with minimum alteration.

Single unit activity recording

Unanesthetized animals were decapitated by guillotine and brains quickly extracted.

The hypothalamus was reduced to 500 μm rectangular coronal slice containing the SCN, the third ventricle and the optic chiasm using fresh razor blades and a mechanical tissue chopper. The slice was maintained in a large-volume brain slice chamber perfused with Earle's balanced salt solution (EBSS, HyClone) supplemented with glucose, bicarbonate and Gentamicin [25]. The chamber was maintained at constant temperature of 37 °C and the EBSS was saturated with 95% O_2:5% CO_2. SCN neurons maintain a rhythm of single unit activity (SUA) *in vitro* that peaks around *circadian time* 7 (CT 7). CT designates the subjective time of day with reference to the intrinsic circadian clock. SUA of an SCN neuron was recorded for 4 min with glass electrodes filled with 5 M NaCl solution; at least 4 neurons were recorded per 60 min [26]. Activities of slices were recorded for 8 h starting at CT 0. Slices were prepared the day before recording during daytime to avoid shifting the intrinsic rhythm associated with cutting the optic nerve during the night. The activities were then averaged over 2 h with 15-min sliding windows and plotted using SigmaPlot. Treatment with peptide was performed by stopping the EBSS flow and filling the chamber for 10 min with EBSS containing the peptide at designated CT times. After 10 min, the EBSS containing peptide was withdrawn and the chamber refilled with regular EBSS, flow was then resumed.

Statistical analysis

Statistical analysis was performed using the GraphPad Prism 6 Software. One-way ANOVA with Dunnett's multiple comparisons test was used to compare magnitudes of

phase-shifts between treatments and control. One-way ANOVA with Bonferroni's multiple comparisons test was used for Western blots and qRT-PCR. $P \leq 0.05$ was considered statistically significant.

2.4 RESULTS

Cbln1 cleavage product in the rat SCN peaks during midday

Cerebellin is the proteolytic product of Cbln1 [27]. Western blot analysis of the SCN at six time points around the day did not show a significant change in the levels of Cbln1 monomer (MW = 25 kDa) when normalized to the non-circadian GAPDH (Fig. 2.2) [28]. On the other hand, the 15 kDa cleavage product of Cbln1 monomer peaks in midday (ZT 8) when compared to three other time points around the day when normalized to GAPDH ($P \leq 0.05$, n = 4) (Fig. 2.2). The level of the 15 kDa Cbln1 cleavage product did not oscillate in the cerebellum (data not shown). The daily peak in the cleavage product, but not the full length Cbln1, indicates diurnal oscillation in peptide cleavage and processing. Specificity of the anti-sera is demonstrated by its immunoreactivity against synthetic cerebellin-short peptide, which was used as the epitope to generate the anti-sera. Anti-sera showed no immunoreactivity against the scrambled control peptide. Possibly due to its small size (Predicted MW = 1.4 kDa) and the limitation of Western blot analysis, cerebellin-short was not observed.

Cbln1 mRNA in the rat SCN increases during late night

To determine whether oscillating levels of cerebellin-short released from the SCN is also controlled at the level of translation, qRT-PCR for Cbln1 mRNA was performed using published primer sets [24]. Cbln1 mRNA levels in the SCN is significantly elevated at late night (ZT 20) compared to three other time points around the day when normalized to the non-circadian housekeeping acidic ribosomal protein (Fig. 2.3).

Affinity purified anti-sera immunoreactivities in the rat SCN are punctate and different from localization of Cbln1

To determine the spatial expression of Cbln1 and cerebellin-short in the SCN, immunohistochemistry was performed with either affinity-purified anti-cerebellin-short anti-sera or an antibody against Cbln1. Cerebellin-short anti-sera immunoreactivity appeared punctate in the cell bodies throughout the SCN (Fig. 2.4A-C). Immunoreactivity appeared punctate and were restricted to the cell bodies, with no staining in processes observed. Cbln1 immunoreactivity on the other hand, showed process-like staining and was localized immediately outside of dorsal SCN along the 3rd ventricle (Fig. 2.4D-F). To determine the temporal pattern of Cbln1 expression in the SCN, DAB immunohistochemistry was performed on fixed coronal brain slices at six different time points around the day-night cycle with the cerebellin-short anti-sera. DAB staining in the SCN with the cerebellin-short anti-sera does not appear to vary over the day (data not shown).

Cerebellin-short advances the phasing of the rhythm of spontaneous neuronal activity in the rat SCN *in vitro.*

In vitro SCN has the ability to maintain spontaneous neuronal activity rhythm, which peaks around mid-day (CT 6.75 ± 0.07; Fig. 2.5A, I) [29]. To investigate whether cerebellin-short, the released form of the peptide, has a functional effect on the circadian time-keeping, synthetic cerebellin-short (100 nM) was applied to the SCN brain slice at CT 7, 14, or 21. These times represent subjective mid-day, early night, and late night, respectively. Synthetic cerebellin-short applied at CT 7 induced a significant phase advance in the SCN spontaneous neuronal activity rhythm (CT 3.75 ± 0.20; n=3; $P \leq 0.001$; Fig. 2.5B, E). When applied at CT 14, cerebellin-short also significantly phase advanced the neuronal activity rhythm (CT 4.75 ± 0.54; n=3; $P \leq 0.01$; Fig. 2.5C, E). The same treatment at CT 21 did not phase shift the SCN (Fig. 2.5D, E). Scrambled peptide did not induce a phase-shift at CT 7 (Fig. 2.5E). Treatment at CT 7 with full-length cerebellin peptide also induced phase-shift at similar magnitude as cerebellin-short (Fig. 2.5E).

2.5 DISCUSSION

Cbln1 and cerebellin-short present an interesting case where both the precursor and the processed peptide were previously shown to have unique functions in biological systems [18,20,21,30]. This study presents, for the first time, a functional role for the cerebellin-short peptide, as a potential circadian peptide in the rat SCN.

Circadian expressions of *Cbln1* mRNA and CBLN1 protein in the rat SCN suggest it is controlled by the circadian clock

Previous studies that examined general expression in the mouse brain did not report Cbln1 mRNA or protein in the SCN [16,24]. However, since Cbln1 mRNA and protein processing oscillate throughout the day, it is possible that previous investigations happened to capture the trough of expression. Alternatively, samples could have been gathered at multiple times of the day, which resulted in data with high variance and was, therefore, regarded as experimental error. Also both studies were performed in mouse, which are physiologically and genetically distinct from rats. Here we demonstrate that Cbln1 mRNA and protein are present in the rat SCN. Both Cbln1 mRNA and protein processing undergo daily oscillations in the SCN, suggesting that Cbln1 transcription and processing are under influence of the circadian clock.

Sequential peaks of mRNA *vs.* protein levels suggest additional controls in translation and/or peptide processing

Our results show that Cbln1 mRNA is present in the SCN at uniform levels throughout the course of the day, but becomes significantly elevated in late night (ZT 20). Although not statistically significant, full length Cbln1 monomer showed a trend of reduced RNA levels from ZT 0 to ZT 20. Interestingly, the 15 kDa cleavage product of the full length Cbln1 showed a significant peak at ZT 8, which is 12 h apart from the mRNA peak. The same oscillation is not observed in the cerebellum, where the level of 15 kDa cleavage product stayed constant. It has previously been observed that the 25

kDa Cbln1 monomer is unstable and easily cleaved at the N-terminus of the cerebellin motif into the 15 kDa cleavage product (Fig. 2.1B) [28]. The mismatch of the two profiles, where only the transcription level is elevated at ZT 20, suggests additional levels of control at either or both translation and/or degradation. A previous study utilizing MS, recorded an oscillation in release of endogenous cerebellin-short from the rat SCN, peaking in the subjective mid-night (CT 16) [13]. This is 8 h after the 15 kDa cleavage product peak at ZT 8 (Fig. 2.2). This suggests that the rate at which Cbln1 is processed into cerebellin and/or cerebellin-short is controlled at the post-translational level and is independent of the abundance of the Cbln1 protein. Also Cbln1 is not likely processed entirely into cerebellin intracellularly. Previous studies in the cerebellum and in cultured cortical neurons showed that functional Cbln1 forms homohexamer or heterohexomers with Cbln2 or Cbln3, and may be secreted in an uncleaved form to facilitate synapse formations and maintenance [15,18,19,31]. Even if the SCN does release Cbln1, previous MS-based peptidomics studies would not have registered uncleaved Cbln1 since at 193 amino acids it is too large for the detection range designated for peptides [15]. Whether uncleaved Cbln1 is also released in the SCN with potential synaptic and/or circadian implications is a subject for further investigation.

Cbln1 immunoreactivity showed different localizations from anti-cerebellin-short immunoreactivity

Cbln1 immunoreactivity is localized immediately dorsal of the SCN along the 3rd

ventricle and demonstrates fibrous staining. Whereas anti-cerebellin-short immunoreactivity is punctuated and localize to the cell bodies throughout the SCN. These staining patterns suggest that immediately outside of the SCN, a portion of Cbln1 remains unprocessed and perhaps functions through the known process of hexamerization and secretion. In the rest of the SCN, Cbln1 might be readily degraded or processed into cerebellin or cerebellin-short to exert the peptide-specific function.

Cerebellin-short advances phasing of the SCN during the day and early night

Exogenous cerebellin-short peptide applied to the SCN brain slice in subjective mid-day (CT 7) and early night (CT 14) phase advanced the intrinsic SCN neuronal firing rhythm. Endogenous release of cerebellin-short at these two times from the SCN is low, suggesting a functional role of cerebellin-short in the circadian signaling within the SCN when the system is perturbed. Despite the growing literature on Cbln1 and the identifications of several Cbln1 receptors (Nrxnβ, GluRD1, GluRD2) [18,19], a receptor has yet to be identified for cerebellin or cerebellin-short. Known Cbln1 receptors cannot function as cerebellin or cerebellin-short receptors. The domains involved in the formation of functional Cbln1 hexomers required for binding to these receptors are removed when cerebellin and cerebellin-short are formed [15,18,32]. Recent crystallography studies also show that domains on the Cbln1 that interact with GluRD2 and Nrxn are outside of the cerebellin motif [28,32]. Whether cerebellin-short exerts its circadian effects through a receptor or via other mechanisms remains a question. The timing of SCN sensitivity to cerebellin-short is not unique. Melatonin

and serotonin elicit phase advances when applied to the rat SCN in the early night and midday respectively [33,34]. Since cerebellin-short also elicits phase advance at these two times of the day, it could signal through related pathways. Whether these regulators of SCN phasing are functionally related requires investigation.

How the full-length Cbln1 is processed into cerebellin peptide is still unclear

This study identifies the presence of Cbln1 in the SCN and identifies cerebellin-short as a novel circadian peptide. However, many questions remain. The proteolytic events generating cerebellin and cerebellin-short from Cbln1 are unclear, and the identification of multiple intermediates suggests the process is complex [15]. Cbln1 is either secreted intact or processed into the cerebellin peptides. Whether these two pathways are exclusive or takes place in the same cell is unknown in the SCN. If both pathways exist in the same cells, then it requires intricate control to balance the levels of Cbln1 and cerebellin peptides. In addition, the 16 amino acid cerebellin peptide also elicited phase shift on the SCN, showing redundancy with cerebellin-short in circadian function. The extra histidine on cerebellin may contribute to longer half-life of the peptide compared to cerebellin-short, providing another level of control. Cbln1 is unusual in that it is transported between cell types in the cerebellum from the granule cells and to the Purkinje cells and the Bergmann glia [35], begging the question whether similar events take place in the SCN and is related to the production, release and circadian function of cerebellin-short.

2.6 FIGURES

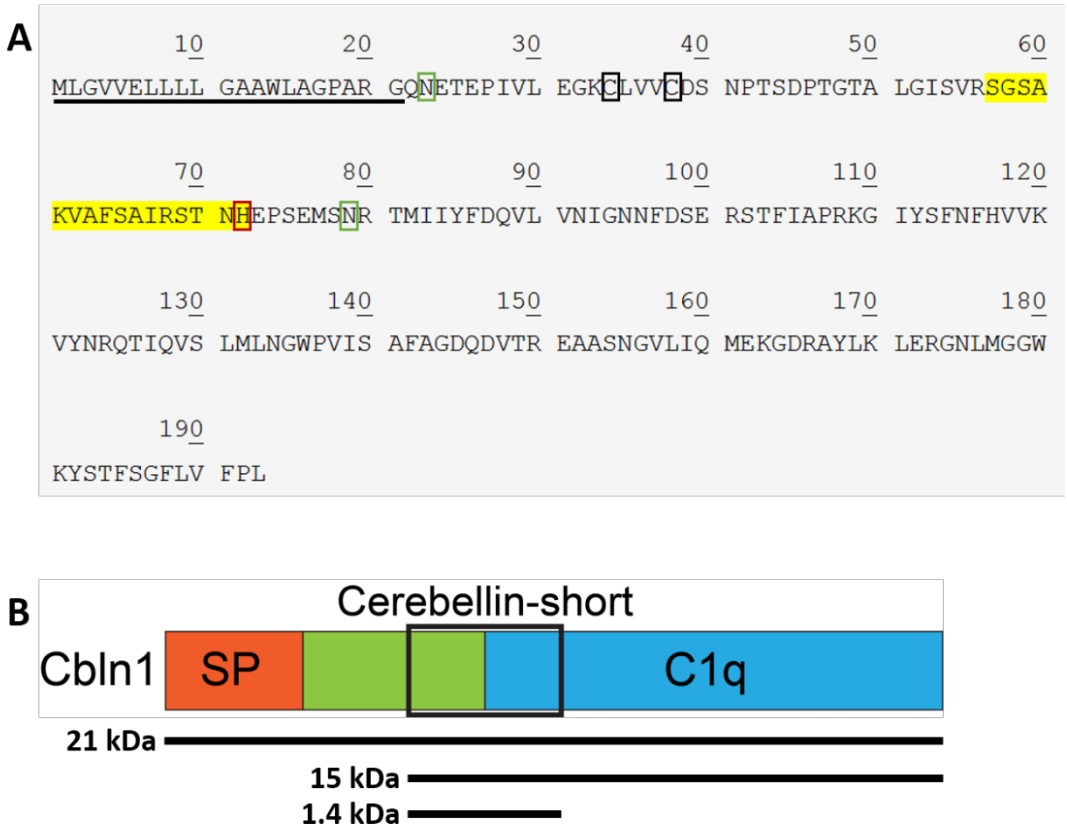

Figure 2.1. Full length amino acid sequence and domains of Cbln1. (A) Amino acid sequence of full length 193 amino acid rat Cbln1 (NP 001102597) [36]. 16 amino acid cerebellin peptide sequence is highlighted in yellow, red box designates C-terminus Histidine truncated from cerebellin-short. Green boxes designate glycosylation sites of Cbln1 at Arginine 23 & 79. Black boxes designate Cystine 34 & 38 responsible for dimerization of Cbln1 [15]. Black underline designates the signal peptide sequence. (B) Schematic of Cbln1, with C-terminus signal peptide and N-terminus C1q motif. Predicted molecular weights base on amino acid sequences of full length and the two cleaved forms of Cbln1 are listed.

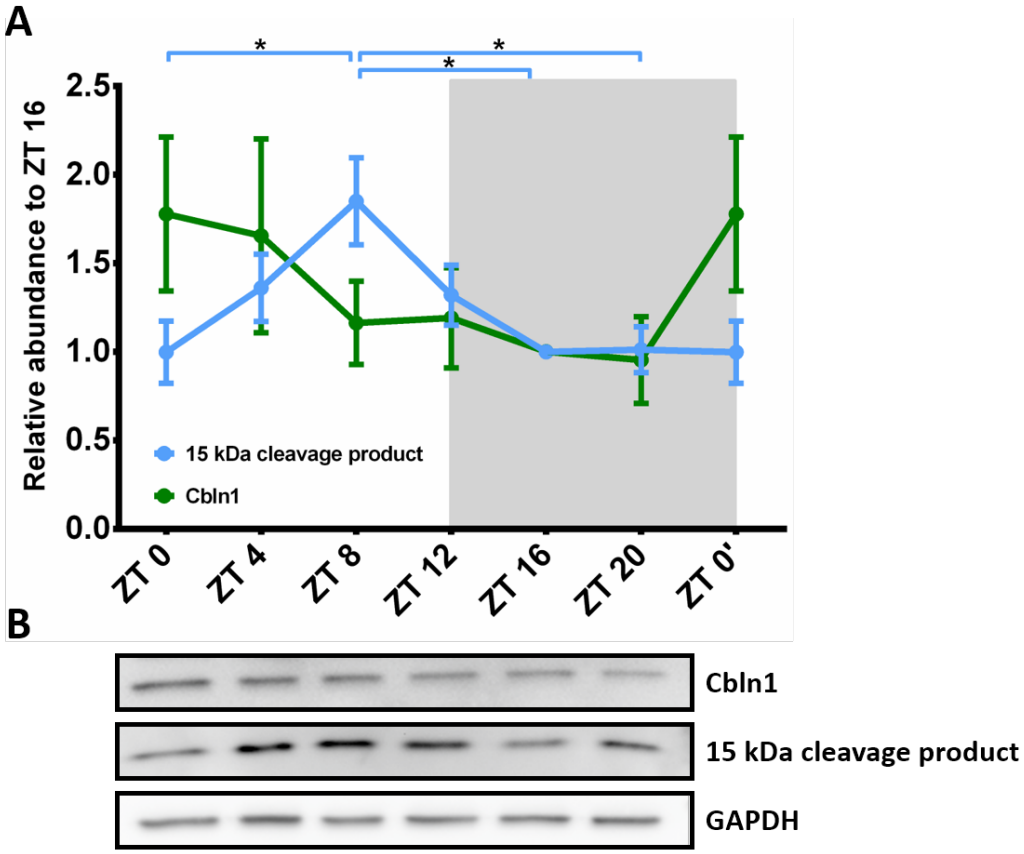

Figure 2.2. Cbln1 mRNA exhibit diurnal variations in the rat SCN. (A) Cbln1 mRNA level is uniform from dawn (ZT 0) through early night (ZT 16), but is elevated in the late night (ZT 20) compared to ZT 0, ZT 4 and ZT 12. Graph shows mean ± SEM, one-way ANOVA with Bonferroni's multiple comparisons test, * $P \leq 0.05$ ** $P \leq 0.01$, n = 4. ZT 0 is double plotted to show complete 24 h. (B) Representative agarose gel of Cbln1 qRT-PCR products at each time point shown in duplicates, along with the RT (-) and cDNA (-) controls.

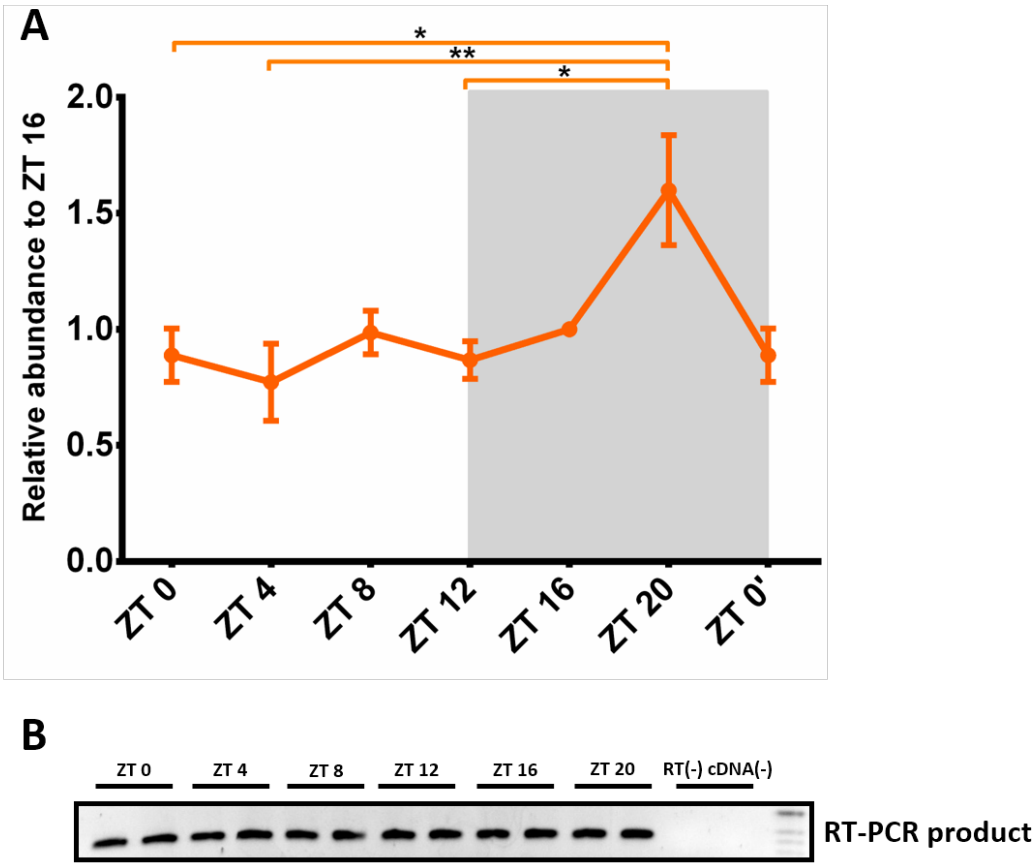

Figure 2.3. The 15 kDa cleavage product of Cbln1 protein exhibits diurnal variations in the rat SCN, while the full length Cbln1 levels remain stable. (A) Levels of full-length Cbln1 (green) showed no significant variation throughout the day. Levels of the 15 kDa cleavage product (blue) is significantly elevated at midday (ZT 8) compared to ZT 0, ZT 16 and ZT 20. Plotted are means ± SEM, one-way ANOVA with Bonferroni's multiple comparisons test, * $P \leq 0.05$, n = 4. ZT 0 is double-plotted to show complete 24 h. (B) Representative Western Blot of full length Cbln1, the 15 kDa cleavage product and GAPDH from the same blot are shown beneath corresponding to the ZT times in the graph.

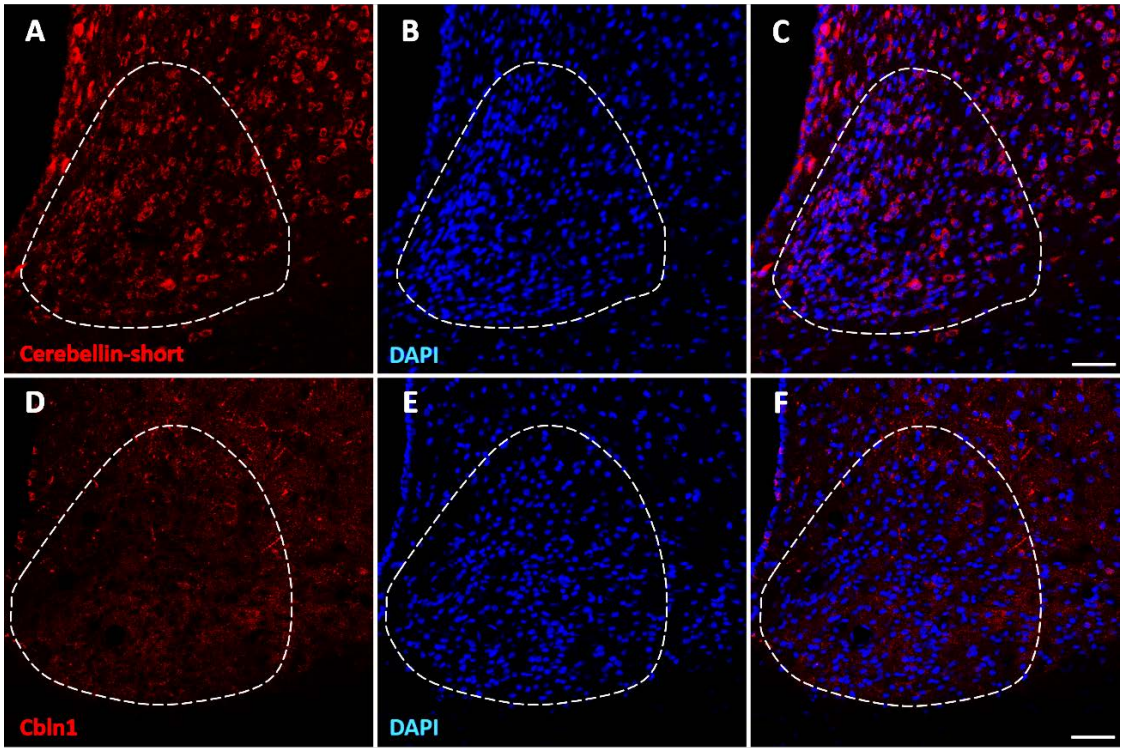

Figure 2.4. Anti-cerebellin-short and Cbln1 immunoreactivities in the rat SCN show different localizations. Confocal image of ZT 8 medial caudal SCN immunostained with anti-cerebellin-short anti-sera (A) or anti-Cbln1 (D) (red), and DAPI (B and E) (blue). When merged, anti-cerebellin-short immunoreactivity showed punctate staining in the cell bodies throughout the SCN (C). Anti-Cbln1 on the other hand, showed fibrous staining immediately dorsal to the SCN along the 3rd ventricle (F). White dotted lines outline the SCN based on DAPI. Scale bar: 50 μm.

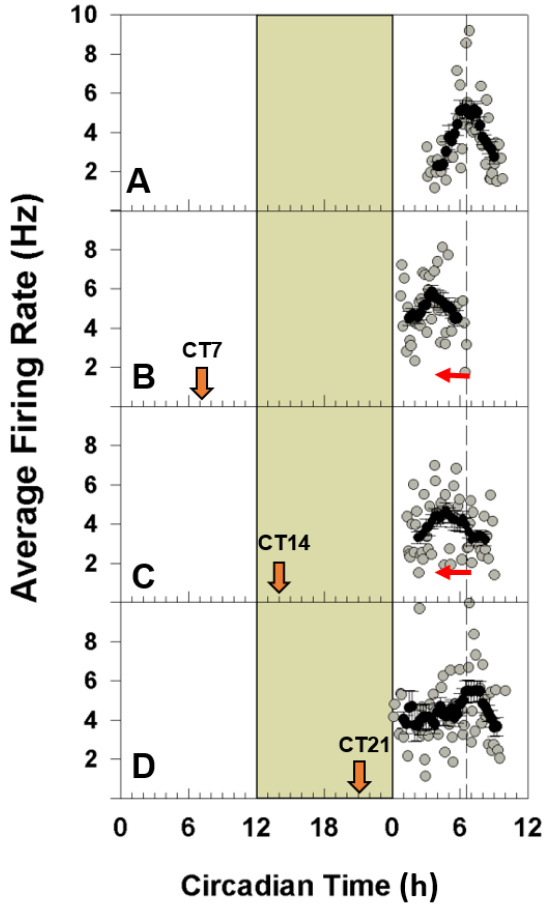

Figure 2.5. Treatment with synthetic cerebellin-short peptide at CT 7 and CT 14 phase advances the circadian rhythm in SCN neuronal activity. (A) SCN extracellular single unit recording of spontaneous neuronal firing rate peaks at CT 6.75 ± 0.07 (indicated by the vertical dotted line.) (B, C) Brief application of a synthetic cerebellin-short peptide (SGSAKVAFSAIRSTN, 100 nM, 10-min bath application) at CT 7 or CT 14 advances the phase of neuronal activity. (D) Treatment at CT 21 has no effect on the neuronal firing peak. Orange arrow: treatment time. Red arrow: phase shift. Grey circle: individual recorded neurons. Black circle: 2-h sliding window average.)

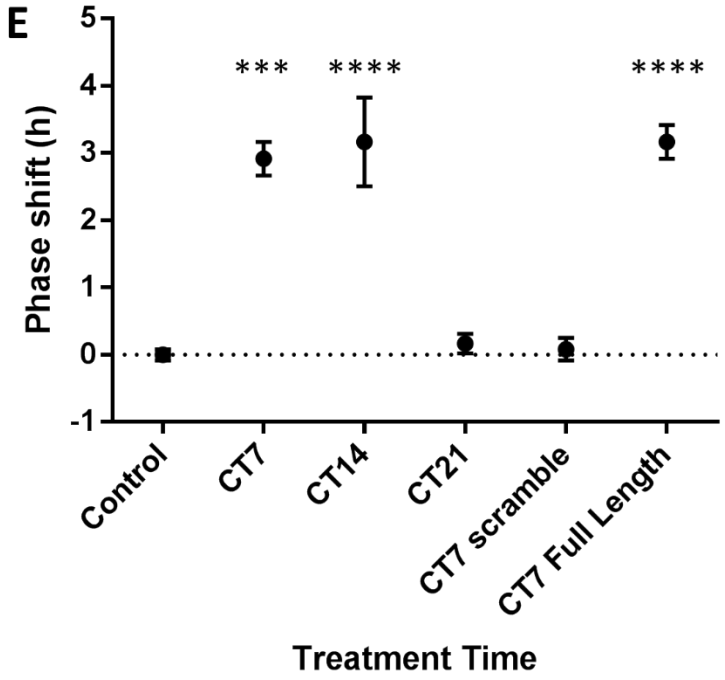

Figure 2.5 (cont.). Treatment with synthetic cerebellin-short peptide at CT 7 and CT 14 phase advances the circadian rhythm in SCN neuronal activity. (E) Mean data for effects of the synthetic cerebellin-short peptide or the scrambled peptide (n = 3). Treatment at CT 7 and CT 14 phase advances the rat SCN neuronal firing peak significantly (CT 3.75 ± 0.20 and C T4.75 ± 0.54, respectively) compared to the control time-of-peak (CT 6.75 ± 0.07). Neither the same treatment at CT 21 nor treatment with scrambled peptide (100 nM, 10-min bath application) at CT 7 altered phasing of this rhythm. Treatment with synthetic cerebellin peptide (100 nM, 10-min bath application) at CT 7 induced phase shift similar to cerebellin-short. Graph shows mean ± SEM, One-way ANOVA with Dunnett's post-test, *** $P \leq 0.001$ **** $P \leq 0.0001$ n = 3.

2.7 REFERENCES

1. Nishino H, Koizumi K, Brooks CMCCM. The role of suprachiasmatic nuclei of the hypothalamus in the production of circadian rhythm. Brain Res. 1976;112: 45–59.

2. Roenneberg T, Wirz-Justice A, Merrow M. Life between Clocks: Daily Temporal Patterns of Human Chronotypes. J Biol Rhythms. 2003;18: 80–90.

3. Gillette MU, Sejnowski TJ. Physiology. Biological clocks coordinately keep life on time. Science. 2005;309: 1196–8.

4. Moore RY, Speh JC, Leak RK. Suprachiasmatic nucleus organization. Cell Tissue Res. 2002;309: 89–98.

5. Dibner C, Schibler U, Albrecht U. The mammalian circadian timing system: organization and coordination of central and peripheral clocks. Annu Rev Physiol. 2010/02/13. 2010;72: 517–549.

6. Gillette MU, Reppert SM. The hypothalamic suprachiasmatic nuclei: circadian patterns of vasopressin secretion and neuronal activity in vitro. Brain Res Bull. Elsevier; 1987;19: 135–139.

7. Francl J, Kaur G, Glass J. Regulation of vasoactive intestinal polypeptide release in the suprachiasmatic nucleus circadian clock. Neuroreport. 2010;21: 1055–1059.

8. Romijn H, Sluiter A, Pool C. Differences in colocalization between Fos and PHI, GRP, VIP and VP in neurons of the rat suprachiasmatic nucleus after a light stimulus during the phase delay versus. J Comp Neurol. 1996;372: 1–8.

9. Atkins Jr. N, Mitchell JW, Romanova E V, Morgan DJ, Cominski TP, Ecker JL, et al. Circadian integration of glutamatergic signals by little SAAS in novel suprachiasmatic circuits. PLoS One. United States; 2010;5: e12612.

10. Colwell CS, Michel S, Itri J, Rodriguez W, Tam J, Lelievre V, et al. Disrupted circadian rhythms in VIP- and PHI-deficient mice. Am J Physiol Regul Integr Comp Physiol. 2003;285: R939-49.

11. Maywood ES, Reddy AB, Wong GK, O'Neill JS, O'Brien JA, McMahon DG, et al. Synchronization and maintenance of timekeeping in suprachiasmatic circadian clock cells by neuropeptidergic signaling. Curr Biol. 2006/03/21. 2006;16: 599–605.

12. Lee JE, Atkins Jr. N, Hatcher NG, Zamdborg L, Gillette MU, Sweedler J V, et al. Endogenous peptide discovery of the rat circadian clock: a focused study of the suprachiasmatic nucleus by ultrahigh performance tandem mass spectrometry. Mol Cell Proteomics. United States; 2010;9: 285–297.

13. Hatcher NG, Atkins Jr. N, Annangudi SP, Forbes AJ, Kelleher NL, Gillette MU, et al. Mass spectrometry-based discovery of circadian peptides. Proc Natl Acad Sci U S A. United States; 2008;105: 12527–12532.

14. Slemmon JR, Blacher R, Danho W, Hempstead JL, Morgan JI. Isolation and sequencing of two cerebellum-specific peptides. Proc Natl Acad Sci U S A. 1984;81: 6866–70.

15. Bao D, Pang Z, Morgan JI. The structure and proteolytic processing of Cbln1 complexes. J Neurochem. England; 2005;95: 618–629.

16. Wei P, Smeyne RJ, Bao D, Parris J, Morgan JI. Mapping of Cbln1-like immunoreactivity in adult and developing mouse brain and its localization to the endolysosomal compartment of neurons. Eur J Neurosci. France; 2007;26: 2962–2978.

17. Hirai H, Pang Z, Bao D, Miyazaki T, Li L, Miura E, et al. Cbln1 is essential for synaptic integrity and plasticity in the cerebellum. Nat Neurosci. United States; 2005;8: 1534–1541.

18. Matsuda K, Miura E, Miyazaki T, Kakegawa W, Emi K, Narumi S, et al. Cbln1 is a ligand for an orphan glutamate receptor delta2, a bidirectional synapse organizer. Science. United States; 2010;328: 363–368.

19. Yasumura M, Yoshida T, Lee SJ, Uemura T, Joo JY, Mishina M. Glutamate receptor delta1 induces preferentially inhibitory presynaptic differentiation of cortical neurons by interacting with neurexins through cerebellin precursor protein subtypes. J Neurochem. 2011/12/24. 2011;

20. Mazzocchi G, Andreis PG, De Caro R, Aragona F, Gottardo L, Nussdorfer GG. Cerebellin enhances in vitro secretory activity of human adrenal gland. J Clin Endocrinol Metab. 1999;84: 632–5.

21. Albertin G, Malendowicz LK, Macchi C, Markowska A, Nussdorfer GG. Cerebellin stimulates the secretory activity of the rat adrenal gland: in vitro and in vivo studies. Neuropeptides. 2000;34: 7–11.

22. Gardiner J V, Beale KE, Roy D, Boughton CK, Bataveljic A, Campbell DC, et al. Cerebellin1 is a novel orexigenic peptide. Diabetes Obes Metab. England: Blackwell Publishing Ltd; 2010;12: 883–890.

23. Tischkau SA, Barnes JA, Lin FJ, Myers EM, Barnes JW, Meyer-Bernstein EL, et al. Oscillation and light induction of timeless mRNA in the mammalian circadian clock. J Neurosci. 1999;19: RC15.

24. Miura E, Iijima T, Yuzaki M, Watanabe M. Distinct expression of Cbln family mRNAs in developing and adult mouse brains. Eur J Neurosci. France; 2006;24: 750–760.

25. Zhang L, Kolaj M, Renaud LP. Suprachiasmatic nucleus communicates with anterior thalamic paraventricular nucleus neurons via rapid glutamatergic and gabaergic neurotransmission: state-dependent response patterns observed in vitro. Neuroscience. 2006;141: 2059–66.

26. Prosser RA, McArthur AJ, Gillette MU. cGMP induces phase shifts of a mammalian circadian pacemaker at night, in antiphase to cAMP effects. Proc Natl Acad Sci. National Acad Sciences; 1989;86: 6812.

27. Urade Y, Oberdick J, Molinar-Rode R, Morgan JI. Precerebellin is a cerebellum-specific protein with similarity to the globular domain of complement C1q B chain. Proc Natl Acad Sci U S A. UNITED STATES; 1991;88: 1069–1073.

28. Cheng S, Seven AB, Wang J, Skiniotis G, Özkan E. Conformational Plasticity in the Transsynaptic Neurexin-Cerebellin-Glutamate Receptor Adhesion Complex. Structure. 2016;24: 2163–2173.

29. Green DJ, Gillette R. Circadian rhythm of firing rate recorded from single cells in the rat suprachiasmatic brain slice. Brain Res. 1982;245: 198–200.

30. Mugnaini E, Dahl AL, Morgan JI. Cerebellin is a postsynaptic neuropeptide. Synapse. 1988;2: 125–38.

31. Ito-Ishida A, Miura E, Emi K, Matsuda K, Iijima T, Kondo T, et al. Cbln1 regulates rapid formation and maintenance of excitatory synapses in mature cerebellar Purkinje cells in vitro and in vivo. J Neurosci. United States; 2008;28: 5920–5930.

32. Elegheert J, Kakegawa W, Clay JE, Shanks NF, Behiels E, Matsuda K, et al. Structural basis for integration of GluD receptors within synaptic organizer complexes. 2016;353.

33. McArthur AJ, Gillette MU, Prosser RA. Melatonin directly resets the rat suprachiasmatic circadian clock in vitro. Brain Res. 1991;565: 158–61.

34. Medanic M, Gillette MU. Serotonin regulates the phase of the rat suprachiasmatic circadian pacemaker in vitro only during the subjective day. J Physiol. 1992;450: 629–42.

35. Wei P, Rong Y, Li L, Bao D, Morgan JI. Characterization of trans-neuronal trafficking of Cbln1. Mol Cell Neurosci. Elsevier Inc.; 2009;41: 258–73.

36. Geer LY, Marchler-Bauer A, Geer RC, Han L, He J, He S, et al. The NCBI BioSystems database. Nucleic Acids Res. 2010;38: D492-6.

CHAPTER THREE: LOCALIZATION AND PROCESSING OF CEREBELLIN-SHORT AND CBLN1 IN THE RAT SUPRACHIASMATIC NUCLEUS

3.1 ABSTRACT

Mammalian circadian rhythm is controlled by the suprachiasmatic nucleus (SCN), which expresses a rich collection of neuropeptides, number of which are crucial for synchronizing the intrinsic rhythm as well as the rhythm in the rest of the brain. One of such small peptide, cerebellin-short, is generated from the cleavage of Cbln1 and undergoes circadian release from the SCN. Cerebellin-short can phase shift the SCN when applied exogenously, yet the source and distribution of cerebellin-short and the precursor Cbln1 in the SCN is unknown. Here we show that cerebellin-short is present in both the AVP- and the VIP-positive cells in the SCN. Cbln1 on the other hand localized to fibers immediately dorsal to the SCN along the 3rd ventricle. Cbln1 is also prominent in the axons and cell bodies of magnocellular neurons in the paraventricular nucleus (PVN) and the supraoptic nucleus (SON). Upon synaptosome fractionation, a 15 kDa cleavage product of Cbln1 is enriched in both the SCN and the cerebellum. These results suggest that Cbln1 is rapidly processed into cerebellin-short at the synapse and widely distributed in the SCN. Uncleaved Cbln1 may also serve functions in the PVN and the SON distinct from the circadian modulation by cerebellin-short in the SCN.

3.2 INTRODUCTION

Circadian rhythms in mammals are controlled by the suprachiasmatic nucleus (SCN), a bilateral nucleus located in the base of the hypothalamus immediately above the optic chiasm [1]. Containing ~10,000 cells, the architecture of the SCN is complex, with interconnected sub regions defined by neuropeptide profiles and specific network properties [2]. The SCN is conventionally divided into a core region or the ventrolateral SCN, and a shell region or the dorsomedial SCN [2]. Ventrolateral SCN is characterized by the expression the vasoactive intestinal peptide (VIP), and is innervated by the retinohypothalamic tract (RHT) to receive direct photic input from the retina [3–5]. Upon light stimulation, glutamate (GLU) and pituitary adenylate cyclase-activation peptide (PACAP) released from the RHT leads to the secretion of VIP, a peptide known to synchronize the SCN [3,5]. Deletion of VIP or its receptor VPAC2 leads to impaired behavior rhythms and the loss of synchrony, highlighting the importance of VIP in circadian time keeping [6–8]. The dorsomedial SCN receives innervations from the ventrolateral SCN and is characterized by the expression of arginine vasopressin (AVP) [2,9,10]. The dorsomedial SCN acts as an output, with the circadian rhythm communicated to the rest of the brain [11,12]. Tempering with the core clock components Bmal1 or casein kinase 1 δ (CK1δ) in the AVP cells have consequences in the amplitude and period of the SCN rhythm, demonstrating the importance of functional AVP cells in circadian time keeping [13,14]. Neuropeptides can influence the circadian clock by phase-shifting the internal rhythm of the SCN. For example, VIP and gastrin releasing peptide (GRP) both phase-shift the SCN similar to

the light response [15–17]. Recently it was discovered that little SAAS, a cleavage product of ProSAAS highly expressed in the central region of the SCN, induces phase-delay in the early night [18,19]. In the previous chapter, it was shown that cerebellin-short can phase-advance the SCN both during the day and in the early night.

In the hypothalamus, SCN interacts with other hypothalamic nuclei to control homeostasis, hormone secretion and metabolism (reference). SCN efferent innervate other hypothalamic nuclei including the paraventricular nucleus (PVN), the supraoptic nucleus (SON) and the arcuate nucleus (ARC) [11,12,20,21]. SCN also receives neuropeptide Y (NPY) and GABA through innervations from the intergeniculate leaflet (IGL), serotonin from the raphe nuclei, and melatonin from the pineal gland [2,9,22]. NPY, GABA, serotonin and melatonin serve as inputs and exert phase-shifts in the SCN with specific windows of action [23–28].

Cerebellin-short was discovered in high throughput mass spectrometry screening of releasate from the SCN with a circadian release pattern peaking during the middle of the night [19,29]. Cerebellin-short is the 15 amino acid cleavage product of the precursor protein Cbln1. Cbln1 has well established formation and maintenance functions in the cerebellum parallel fiber-Purkinje cell synapses [30–32], and has recently been implicated to participate in synapse formation in the hippocampus [33,34]. Previous low resolution whole brain *in situ* hybridization and immunostaining

studies suggested that Cbln1 is widely expressed in the hypothalamus [35–37], yet little follow up study has been done on Cbln1 in this region of the brain. Since cerebellin-short is released from the SCN, the precursor Cbln1 is either endogenously expressed in the SCN or transported to the SCN via afferents. In the cerebellum, Cbln1 undergoes complex processing with multiple intermediates to yield cerebellin peptides [38]. Whether the same process takes place at the SCN is unknown.

This study describes the difference in localization between Cbln1 and its processing intermediate in the rat hypothalamus. Region-specific distributions of cerebellin-short in the SCN were explored, and the subcellular distribution of Cbln1 versus processing intermediates in the SCN was examined.

3.3 MATERIALS AND METHODS

Animal

Long Evans/BluGill rats of both genders (University of Illinois, Urbana, IL) between the ages of 7 to 13 weeks were used for adult rat experiments. The colony is inbred, and genomic scan revealed one allele at each locus examined. Rats are housed under 12h:12h light-dark cycle with constant temperature, humidity, with access to food and water *ad libtium*. *Zeitgeber time* (ZT), standardized to the environmental light cycle, is designated ZT 0 when the light turns on and ZT 12 when the light goes off.

Tissue acquisition

For synaptosomal fractionation experiments, unanesthetized animals were decapitated by guillotine at ZT 8 and the brain quickly extracted. The hypothalamus was surgically reduced to a 1 mm thick coronal slice containing the SCN, the third ventricle and the optic chiasm using fresh razor blades on a mechanical tissue chopper. A tissue puncher (r = 1.5 mm) was used to isolate the bilateral SCN from the slice, which is immediately submerged in 9 volumes of chilled homogenizing media (0.32 M sucrose, 50 mM Tris-HCl, pH 8) containing protease and kinase inhibitor cocktails. Cerebellum tissue was obtained from the same brain by reducing the cerebellum into a 1 mm thick sagittal slice.

For fixed tissue collection, animals were euthanized with 1 ml Euthasol (Virbac) at designated ZT times and perfused through the heart with 300 ml of 0.9% saline, followed by 300 ml of 4% paraformaldehyde (PFA, Sigma-Aldrich) in 0.1 M PBS. The brain was removed and fixed in 4% PFA overnight at 4 °C, then transferred to 30% sucrose solution in PBS for 72 hrs at 4 °C for cryo-protection. Coronal brain sections (40 μm) were obtained by cryostat (Microm).

For fixed tissue from the Astrobow mice, adult animals were euthanized with 0.1 ml Euthasol and perfused through the heart with 50 ml of 0.9% saline, followed by 50 ml of 4% PFA in 0.1 M PBS. The brain was removed and fixed in 4% PFA overnight at 4 °C, followed by 40 μm sectioning at room temperature on a vibratome in PBS.

Immunohistochemistry

To examine possible region-specific localizations of Cbln1/cerebellin short in the SCN, 40 μm coronal brain sections were antigen retrieved with 10 mM sodium citrate (pH 9) at 75 °C for 30 min [39]. Treated slices were blocked in 0.3 % Triton X-100 PBS with 5 % normal goat serum (Vector Lab) or normal donkey serum (Jackson ImmunoResearch) at room temperature for 1 h. Slices were exposed to either 1:1,000 rabbit polyclonal anti-Cbln1 (ab92526, Abcam) or 1:2,000 affinity-purified rabbit anti-cerebellin-short antisera in 0.3 % Triton X-100 PBS with 2 % normal goat serum or 2 % normal donkey serum for 48 h at 4 °C. The AVP and the VIP regions of the SCN were immunostained with guinea pig anti-AVP (T-5048, Peninsula Laboratories International) and guinea pig anti-VIP (T-5030, Peninsula Laboratories International) at 1:1,000 dilutions. Purkinje cells in the cerebellum were identified with mouse anti-calbindin D-28K (C9848, Sigma-Aldrich) at 1:1,000 dilution. Lysosomes were identified with mouse anti-cathepsin D (ab6313, Abcam) at 1:500 dilution. After primary antibody incubation, slices were washed 3 x 10 min with PBS at room temperature. Slices were then incubated with the appropriate goat or donkey secondary antibodies conjugated to Alexa flour 488, 568, or 633 (Invitrogen) at 1:1,000 dilutions in 0.3% Triton-X 100 with 2% normal goat or donkey serum at room temperature for 1 h. Nuclei were counter staining with DAPI (Thermo Fisher). Slices were mounted on gelatin-coated Superfrost microscope slides and coverslipped with Prolong Gold Antifade (Thermo Fisher).

Image acquisition

Confocal immunofluorescence images were captured on the LSM-710 confocal microscope (Zeiss). Image acquisition parameters (gain, offset, aperture, scan properties and laser power) were optimized for each objective and kept constant across repeated samples. Captured images were compiled in Zen2 and Adobe Photoshop CC with minimum alteration.

Cell counting

Z-stack images of the SCN were captured with 20x objective at 1 μm z-intervals. Raw images were divided with 8x8 grids and counted manually. SCN from at least 3 animals with at least 3 slices per animal were counted.

Synaptosomal fractionation and Western blot

Synaptosomal fractionation protocol was based on previous publication [38]. Briefly, tissues in 9 volumes of the homogenizing buffer were homogenized with 4 strokes by a plastic pestle in 1.5 ml tubes on ice. The homogenate was centrifuged at 700 x g for 10 min at 4 °C to pellet the nuclei/cell debris (P1) and the supernatant was collected (S1, post nuclear fraction). The S1 fraction was further centrifuged at 11,000 x g for 15 min at 4 °C to separate the cytosol and light membrane supernatant fraction (S2) from the crude synaptosomal pellet fraction (P2). The P2 fraction containing crude synaptosomes was washed with the homogenizing buffer twice and lysed in RIPA

buffer containing protease inhibitors. At this point protein concentrations of the S2 and the P2 fractions were assessed with a BCA kit (Thermo Fisher).

For Western blot analysis, S2 or P2 fractions containing 10 μg of protein were mixed with 5x loading buffer containing sodium dodecyl sulfate (SDS) and beta mercaptoethanol and denatured at 60 °C for 10 min. Denatured samples were resolved on 4 – 20% SDS-PAGE (Bio-Rad) and transferred to polyvinvldifluoride (PVDF) membrane (Millipore). Cbln1 and cleavage products were detected with either 1:1,000 dilution of rabbit polyclonal anti-precerebellin antibody (PA5-20159, Thermo Fisher) or 1:1,000 affinity-purified rabbit anti-cerebellin-short antisera, followed by 1:2,500 dilution of HRP-conjugated goat anti-rabbit antibody and visualized with SuperSignal Femto Maximum Sensitivity Substrate (Thermo Fisher). The membrane was then subjected to 1:10,000 dilution of rabbit anti-GAPDH antibody (G-9545, Sigma-Aldrich), followed by 1:2,500 HRP-conjugated goat anti-rabbit antibody and visualized. Protein levels were quantified by band intensities and normalized to GAPDH.

Statistical analysis

Unpaired two-tailed student's t-test was used to compare between the band intensities and the ratios for the synaptosomal fractionation experiments using the GraphPad Prism 6 software. $P \leq 0.05$ was considered statistically significant.

3.4 RESULTS

Cerebellin-short and Cbln1 immunoreactivities localize differently in the rat cerebellum

Previous studies reported different localizations of cerebellin-short and Cbln1 immunoreactivities (IR) in the cerebellum. To confirm the specificity of the cerebellin-short and the Cbln1 antibodies used for this investigation, immunofluorescence was performed in the rat cerebellum. Cerebellin-short IR were punctate and mainly localized between the Purkinje cell bodies in the Purkinje cell layer (Fig. 3.1A-D). Cbln1 IR on the other hand were localized to the molecular layer and concentrated around the dendritic trees of the Purkinje cells (Fig. 3.1E-H). These results agreed with previous publications [37,40] and suggested that the antibodies are specific to their respective targets.

Cerebellin-short immunoreactivities co-localize with AVP- and VIP- positive cells in the SCN

To examine possible region-specific localizations of the cerebellin-short peptide in the rat SCN, brain slices collected at ZT 8 were stained for both cerebellin-short and either AVP or VIP. AVP staining defined the dorsomedial region, while VIP staining marked the ventrolateral region of the SCN (Fig. 3.2B, 3.2F). Cerebellin-short IR appeared to be punctate around the cell bodies, and showed substantial overlap with both the AVP and the VIP cells (Fig. 3.2D & 3.2H). Cerebellin-short IR in the cell bodies appeared

stronger immediately outside of the SCN (Fig. 3.2A & 3.2E). Of all the counted AVP and VIP positive cells in the SCN, approximately 80% of the AVP- and VIP-positive cells were also positive for cerebellin-short IR. The percentages of AVP and VIP cells positive for cerebellin-short IR were not significantly different (data not shown).

Cbln1 immunoreactivities localized immediately dorsal to the SCN and is widely present in the hypothalamus

To examine the potential difference in localization between cerebellin-short and its precursor Cbln1, brain slices collected at ZT 8 were stained for Cbln1 alone with AVP to mark the SCN. Interesting, the strongest Cbln1 IR were immediately dorsal to the SCN along the 3rd ventricle, with patterns that resemble neuronal fibers (Fig. 3.3). The fibrous IR showed minimal overlap with the SCN and mostly terminated at the boundary of the dorsal medial SCN marked by both DAPI and AVP. Some AVP positive fibers extending from the SCN were also positive for Cbln1 IR, suggesting the presence of Cbln1 in these AVP cells.

Outside of the SCN, intense Cbln1 IR were observed in other hypothalamic nuclei including the paraventricular nucleus (PVN) (Fig 3.4A), the median eminence (ME) (Fig. 3.4B), and the supraoptic nucleus (SON) (Fig. 3.4C-F). Cbln1 IR were also prominent along the axonal tracks that project from the PVN and the SON towards the posterior pituitary. In the SON, Cbln1 IR (Fig. 3.4C) and AVP (Fig. 3.4D) showed no

co-localization, indicating the absence of Cbln1 in the AVP magnocellular neurons of the SON.

Both cerebellin-short and Cbln1 immunoreactivities do not co-localize with GFAP-positive astrocytes in the mouse SCN

To determine whether Cbln1 and cerebellin-short in the SCN are also present in glial cells, immunofluorescence was performed on the transgenic Brainbow GFAP-Cre mouse line that stochastically expresses fluorescent proteins in GFAP-positive cells. Upon SCN staining, both the cerebellin-short and Cbln1 IR showed no co-localization with GFAP-induced Brainbow fluorescence in the mice SCN (Fig. 3.5).

The 15 kDa cleavage product of Cbln1 is enriched in the crude synaptosomal fraction in both the SCN and the cerebellum

Cbln1 undergoes extensive processing to yield cerebellin peptides. One of the processing intermediate is the 15 kDa cleavage product discussed in the previous chapter formed by the cleavage of Cbln1 at the N-terminus of the cerebellin sequence. The 15 kDa cleavage product is recognized by the cerebellin-short antisera on Western blot, whereas the ~1.4 kDa cerebellin peptides were not observed possibly due to their low molecular weight and the detection limit of the Western blot technique. To examine the processing of Cbln1 in the SCN, SCN tissue was subjected to synaptosomal fractionation by centrifugation followed by electrophoresis on SDS-

PAGE and detection by Western blot. Both Cbln1 and the 15 kDa cleavage product were present in the cytosol and light membrane fraction (S2), but the 15 kDa cleavage product was enriched in the crude synaptosome fraction (P2) of the SCN with minimal amounts of Cbln1 observed (Fig.3.6A). A similar pattern was also observed in the cerebellum, although slightly higher amounts of Cbln1 was observed in the P2 fraction compared to the SCN (Fig. 3.6A). These results were initially puzzling, as Cbln1 was observed in the SCN S2 fraction but Cbln1 IR were minimal in the SCN. One possible explanation is that during tissue acquisition Cbln1 in neuronal processes dorsal to the SCN (Fig. 3.3A) were inevitably collected due the size of the biopsy punch.

In the S2 fraction of the SCN, the amount of Cbln1 was generally higher than the 15 kDa cleavage product when normalized to GAPDH, although the difference was not statistically significant (Fig. 3.6B) (Unpaired t-test, P-value = 0.194). In the P2 fraction, the opposite trend was observed (Fig. 3.6C) (Unpaired t-test, P-value = 0.0551). When the 15 kDa cleavage product to Cbln1 ratio was compared between the SCN S2 and the P2 fractions, the P2 fraction had significant enrichment of the 15 kDa cleavage product compared to the S2 fraction (Fig. 3.6D) (Unpaired t-test, P-value = 0.0137). In the S2 fraction of the cerebellum, the amount of Cbln1 was significantly higher than the 15 kDa cleavage product when normalized to GAPDH (Fig. 3.6E) (Unpaired t-test, P-value = 0.0025). In the P2 fraction, the 15 kDa cleavage product was significantly higher than Cbln1 (Fig. 3.6F) (Unpaired t-test, P-value = 0.0047). The ratio of 15 kDa cleavage product to Cbln1 in the cerebellum was also significantly

higher in the P2 fraction compared to the S2 fraction (Fig. 3.6G) (Unpaired t-test, P-value = 0.0032).

3.5 DISCUSSION

Cerebellin-short IR showed high overlap with both AVP and VIP cells in the SCN

Cerebellin-short IR were predominantly punctate in the neuronal cell bodies, with some puncta localized to the lysosomes as previously reported (data not shown) [35,37]. Localization to the lysosomes indicates the possibility of active degradation. Transfer of Cbln1 from presynaptic granule cells to postsynaptic Purkinje cells and Bergmann glia were previously described in the cerebellum [37]. Secreted Cbln1 at the synapse were speculated to be internalized through the endosomal pathway, some of which may be shuttled to the lysosomes for degradation [37]. Lysosomes might also process Cbln1 into cerebellin peptides for alternative functions in the cerebellum yet to be discovered. In the SCN the same mechanism might be in place to impose circadian modulation on the level of available cerebellin-short peptides. Alternatively, localization of cerebellin-short IR to the lysosomes might be a part of a secretion mechanism involving the fusion of lysosomes to the plasma membrane [41,42].

When the entire SCN was analyzed, cerebellin-short IR did not localize exclusively to either the dorsomedial or the ventrolateral SCN designated by AVP and VIP. Instead, around 80% of both AVP and VIP cells in the SCN were positive for cerebellin-short

IR. This result suggests that cerebellin-short is widely present throughout the SCN and might functionally connect the two regions critical to circadian time keeping.

Cbln1 IR is prevalent in the hypothalamus and distinct from cerebellin-short IR in the SCN

In contrast to the cerebellin-short IR, Cbln1 IR were minimal in the SCN but were prominent in processes immediately dorsal to the SCN along the 3rd ventricle. SCN is known to project directly to the PVN and the sub-paraventricular area [43], suggesting the possibility of Cbln1 transport between the SCN and the PVN. This speculation is supported by the observation of high amounts of Cbln1 IR in the PVN magnocellular neuron cell bodies and axons. Magnocellular neurons from the PVN project to the posterior pituitary through the hypothalamo-neurohypophysial system, where peptides and hormonal signals are released into the bloodstream [44,45]. Previous study also reported presence of Cbln1 in the posterior pituitary [46,47]. One possibility is that Cbln1 from the SCN is transported to the PVN and the posterior pituitary for functions distinct from the circadian modulation conferred by cerebellin-short in the SCN discussed in the previous chapter. Alternatively, Cbln1 is transported from the PVN to the SCN, which is then processed into cerebellin-short to modulate circadian rhythm.

Cbln1 IR were also observed in the SON magnocellular neurons and were distinct from the AVP cells. Like the PVN, magnocellular neurons from the SON also project

axons to the posterior pituitary [44,45]. Synthetic cerebellin peptide was known to stimulate the release of norepinephrine from rat adrenal glands [48,49], suggesting the involvement of Cbln1 in the hypothalamic-pituitary-adrenal axis.

Cbln1 and cerebellin-short are neuronal in the SCN

Astrocytes in the SCN are an integral part in facilitating circadian rhythm [50–52]. As mentioned previously, Cbln1 can be transferred from the granule cells to the Bergmann glia in the cerebellum. This observation raised the question whether Cbln1 and cerebellin-short in the SCN could also be present in astrocytes. Upon staining in GFAP-Cre Astrobow mice, cerebellin-short IR co-localized with GFAP-positive Bergmann glia in the cerebellum (data not shown), confirming previously published results. In contrast, neither Cbln1 nor cerebellin-short IR were observed in SCN GFAP-positive astrocytes, suggesting their neuronal origins.

Processing of Cbln1 into cerebellin peptides takes place at the synapse or lysosomes

Cbln1 undergo extensive processing through multiple intermediates to yield the cerebellin peptides [38]. At the N-terminus of the cerebellin sequence in Cbln1, a cleavage site similar to that in proTNα is present [38,53]. ProTNFα is cleaved by the TACE metalloprotease to release TNFα, suggesting the possibility that TACE could also cleave Cbln1. At the C-terminus of the cerebellin sequence endopeptidase possibly responsible for the cleavage has yet to be identified. The 15 kDa cleavage

product observed in this investigation most likely corresponded to the C-terminal product when Cbln1 is cleaved at the N-terminus of the cerebellin sequence. This cleavage was previously reported to be common and happened spontaneously when recombinant Cbln1 was being prepared for crystallography structural studies [54]. Beyond these observations, the exact steps and enzymes involved in the complete processing of Cbln1 into cerebellin peptides remain largely a mystery.

Cerebellin peptides was previously described to be enriched in the crude synaptosomal fraction of the cerebellum when examined with HPLC [55]. This observation agrees with the result of this investigation, as the 15 kDa processing intermediate was enriched in the crude synaptosomal fraction of the cerebellum and the SCN. Crude synaptosomal enrichments of the 15 kDa cleavage product in both the cerebellum and the SCN suggest that subsequent cleavages of Cbln1 at the C-terminus of the cerebellin sequence to produce cerebellin peptides take place at the synapse. The diminished amounts of Cbln1 in the P2 fractions suggest that Cbln1 levels are low in the synapse relative to cerebellin peptides, perhaps due to rapid secretion or turnover. 15 kDa cleavage product could also be in other membrane-bound vesicles of similar densities to synaptosomes. Electron microscopy study showed that lysosomes are sometimes observed in crude synaptosomal preparations due to their similar densities with synaptosomes [56]. As discussed earlier, lysosomes possibly modulate the level of Cbln1 through degradation/cleavage. This mechanism can simultaneously produce cerebellin peptides, providing a possible control mechanism for the functionally

distinct yet intertwined Cbln1 and cerebellin peptide. The question remains whether Cbln1 is secreted in the SCN and functionally participates in either synapse formation or circadian time keeping.

Data presented in this investigation suggest active processing of Cbln1 into cerebellin peptides in both the AVP and VIP regions of the SCN. Processing of Cbln1 into cerebellin peptides in the SCN happens at either or both the synapse and the lysosomes. Outside of the SCN, Cbln1 is observed in the PVN and the SON and possibly confer functions in the hypothalamic-pituitary-adrenal axis distinct from the circadian modulatory function of cerebellin-short described in the previous chapter.

3.6 FIGURES

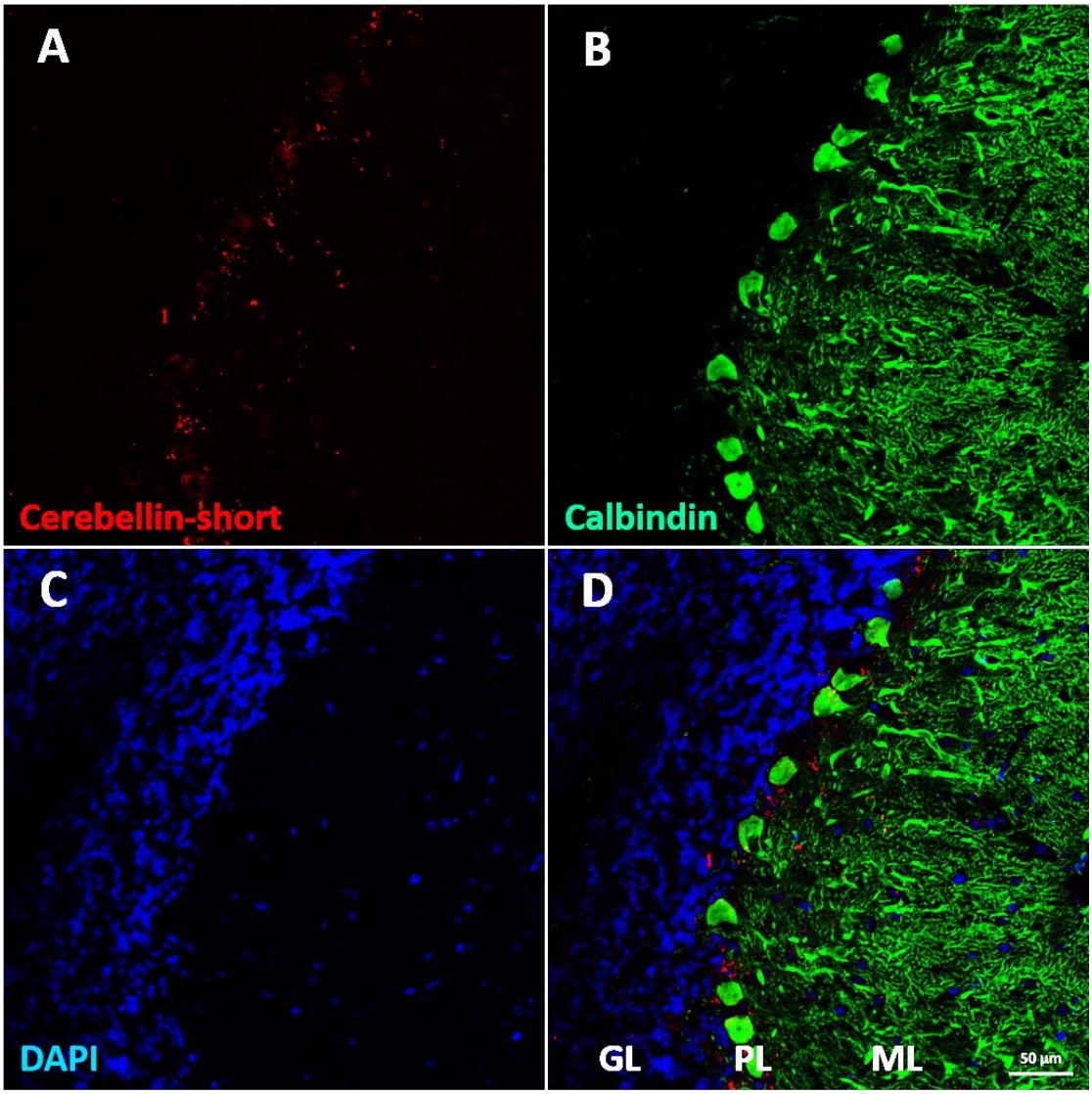

Figure 3.1. Cerebellin-short and Cbln1 IR show different localization in the rat Cerebellum. (A) Confocal images of ZT 8 cerebellum immunostained with anti-cerebellin-short (A) or anti-Cbln1 (E) (red), anti-calbindin D-28K (B and F) (green), and DAPI (C and G) (blue). When merged, anti-cerebellin short IR localized in puncta at the Purkinje cell layer around the cell bodies or Purkinje cells and Bergmann glia (D). Anti-Cbln1 on the other hand were localized along the Purkinje cell dendritic trees (H). 2x2 tile scanned with 40x objective (A-D). Single 40x image (E-H). Scale bar: 50 µm (A-D), 20 µm (E-H). ML: Molecular layer, PL: Purkinje cell layer: GL: Granule cell layer.

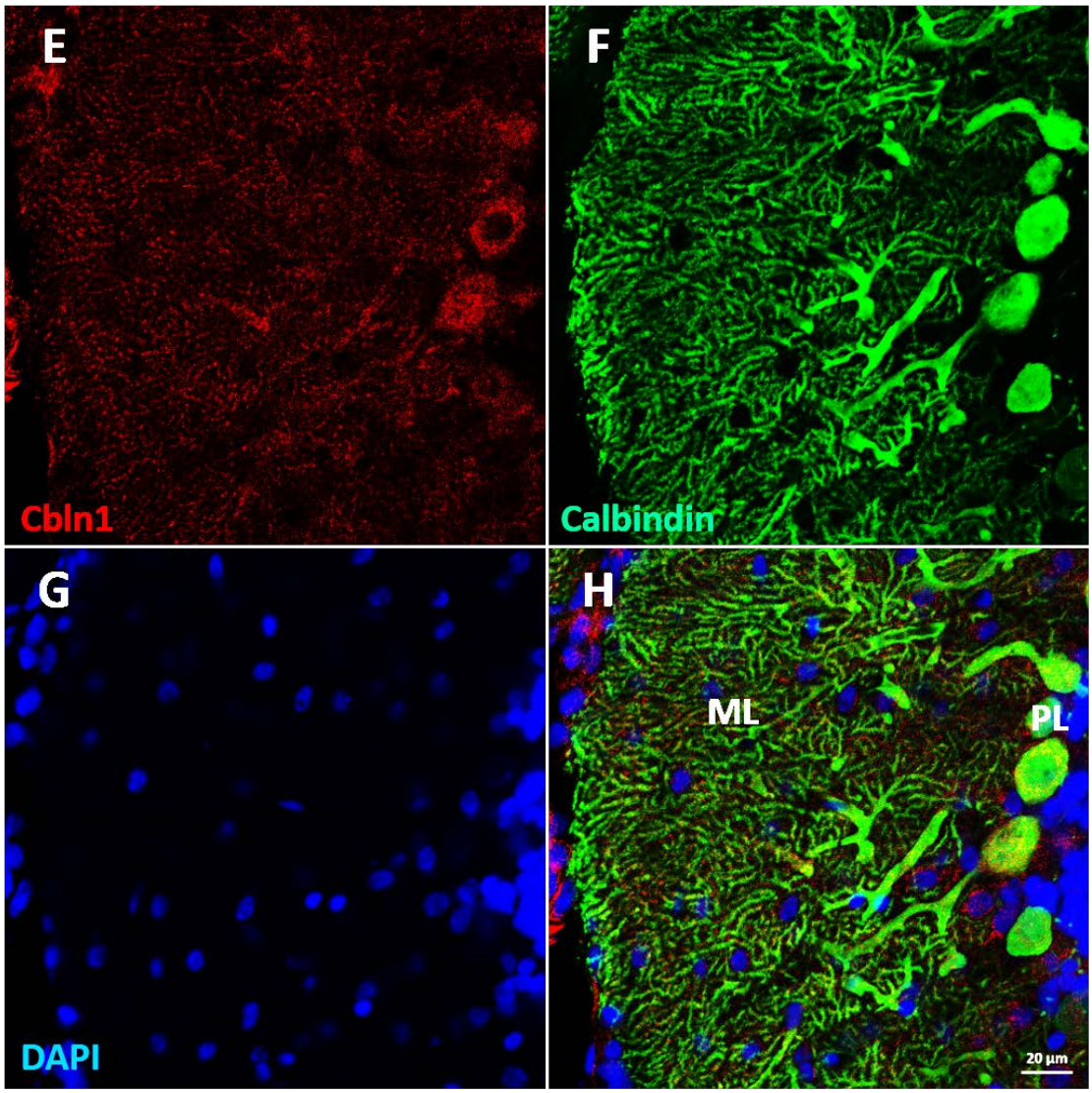

Figure 3.1 (cont.). Cerebellin-short and Cbln1 IR show different localization in the rat Cerebellum.

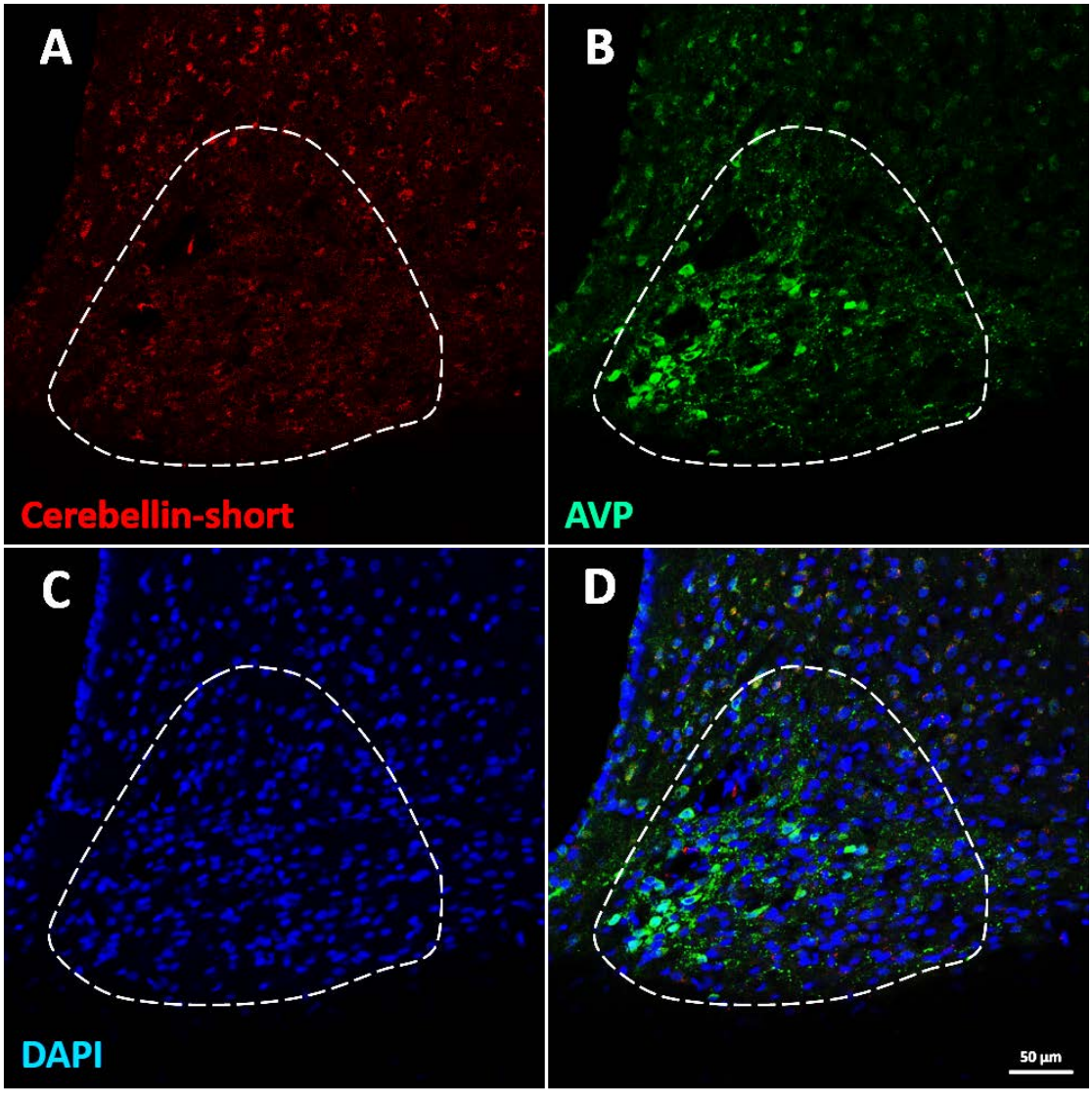

Figure 3.2. Cerebellin-short IR co-localize with both AVP and VIP positive cells in the rat SCN. 2x2 tile scanned 40x confocal images of ZT 8 medial SCN immunostained with anti-cerebellin-short (A and E) (red), anti-AVP (B) or anti-VIP (F) (green), and DAPI (C and G). When merged, anti-cerebellin-short IR showed punctate staining in the cell bodies of both AVP and VIP positive cells (D and H). Scale bar: 50 µm. White dotted lines outline the SCN based on DAPI.

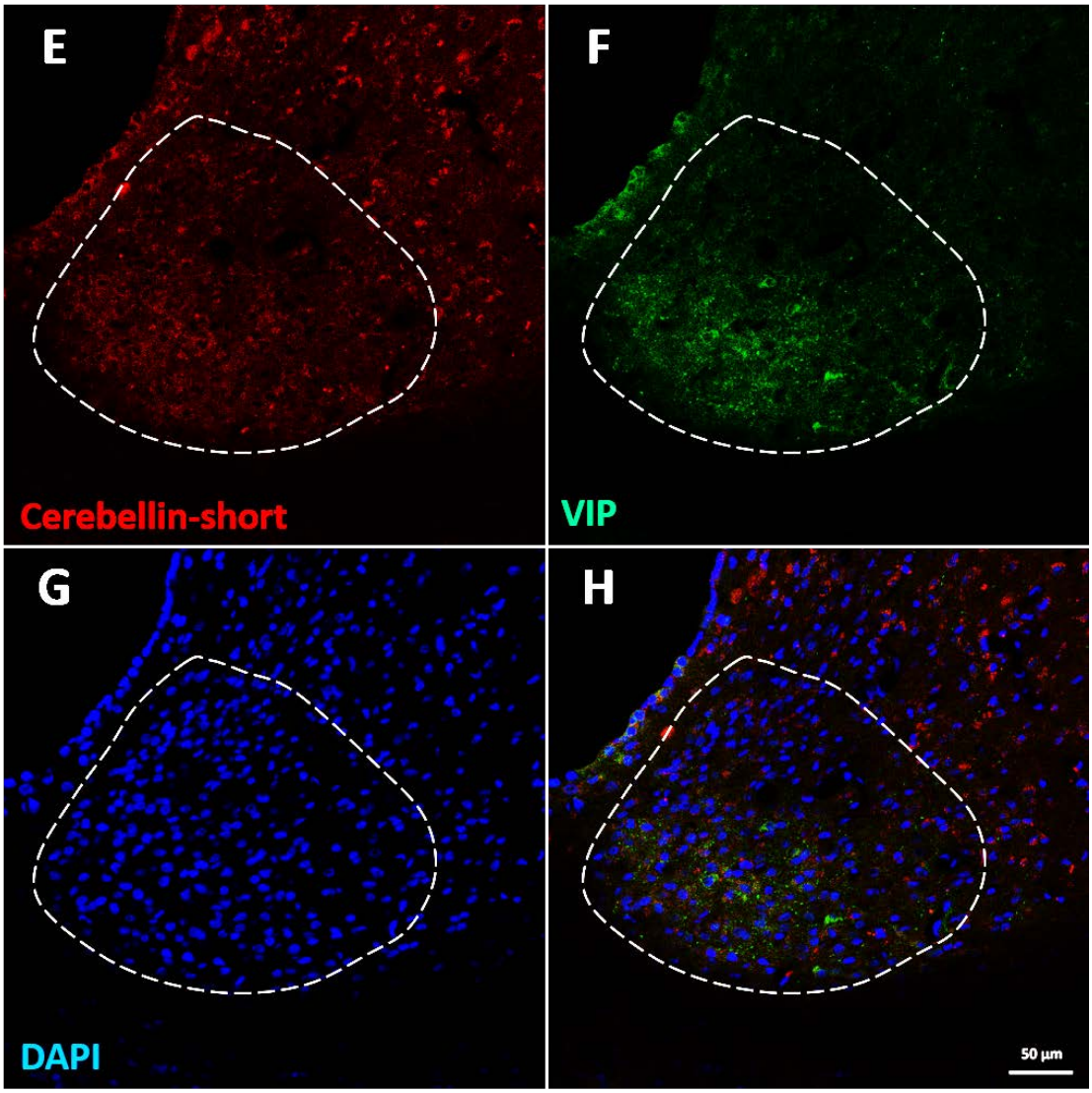

Figure 3.2 (cont.). Cerebellin-short IR co-localize with both AVP and VIP positive cells in the rat SCN.

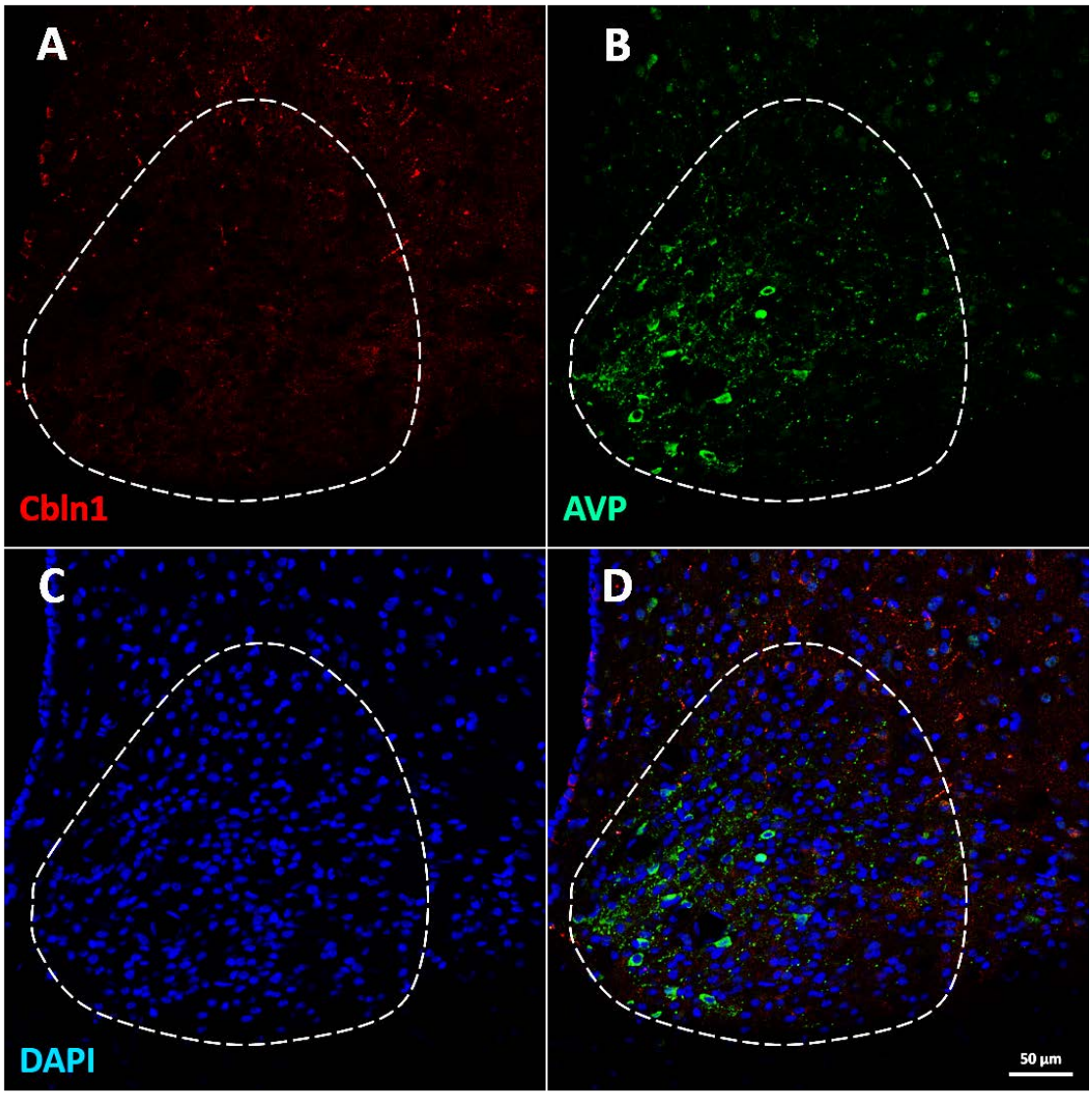

Figure 3.3. Cbln1 IR are fibrous and immediately dorsal to the SCN. 2x2 tile scanned 40x confocal images of ZT 8 medial SCN immunostained with anti-Cbln1 (A) (red), anti-AVP (B) (green), and DAPI (C) (blue). When merged, Cbln1 IR appeared fibrous immediately dorsal to the SCN along the 3rd ventricle. Minimal Cbln1 IR was observed within the SCN (D). White dotted lines outline the SCN based on DAPI. Scale bar: 50 µm.

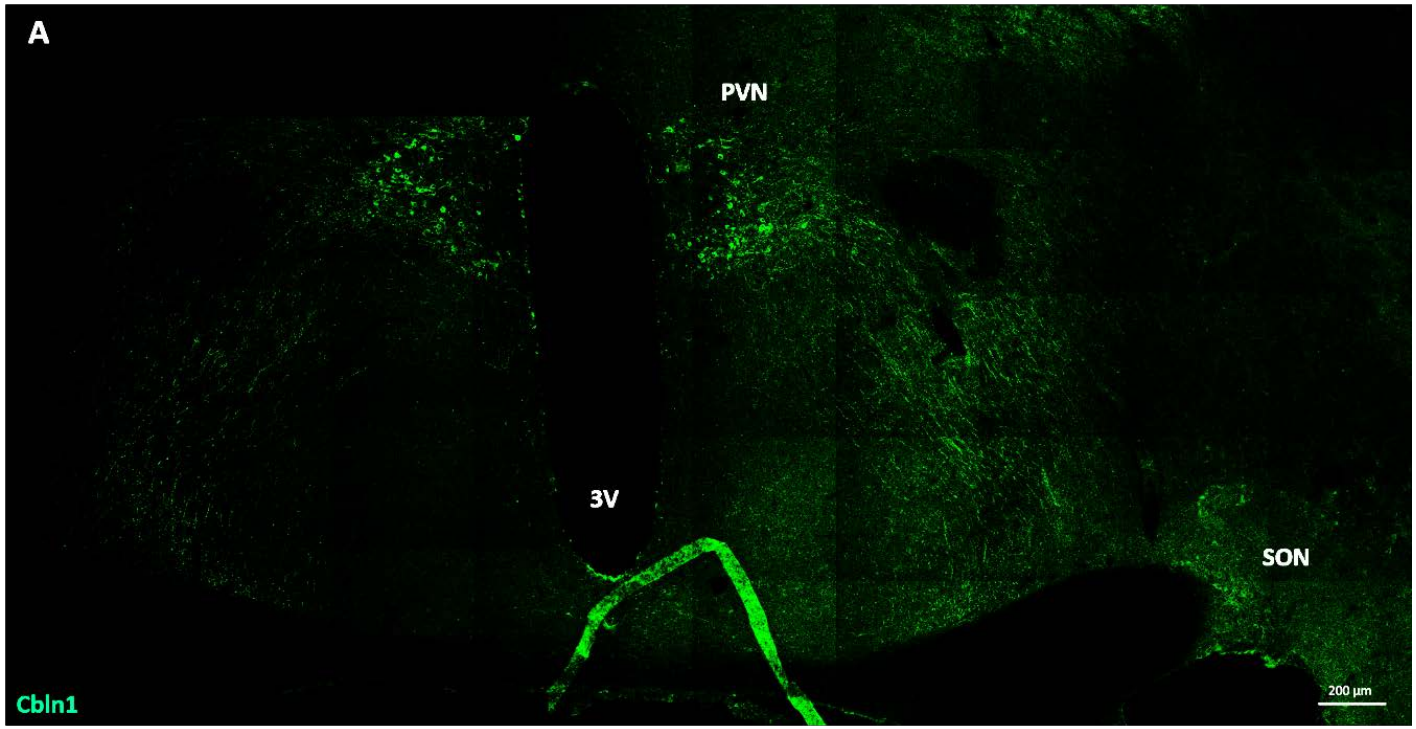

Figure 3.4. Cbln1 IR are present in multiple rat hypothalamic nuclei and neuronal processes. Tile scanned 20x confocal images of ZT 8 hypothalamus immunostained with anti-Cbln1 in green (A and B). Magnocellular neurons in the PVN and their axons projecting through the hypothalamus showed intense Cbln1 IR (A). 3V: 3rd ventricle. Scale bar: 200 µm (A and B).

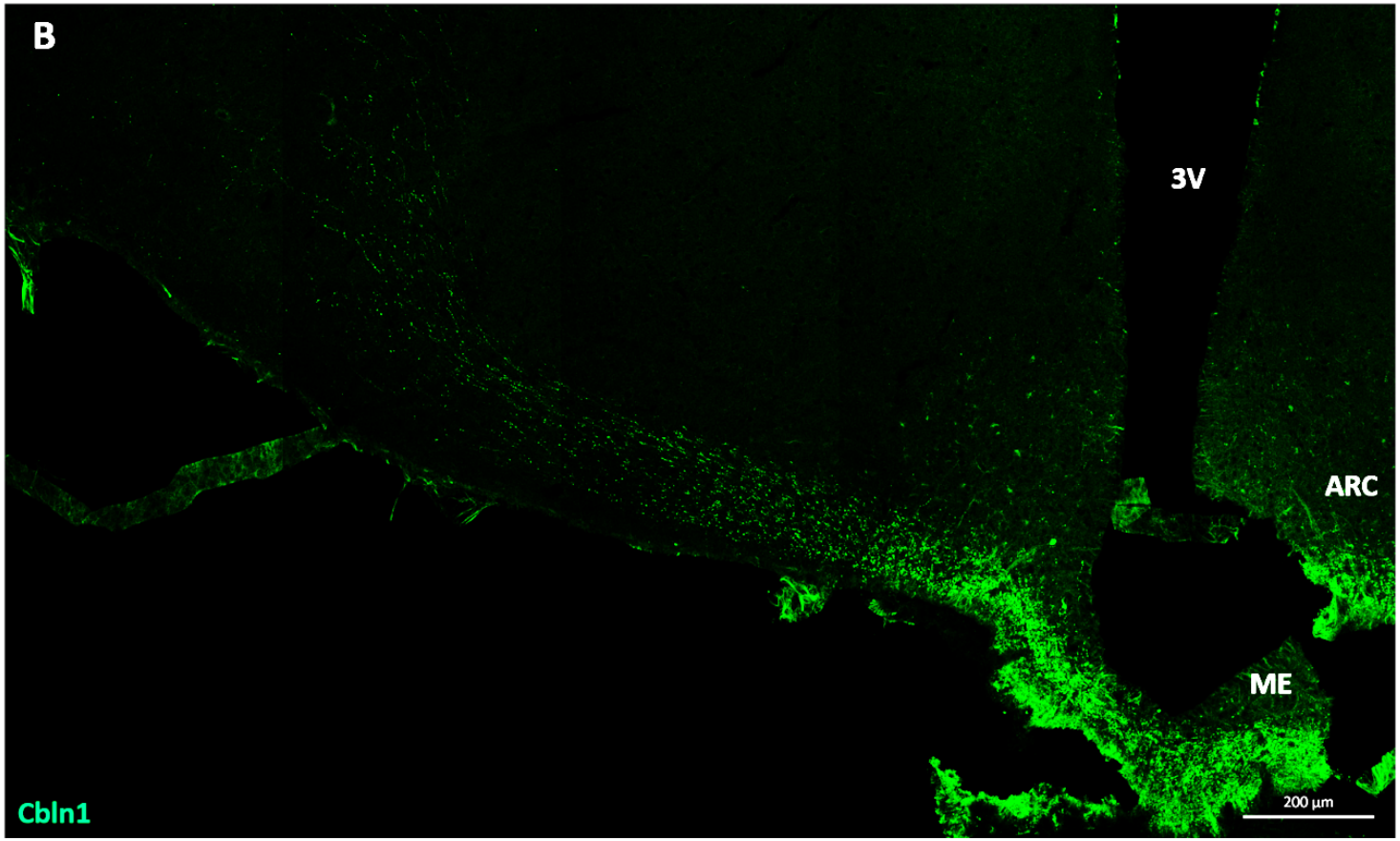

Figure 3.4 (cont.). Cbln1 IR are present in multiple rat hypothalamic nuclei and neuronal processes. Tile scanned 20x confocal images of ZT 8 hypothalamus immunostained with anti-Cbln1 in green (A and B). Strong Cbln1 IR was observed in the median eminence (ME) and the PVN magnocellular axonal projections toward the posterior pituitary, while weaker staining was observed at the arcuate nucleus (ARC) (B). 3V: 3rd ventricle. Scale bar: 200 µm (A and B).

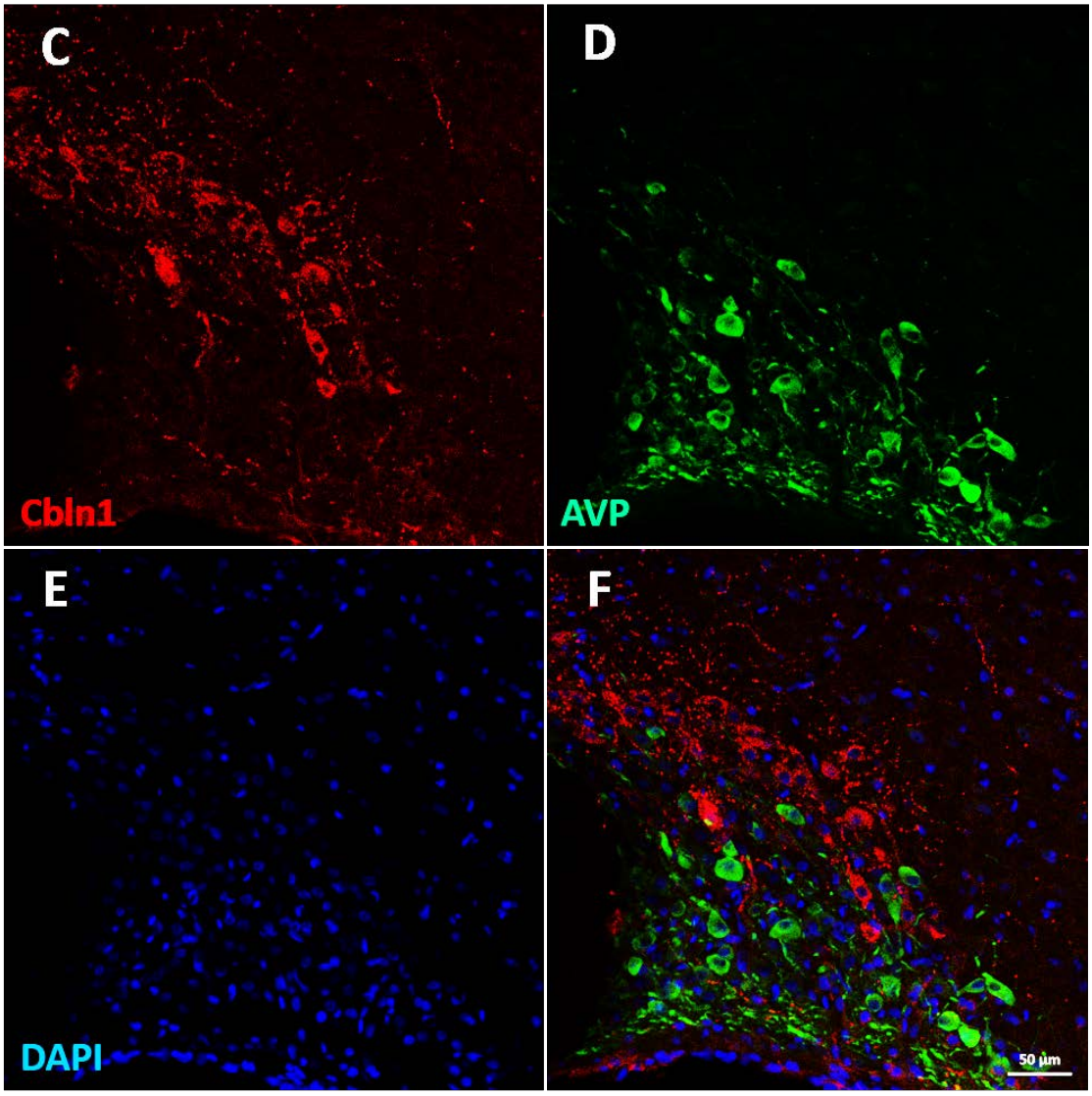

Figure 3.4 (cont.). Cbln1 IR are present in multiple rat hypothalamic nuclei and neuronal processes. The SON was immunostained with anti-Cbln1(C) (red), anti-AVP (D) (green) and DAPI (E) (blue). When combined, Cbln1 IR localized to magnocellular neurons and their processes distinct from those positive for AVP (F). Scale bar: 50 µm (C-F).

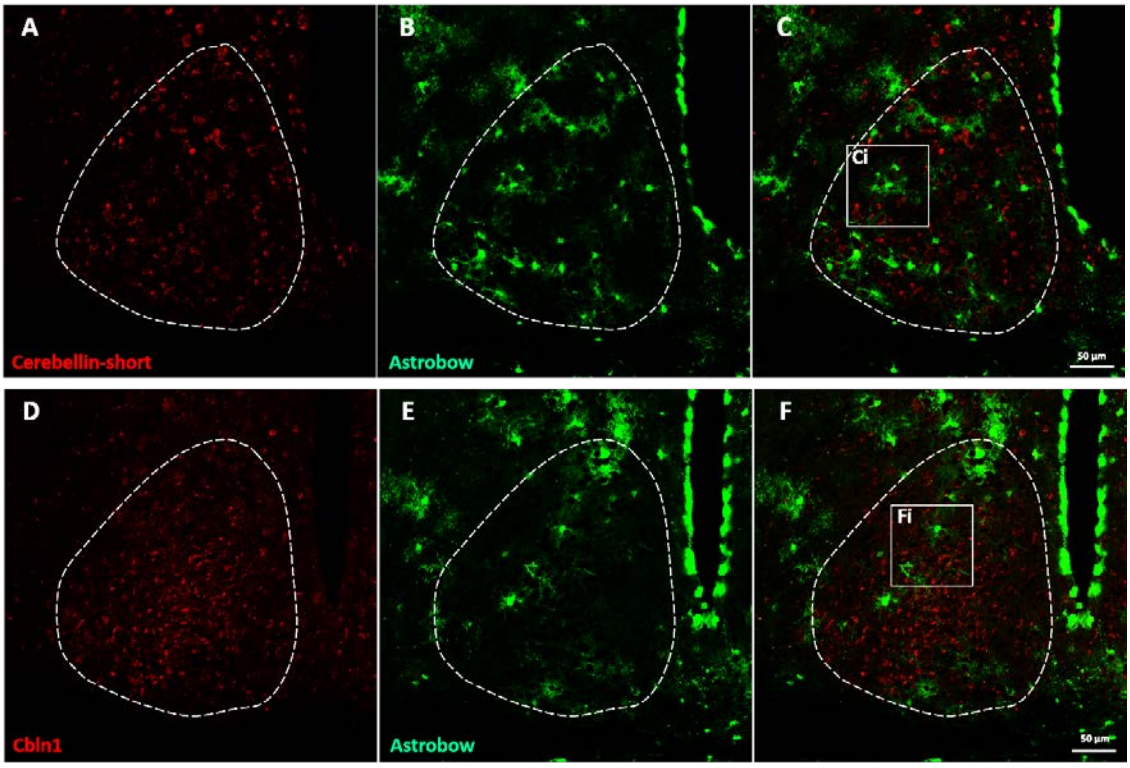

Figure 3.5. Both cerebellin-short and Cbln1 IR do not co-localize with GFAP-expressing astrocytes in the mouse SCN. 2x2 tile scanned 40x confocal images of ZT 8 medial SCN of transgenic GFAP-Cre Brainbow mice immunostained with anti-cerebellin-short (A) or anti-Cbln1 (D) (Alexa 633 pseudo-colored red). Fluorescent signals from YFP and RFP captured through different channels were combined and pseudo-colored green for the ease of viewing (B and E). When combined, both anti-cerebellin-short and Cbln1 IR showed punctate staining in the cell bodies, which did not co-localize with GFAP-expressing astrocytes in the mouse SCN (C and F). Scale bar: 50 µm.

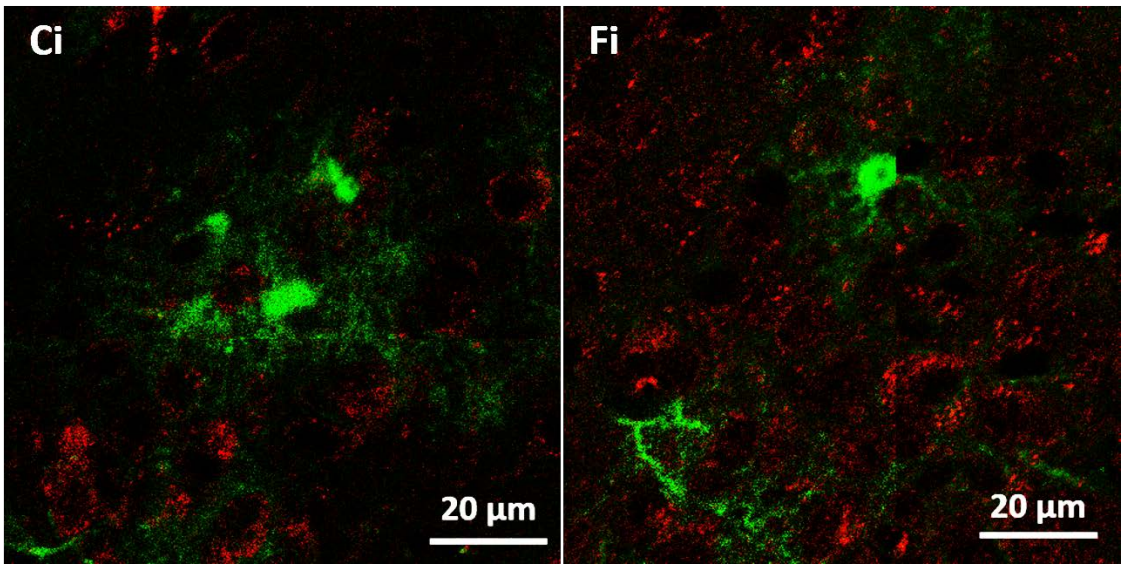

Figure 3.5 (cont.). Both cerebellin-short and Cbln1 IR do not co-localize with GFAP-expressing astrocytes in the mouse SCN. Zoomed in images showing no overlap between either cerebellin-short or Cbln1 IR with astrocyte fluorescence (Ci and Fi) Scale bar: 20 µm.

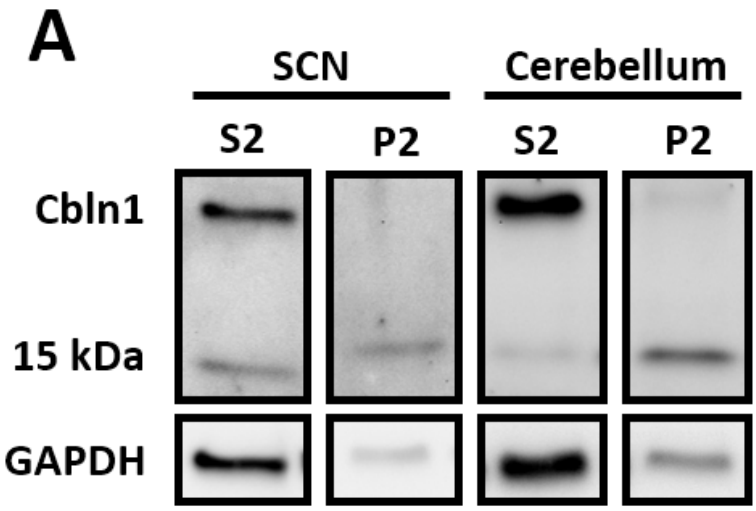

Figure 3.6. The 15 kDa cleavage product of Cbln1 is enriched in the crude synaptosomal fractions of both the SCN and the cerebellum. (A) The cytosol light membrane fractions (S2) and the crude synaptosome fractions (P2) from ZT 8 SCN and cerebellum were immunoblotted with anti-Cbln1 and anti-cerebellin-short. Anti-Cbln1 detected a single band ~25 kDa, corresponding to Cbln1. Anti-cerebellin-short detected a single band ~15 kDa, corresponding to the C-terminal portion of Cbln1 cleaved at the N-terminus of the cerebellin sequence. Cbln1 was high in the S2 fractions of both the SCN and the cerebellum, but the amount diminished in the P2 fractions. 15 kDa cleavage product were low in the S2 fractions in both the SCN and the cerebellum, but enriched in P2 fractions from both regions compared to Cbln1. GAPDH were immunoblotted to standardize intensities between biological replicates.

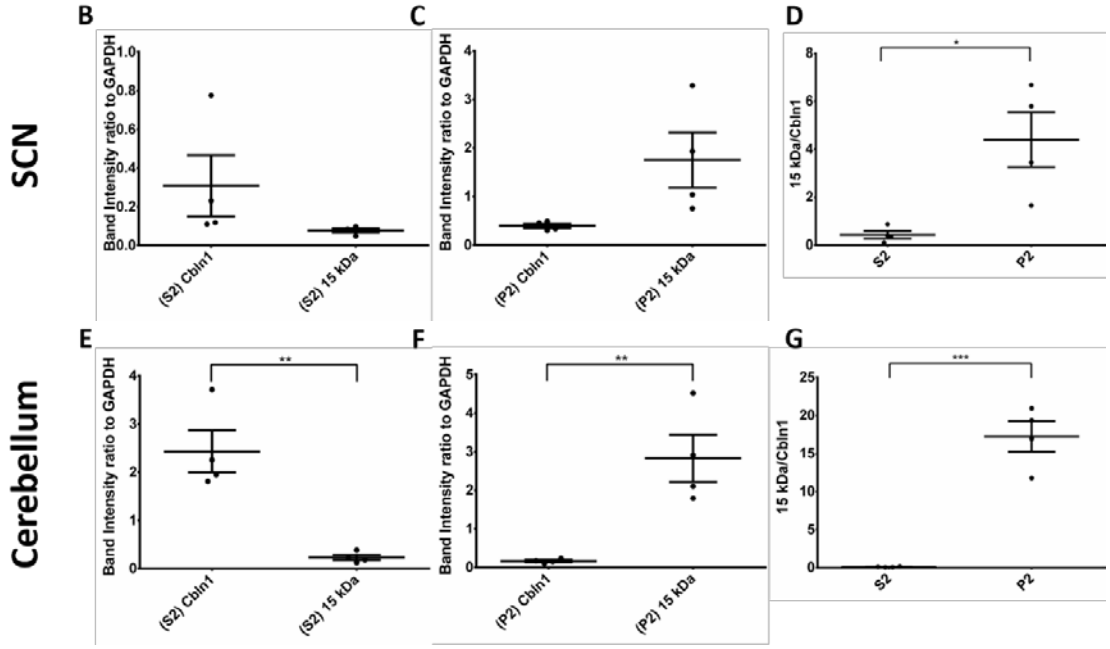

Figure 3.6 (cont.). The 15 kDa cleavage product of Cbln1 is enriched in the crude synaptosomal fractions of both the SCN and the cerebellum. The intensities of Cbln1 and 15 kDa cleavage products in the S2 and the P2 fractions from both brain regions were compared separately after normalizing to GAPDH (B, C, E and F). The ratios of band intensities of 15 kDa cleavage product to Cbln1 were also compared between the S2 and the P2 fractions in both brain regions (D and G). Results showed significant enrichment of the 15 kDa cleavage product in the P2 fractions from both brain regions. Graphs show mean ± SEM, unpaired two-tailed t-test, * $P \leq 0.05$ ** $P \leq 0.01$, $n = 4$.

3.7 REFERENCES

1. Nishino H, Koizumi K, Brooks CMCCM. The role of suprachiasmatic nuclei of the hypothalamus in the production of circadian rhythm. Brain Res. 1976;112: 45–59.

2. Moore RY, Speh JC, Leak RK. Suprachiasmatic nucleus organization. Cell Tissue Res. 2002;309: 89–98.

3. Dibner C, Schibler U, Albrecht U. The mammalian circadian timing system: organization and coordination of central and peripheral clocks. Annu Rev Physiol. 2010/02/13. 2010;72: 517–549.

4. Gillette MU. The suprachiasmatic nuclei: circadian phase-shifts induced at the time of hypothalamic slice preparation are preserved in vitro. Brain Res. 1986;379: 176–181.

5. Francl J, Kaur G, Glass J. Regulation of vasoactive intestinal polypeptide release in the suprachiasmatic nucleus circadian clock. Neuroreport. 2010;21: 1055–1059.

6. Fan J, Zeng H, Olson DP, Huber KM, Gibson JR, Takahashi JS. Vasoactive Intestinal Polypeptide (VIP)-Expressing Neurons in the Suprachiasmatic Nucleus Provide Sparse GABAergic Outputs to Local Neurons with Circadian Regulation Occurring Distal to the Opening of Postsynaptic GABAA Ionotropic Receptors. J Neurosci. 2015;35: 1905–20.

7. Harmar AJ, Marston HM, Shen S, Spratt C, West KM, Sheward WJ, et al. The VPAC2 receptor is essential for circadian function in the mouse suprachiasmatic nuclei. Cell. 2002;109: 497–508.

8. Colwell CS, Michel S, Itri J, Rodriguez W, Tam J, Lelievre V, et al. Disrupted circadian rhythms in VIP- and PHI-deficient mice. Am J Physiol Regul Integr Comp Physiol. 2003;285: R939-49.

9. Moga MM, Moore RY. Organization of neural inputs to the suprachiasmatic nucleus in the rat. J Comp Neurol. 1997;389: 508–34.

10. Yan L, Karatsoreos I, LeSauter J, Welsh DK, Kay S, Foley D, et al. Exploring spatiotemporal organization of SCN circuits. Cold Spring Harb Symp Quant Biol. 2007;72: 527–541.

11. Campos LMG, Cruz-Rizzolo RJ, Watanabe IS, Pinato L, Nogueira MI. Efferent projections of the suprachiasmatic nucleus based on the distribution of vasoactive intestinal peptide (VIP) and arginine vasopressin (AVP) immunoreactive fibers in the hypothalamus of Sapajus apella. J Chem Neuroanat. Elsevier B.V.; 2014;57–58: 42–53.

12. Li J Da, Hu WP, Zhou QY. The circadian output signals from the suprachiasmatic nuclei. 1st ed. Progress in Brain Research. Elsevier B.V.; 2012.

13. Mieda M, Ono D, Hasegawa E, Okamoto H, Honma K ichi, Honma S, et al. Cellular clocks in AVP neurons of the scn are critical for interneuronal coupling regulating circadian behavior rhythm. Neuron. Elsevier Inc.; 2015;85: 1103–1116.

14. Mieda M, Okamoto H, Sakurai T. Manipulating the Cellular Circadian Period of Arginine Vasopressin Neurons Alters the Behavioral Circadian Period. Curr Biol. Elsevier Ltd; 2016;26: 2535–2542.

15. Gillette MU, Reppert SM. The hypothalamic suprachiasmatic nuclei: circadian patterns of vasopressin secretion and neuronal activity in vitro. Brain Res Bull. Elsevier; 1987;19: 135–139.

16. Gamble KL, Allen GC, Zhou T, McMahon DG. Gastrin-Releasing Peptide Mediates Light-Like Resetting of the Suprachiasmatic Nucleus Circadian Pacemaker through cAMP Response Element-Binding Protein and Per1 Activation. J Neurosci. 2007;27: 12078–12087.

17. Piggins HD, Antle MC, Rusak B. Neuropeptides Phase Shift the Mammalian Circadian Pacemaker. J Neurosci. 1995;15: 5612–5622.

18. Atkins Jr. N, Mitchell JW, Romanova E V, Morgan DJ, Cominski TP, Ecker JL, et al. Circadian integration of glutamatergic signals by little SAAS in novel suprachiasmatic circuits. PLoS One. United States; 2010;5: e12612.

19. Hatcher NG, Atkins Jr. N, Annangudi SP, Forbes AJ, Kelleher NL, Gillette MU, et al. Mass spectrometry-based discovery of circadian peptides. Proc Natl Acad Sci U S A. United States; 2008;105: 12527–12532.

20. Kalsbeek a, Palm IF, La Fleur SE, Scheer F a JL, Perreau-Lenz S, Ruiter M, et al. SCN outputs and the hypothalamic balance of life. J Biol Rhythms. 2006;21: 458–69.

21. Leak R. Topographic organization of suprachiasmatic nucleus projection neurons. J Comp Neurol. 2001;334: 312–334.

22. Pickard GE, Rea M a. Serotonergic innervation of the hypothalamic suprachiasmatic nucleus and photic regulation of circadian rhythms. Biol Cell. 1997;89: 513–23.

23. Prosser R a. Melatonin inhibits in vitro serotonergic phase shifts of the suprachiasmatic circadian clock. Brain Res. 1999;818: 408–13.

24. Medanic M, Gillette MU. Serotonin regulates the phase of the rat suprachiasmatic circadian pacemaker in vitro only during the subjective day. J Physiol. 1992;450: 629–42.

25. Gillette MU, Mitchell JW. Signaling in the suprachiasmatic nucleus: Selectively responsive and integrative. Cell Tissue Res. 2002;309: 99–107.

26. Besing RC, Hablitz LM, Paul JR, Johnson RL, Rebecca A, Gamble KL, et al. NPY-Induced Phase Shifts of PER2::LUC Rhythms are Mediated by Long-Term Suppression of Neuronal Excitability in a Phase-Specific Manner. Chronobiol Int. 2013;29: 91–102.

27. Dubocovich ML. Melatonin receptors: role on sleep and circadian rhythm regulation. Sleep Med. 2007;8 Suppl 3: 34–42.

28. Albers HE, Walton JC, Gamble KL, McNeill JK, Hummer DL. The dynamics of GABA signaling: Revelations from the circadian pacemaker in the suprachiasmatic nucleus. Frontiers in Neuroendocrinology. 2017.

29. Lee JE, Atkins Jr. N, Hatcher NG, Zamdborg L, Gillette MU, Sweedler J V, et al. Endogenous peptide discovery of the rat circadian clock: a focused study of the suprachiasmatic nucleus by ultrahigh performance tandem mass spectrometry. Mol Cell Proteomics. United States; 2010;9: 285–297.

30. Hirai H, Pang Z, Bao D, Miyazaki T, Li L, Miura E, et al. Cbln1 is essential for synaptic integrity and plasticity in the cerebellum. Nat Neurosci. United States; 2005;8: 1534–1541.

31. Matsuda K, Miura E, Miyazaki T, Kakegawa W, Emi K, Narumi S, et al. Cbln1 is a ligand for an orphan glutamate receptor delta2, a bidirectional synapse organizer. Science. United States; 2010;328: 363–368.

32. Uemura T, Lee SJ, Yasumura M, Takeuchi T, Yoshida T, Ra M, et al. Trans-synaptic interaction of GluRdelta2 and Neurexin through Cbln1 mediates synapse formation in the cerebellum. Cell. United States: Elsevier Inc; 2010;141: 1068–1079.

33. Ito-Ishida A, Miura E, Emi K, Matsuda K, Iijima T, Kondo T, et al. Cbln1 regulates rapid formation and maintenance of excitatory synapses in mature cerebellar Purkinje cells in vitro and in vivo. J Neurosci. United States; 2008;28: 5920–5930.

34. Ryu K, Yokoyama M, Yamashita M, Hirano T. Induction of excitatory and inhibitory presynaptic differentiation by GluD1. Biochem Biophys Res Commun. Elsevier Inc.; 2012;417: 157–161.

35. Wei P, Smeyne RJ, Bao D, Parris J, Morgan JI. Mapping of Cbln1-like immunoreactivity in adult and developing mouse brain and its localization to the endolysosomal compartment of neurons. Eur J Neurosci. France; 2007;26: 2962–2978.

36. Miura E, Iijima T, Yuzaki M, Watanabe M. Distinct expression of Cbln family mRNAs in developing and adult mouse brains. Eur J Neurosci. France; 2006;24: 750–760.

37. Wei P, Rong Y, Li L, Bao D, Morgan JI. Characterization of trans-neuronal trafficking of Cbln1. Mol Cell Neurosci. Elsevier Inc.; 2009;41: 258–73.

38. Bao D, Pang Z, Morgan JI. The structure and proteolytic processing of Cbln1 complexes. J Neurochem. England; 2005;95: 618–629.

39. Jiao Y, Sun Z, Lee T, Fusco FR, Kimble TD, Meade C a., et al. A simple and sensitive antigen retrieval method for free-floating and slide-mounted tissue sections. J Neurosci Methods. 1999;93: 149–162.

40. Miura E, Matsuda K, Morgan JI, Yuzaki M, Watanabe M. Cbln1 accumulates and colocalizes with Cbln3 and GluRdelta2 at parallel fiber-Purkinje cell synapses in the mouse cerebellum. Eur J Neurosci. 2009/03/03. 2009;29: 693–706.

41. Nickel W, Rabouille C. Mechanisms of regulated unconventional protein secretion. Nat Rev Mol Cell Biol. 2009;10: 148–55.

42. Raposo G, Stoorvogel W. Extracellular vesicles: Exosomes, microvesicles, and friends. J Cell Biol. 2013;200: 373–383.

43. Vrang N, Larsen PJ, Moller M, Mikkelsen JD. Topographical organization of the rat suprachiasmatic-paraventriocular projection. J Comp Neurol. 1995;353: 585–603.

44. Saeb-Parsy K, Lombardelli S. Neural connections of hypothalamic neuroendocrine nuclei in the rat. J. 2000;12: 635–48.

45. Ludwig M, Stern J. Multiple signalling modalities mediated by dendritic exocytosis of oxytocin and vasopressin: Figure 1. Philos Trans R Soc B Biol Sci. 2015;370: 20140182.

46. Rucinski M, Malendowicz LK. Precerebellin-related genes and precerebellin 1 peptide in endocrine glands of the rat - pattern of their expression. Int J Mol Med. Greece; 2009;23: 113–119.

47. Gardiner J V, Beale KE, Roy D, Boughton CK, Bataveljic A, Campbell DC, et al. Cerebellin1 is a novel orexigenic peptide. Diabetes Obes Metab. England: Blackwell Publishing Ltd; 2010;12: 883–890.

48. Albertin G, Malendowicz LK, Macchi C, Markowska A, Nussdorfer GG. Cerebellin stimulates the secretory activity of the rat adrenal gland: in vitro and in vivo studies. Neuropeptides. 2000;34: 7–11.

49. Mazzocchi G, Andreis PG, De Caro R, Aragona F, Gottardo L, Nussdorfer GG. Cerebellin enhances in vitro secretory activity of human adrenal gland. J Clin Endocrinol Metab. 1999;84: 632–5.

50. Brancaccio M, Patton AP, Chesham JE, Maywood ES, Hastings MH. Astrocytes Control Circadian Timekeeping in the Suprachiasmatic Nucleus via Glutamatergic Signaling. Neuron. 2017; 1–16.

51. Barca-Mayo O, Pons-Espinal M, Follert P, Armirotti A, Berdondini L, De Pietri Tonelli D. Astrocyte deletion of Bmal1 alters daily locomotor activity and cognitive functions via GABA signalling. Nat Commun. Nature Publishing Group; 2017;8: 14336.

52. Burkeen JF, Womac AD, Earnest DJ, Zoran MJ. Mitochondrial calcium signaling mediates rhythmic extracellular ATP accumulation in suprachiasmatic nucleus astrocytes. J Neurosci. 2011;31: 8432–40.

53. Fricker LD. Analysis of mouse brain peptides using mass spectrometry-based peptidomics: implications for novel functions ranging from non-classical neuropeptides to microproteins. Mol Biosyst. 2010;6: 1355.

54. Cheng S, Seven AB, Wang J, Skiniotis G, Özkan E. Conformational Plasticity in the Transsynaptic Neurexin-Cerebellin-Glutamate Receptor Adhesion Complex. Structure. 2016;24: 2163–2173.

55. Slemmon JR, Blacher R, Danho W, Hempstead JL, Morgan JI. Isolation and sequencing of two cerebellum-specific peptides. Proc Natl Acad Sci U S A. 1984;81: 6866–70.

56. Cotman C, Brown DH, Anderson NG. Analytical Sedimentation and Differential Properties Lysosomes Centrifugation : from Rat Brain An Analysis Homogenates of the of Synaptosomes , Mitochondria. Arch Biochem. 1970;136: 436–447.

CHAPTER FOUR: METABOLOMIC AND LIPIDOMIC CHANGES DURING LONG TERM POTENTIATION REVEALED BY MASS SPECTROMETRY IMAGING IN THE MOUSE HIPPOCAMPUS[1]

4.1 ABSTRACT

Brain plasticity is well known as the underlying mechanism for memory encoding in the brain. Long term potentiation (LTP) is the best-studied tissue model for learning and memory, and tracking the chemical changes during LTP is critical for unveiling the mechanism of the process. However, due to the technical limitation, majority of the molecular studies of LTP focused on primary messengers and large proteins. On the other hand, signaling lipids and small signaling metabolites are less studied. In this work, we used dopamine (DA)-modified TiO_2-assisted laser desorption/ionization (LDI)-mass spectrometry imaging (MSI) to spatially track the metabolomic and the lipidomic changes in the hippocampus after LTP induction in the Schaffer collateral-CA1 pathway. In the CA1 region we observed the increase of creatine, spermine, and

[1] This work was done in collaboration with Qian Wu Ph.D. from the lab of Prof. Jonathan Sweedler of analytical chemistry at the University of Illinois at Urbana-Champaign. This work was supported by the Center for Nutrition, Learning and Memory (CNLM) with funding from Abbott's Nutrition Business. Qian Wu assembled the initial manuscript, and James Chu edited the manuscript extensively in preparation for submission for publication. James Chu performed the LTP recordings and analyzed the electrophysiological data. Qian Wu performed the MSI experiments and analyzed analytical chemistry data. Ann Benefiel and Mia Yu Ph.D. provided animal care. Jennifer Mitchell Ph.D., Stas Rubakhin Ph.D., Prof. Martha Gillette and Prof. Jonathan Sweedler provided guidance for experiments and manuscript assembly.

two amino acids. In the CA2/3 region we observed the increase of ceramide, four fatty acids, three phosphatidylethanolamine (PE) and the decrease of creatinine and one phosphatidylcholine (PC). These changes dominated the differences between LTP versus control hippocampal slices from mice 8 month in age. The magnitude of chemical changes is correlated to the magnitude of LTP-induction. Majority of the observed chemical changes agree with previously reported LTP signaling pathways or the related pathways downstream of Ca^{2+} flux. Creatinine/creatine changes can be attributed to energy shuttling, fatty acids/PC/PE changes fall under polyunsaturated fatty acids (PUFA) signaling, ceramides and cholesterol are related to lipid rafts, GABA change is related to neurotransmission, and spermine change is related to NMDA receptor activation. We demonstrate the first use of MSI to simultaneously visualize multiple previous reported LTP chemical changes. In addition, we observed cholesterol changes that cannot be explained by known pathways and pyroglutamate changes not previously reported. These results provided important new information for the molecular substrates of brain plasticity.

4.2 INTRODUCTION

The brain can adapt to the environment by forming new connections or changing the strength of existing connections between neurons. This process is known as brain plasticity [1]. Brain plasticity is widely assumed to be the mechanism by which memory is encoded and stored in the central nervous system. Long term potentiation (LTP) is the best studied brain plasticity mechanism [2], in which synaptic potentials,

evoked by low-frequency stimulation, are observed to increase in amplitude as a consequence of a brief pulse of high-frequency stimulation or the pairing of presynaptic activity with postsynaptic depolarization. To this day, LTP remains the most widely used model for the study of learning and memory in vertebrates [3].

The molecular mechanism of LTP is well dissected in the past decades, with efforts largely focused on small primary messengers such as neurotransmitters and large proteins such as enzymes and receptors [4]. However, lipids which makes up more than half of the human brain in dry weight received much less attention. Recent advances in cell biology, synaptic physiology and receptor pharmacology lead to the discoveries that lipids have broad information carrying roles in the CNS, including altering the geometric properties and supramolecular organization of neuronal/glial membranes and taking role as ligands for proteins, secondary messenger or precursor of other signaling molecules [5,6]. For example, the dissociations of phospholipids into cone-shaped fatty acids and lysophospholipids at cell membrane have important roles in synaptic vesicle exocytosis [7]. The dissociation of PC can generate platelet-activating factor which is a retrograde messenger that activates the presynaptic mechanisms facilitating synaptic plasticity during LTP [8]. PUFA such as DHA and AA are implicated in neurodegeneration and are precursor of several messenger molecules [6].

To understand the chemical mechanism of lipids and lipid derivatives during memory and learning, imaging techniques that track lipidomic changes during plasticity are critical. However, imaging of lipidomic changes during brain plasticity are scarce; most imaging techniques used to study LTP are specific for small metabolites or larger proteins. Optical imaging with voltage-sensitive dyes are used to visualize neurons [9] and Ca^{2+} sensitive dyes are used to capture Ca^{2+} fluxes [10]. Fluorescent molecules are used to track small signaling molecule such as NO [11], glutamate [12] and even cholesterol [13], while magnetic resonance spectroscopy (MRS) is used for imaging small metabolites [14]. These methods have been widely employed to track specific signaling molecules for brain or neuronal plasticity. Optical imaging methods have high spatial resolution that allow tracking of target molecules at the synaptic scale, but the number of different molecules that can be simultaneously monitored is limited. MRS imaging is capable of *in vivo* measurements, but suffers from low sensitivity and limited resolution.

Mass spectrometry imaging (MSI) is a sensitive and multiplexed approach for the characterization and localization of a wide range of analytes including small metabolites [15,16], lipids [17], peptides and proteins [18]. The wide analyte spectrum makes MSI an attractive method to simultaneously visualize all the important compounds and identify key signaling substrates. Time-of-flight secondary-ion mass spectrometry has previously been used to produce high-resolution images of the microscopic changes in lipid composition that occur at the fusion sites between two

mating cells of the protozoon Tetrahymena thermophile [7]. Indeed, the goal of profiling large-scale changes in lipid composition or determining the topographical distribution of individual lipid species is no longer beyond reach after the advancement of the MSI technology.

Recently, we developed a new surface-assisted laser desorption/ionization (MALDI)-MSI method with dopamine (DA)-modified TiO_2 monolith. With this improved method, small amino acids, alkaloids, fatty acids together with larger lipids including diglycerides, ceramides, PE and PC can be localized simultaneously in brain tissues in high spatial resolution up to 20 μm [19]. In this work, this unique MSI method was used to track the lipidomics and metabolomics changes associated with the LTP formation, and to identify the most important signaling molecules dominating the changes among the compounds we can detected with this method. Most of the observed changes in chemical compounds agree with reported LTP signaling pathways. In addition, we observed changes in several compounds that were not previously reported. Thus, our results provide a basic chemical information list for further investigation of the molecular mechanism of for LTP and brain plasticity.

4.3 MATERIALS AND METHODS

Chemicals and materials

The following chemicals were purchased from Sigma-Aldrich (St. Louis, MO): n-methyl-D-glucamine, potassium chloride, sodium phosphate monobasic, (+)-sodium L-ascorbate, thiourea, sodium pyruvate, magnesium sulfate anhydrous, picrotoxin, titanium (IV) n-butoxide, dopamine hydrochloride (>98%). Concentrated phosphoric acid (analytical grade), sodium bicarbonate, HEPES, calcium chloride, D-glucose, sodium chloride, acetonitrile, ethanol, and water (liquid chromatography (LC)/MS grade) were purchased from Fisher Scientific (Pittsburgh, PA).

Animal experiments

Inbred C57BL/6 mice of both genders around the age of 8 months were used. Animals were housed under 12h:12h light-dark cycle at 18–26 °C, 30–70% humidity. Food and water were accessible ab libitum. All animal-related procedures, including euthanasia by cervical dislocation, were performed in compliance with local and federal regulations and according to animal use protocols approved by the University of Illinois Institutional Animal Care and Use Committee.

LTP induction

Mouse was cervically dislocated, decapitated and the brain quickly extracted. The brain was chilled in NMDG-artificial cerebral spinal fluid (ACSF) slicing solution at 4 ℃ containing (in mM) NMDG 93, KCl 2.5, NAH_2PO_4, 1.2, $NaHCO_3$ 30, HEPES 20, glucose 25, sodium ascorbate 5, thiourea 2, sodium pyruvate 3, $MgSO_4$ 10 and $CaCl_2$ 0.5, bubbled continuously with 95% O2/ 5% CO_2 [20]. Coronal hippocampal slices, 400 μm thick, were obtained with a Leica vibratome.

After slicing, slices were allowed to recover for 10 min in NMDG-ACSF at 30 °C, then transferred to a submerged recording chamber perfused with ACSF solution (2 ml/min) containing (in mM) NaCl 124, KCl 2.5, NaH_2PO_4 1.2, $NaHCO_3$ 24, HEPES 5, glucose 12.5, $MgSO_4$ 2, $CaCl_2$ 2 and Picrotoxin 50, bubbled continuously with 95% O_2/ 5% CO_2 at 30 °C. Slices were equilibrated in the recording chamber for 1 h before LTP recording.

Stimulations were performed with a concentric bipolar electrode (FHC) placed at the Schaffer collateral between CA3 and CA1, recordings were performed with a tungsten electrode (FHC) placed at the striatum radiatum of CA1. Field excitatory postsynaptic potential (fEPSP) was monitored until stable and input-output curves were obtained. Slices were given test-pulses (0.033 Hz) at ~ 40% maximum fEPSP throughout the recording. After a minimum of 20 min stable baseline recording, LTP was induced by

3 trains of 100 Hz, 1000 ms duration, 15 s interval high frequency stimulations (HFS) at test-pulse strength. For signal acquisition, amplifier gain was set to 1000 and filtered between 1 Hz to 3 kHz. Signals were recorded and processed with pClamp 10 software. To control for the effect of electrode insertions and electrical stimulations on MSI, control slices were generated from the same brains and only subjected to test-pulses without LTP induction. After recording, brain slices were transferred to glass slides covered with Parafilm and flash frozen over dry ice for further cryo-sectioning and MSI.

Synthesis of TiO2 monolith

TiO_2 nanoparticles were prepared using a previously described sol-gel method to hydrolyze titanium(IV) n-butoxide in an ethanol-water solution under acidic condition [21]. Briefly, 3.4 mL of titanium (IV) n-butoxide and 1.6 mL of ethanol were mixed by vortex for 1 min, forming a precursor solution. Then, a solution containing 5 mL of ethanol with 0.1 M nitric acid and 1% HPLC grade water was added dropwise to the vigorously stirred precursor solution, which was cooled in an ice/water bath. TiO_2 structures were formed in this solution (Solution I) during stirring in an ice/water bath for 3 h. To prepare DA-modified TiO_2 monolith deposition mixture, 250 µL of solution I was diluted in 5 mL of reaction solution (solution II) for further hydrolysis/condensation. Solution II consists of 5% water-ethanol solution with 0.005 M DA. The mixture of solution I and solution II was incubated for 1 h.

Sample preparation for MSI

The 400 µm thick frozen coronal brain slices were further cryo-sectioned into sets of 10-µm thick sections using a cryostat (Leica CM3050 S, Leica Biosystems Inc.). Slices with LTP-induction (or pulse test) and the corresponding control slices were paired tightly, thaw-mounted on indium-tin-oxide coated glass slides (Delta Technology Ltd., Loveland, CO) and dried in an N_2-filled desiccator for 20 min.

For TiO_2-assisted LDI, DA-modified TiO_2 monolith deposition mixture were applied to tissue sections by airbrush-assisted deposition. Briefly, 5 mL of the above described, appropriately diluted TiO_2-containing solution were sprayed with a 0.2 mm nozzle airbrush (Paasche Airbrush Company, Chicago, IL), with a nozzle-to-target distance of ~50 cm and nozzle nitrogen gas pressure at 35 psi. The final TiO_2 material layer was ~400 µg/cm^2, determined by comparing sample weight before and after sublimation.

Sample preparation for LC-MS/MS

10-µm thick sections on glass slide are scratched out with needle under microscope according to anatomical morphology. CA1 and CA3 regions of each animal were collected and extracted with 400 µL methanol-chloroform (2:3) solution under sonication on ice in a bath sonicator (8891 Ultrasonic Cleaner, Cole-Parmer, Vernon Hills, IL) for 10 min. The extracts were centrifuged at 6,600 ×g at 4 ºC for 5 min and the supernatants collected (extraction solution I). After centrifugation, the pallets were

extracted with 50 µL methanol-water again under sonication, and the extracts were centrifuged at 6,600 ×g at 4 ºC for 5 min. The supernatant (extraction solution II) was collected for direct injection into LC-MS/MS to detect creatinine. Extraction solution I was divided into two parts. The first part was dried with a gentle N_2 stream at ambient conditions, re-dissolved into 50 µL methanol, and directly injected into LC-MS/MS for to detect cholesterol. The other part was dried with a gentle N_2 stream at ambient conditions, derivatized, and injected into the LC system to validate the MALDI results.

MS analyses

MALDI time-of-flight (TOF)/TOF MSI was performed using an ultrafleXtreme II mass spectrometer (Bruker Daltonics, Billerica, MA) equipped with a solid-state UV Smartbeam II laser. Tandem MS (MS/MS) analysis was used to elucidate the structural properties of the detected compounds. MS/MS was carried out in the LIFT mode utilizing argon as a collision gas at a 2 Da precursor isolation window.

Equipped with a MALDI ion source, a solariX™ XR Fourier transform ion cyclotron resonance (FTICR) mass spectrometer (Bruker Daltonics) was used for high mass resolution and accuracy measurements of the samples previously analyzed via MSI.

Data processing and statistical analysis

The molecular ion distribution images of tissue sections were visualized using flexImaging. Different cell layers in different regions were manually defined according to anatomical morphologies in optical images and ion images, and the spectra in regions of interest (ROI) were exported, imported into ClinProTools (Bruker) with automatic baseline subtraction and total ion count normalization. Peaks were picked with a signal/noise threshold greater than 3 on average spectra and matrix-related peaks were removed. Picked peaks were exported as m/z value-peak intensity tables. For five repeated, combat method [22] was used for normalization to remove batch effect of different slides using online tool (metaboanalysis 3.0, http://www.metaboanalyst.ca/faces/Secure/utils/BatchUpload.xhtml).

After normalization, data from five replicates were combined for multivariate analysis. Principal component analysis (PCA)) was done by OriginPro 8.5 (OriginLab Corporation, Northampton, MA), and Orthogonal partial least squares (OPLS) was done by SIMCA 14.1. For comparison of averaged peak intensities of signals acquired from different brain regions, a two sample t-test was calculated using OriginPro 8.5 to determine significant differences between the average peak intensities of each pair of regions measured in triplicate.

4.4 RESULTS

LTP induction/recording and MS imaging for tracking small metabolites and lipids changes in hippocampus

We previously demonstrated that TiO_2-DA-assisted LDI has higher selectivity and sensitivity for Lewis basic lipids, such as fatty acids, cholesterols, ceramides, DAGs and PEs, in positive mode [19]. In the given mice hippocampus tissue, 35 small molecules (including amino acids, alkaloids, free fatty acids and dipeptides) and over 50 lipids (including cholesterols, ceramides, diacylglycerol (DAG), GlcCer, phosphatidic acid (PA), PE-Cer, PCs and PEs) were detected with TiO_2-DA monolith-assisted LDI MSI and identified with FTICR MS and MALDI MS/MS.

Schaffer collateral axons running from CA3 to CA1 were used for field stimulation, and the stimulating electrode was placed near the sr of CA2 where most of Schaffer collateral axons are present (Fig. 4.1A). fEPSP was recorded near the sr and the slm of CA1, which contain most of the Schaffer collateral axonal terminals that synapse onto the CA1 pyramidal cells dendrites. A sample recording correlating time to mean percentage (%) fEPSP slope to baseline before and after LTP induction is shown in Figure 5.1B.

To detect the spatio-chemical changes of the hippocampus after LTP induction, mouse brain was sectioned and divided into two sides. One side was used for

LTP induction, while the other side was used as untouched control incubated in the same condition as the LTP side (two sides are selected randomly every time). Slices were frozen immediately after LTP recording, and further sectioned into 10-um slices for TiO_2-DA-assisted LDI MSI (Fig. 4.1C). This procedure identifies compounds involved in LTP formation. To distinguish the changes induced by HFS LTP induction versus test pulses, separate control slices exposed to test pulses only were prepared and compared to untouched controls.

Though symmetric contralateral hippocampal slices were used for experiment and control, different matrix effects, such as salt content and surface properties, can also contribute to artifacts in MSI signal. Thus, to demonstrate that the detected signals indeed correspond to changes in compound levels, we used LC-MS/MS to validate MSI results for several important biomarkers. All detected compounds have correlation coefficient > 0.9 except for cholesterol. Low correlation of cholesterol may be due to its high concentration in the fiber tracts, which potentially contaminated the hippocampal tissue when tissue scratching was done for LC-MS/MS.

Untargeted analysis of chemical changes after LTP

We used multivariate analysis to find spatio-chemical changes in metabolites and lipids of the hippocampus after LTP induction. MSI data in hippocampus was separated into so, sp, sr and slm cell layers of CA1, CA2 and CA3 sub regions

according to anatomical morphology in optical images as well as ion images of some representative compounds. Mass spectra from different selected layers were exported and analyzed with PCA, a complementary multivariate analysis technique.

Score plot of PCA shows that the CA2 and the CA3 regions have the most separation between control (black dots) and LTP sample (red dots) (Figure 4.2A). For the CA1 region, control and LTP sample cannot be separated in most of the layers except for the so layer. In the CA1 so layer, two samples can be separated in the PC1 axis. For the CA2 regions, samples can be separated in all the layers in the PC3 axis. For the CA3 region, only the slm layer have obvious separation of two sample dots in the PC3 axis. It can be seen that the CA2 region, where the stimulating electrode is placed, had the most obvious separation. The slm and sr layers containing most of the Schaffer collateral axons have the largest separations in both the CA2 and the CA3, so the changes from PCA correspond to the position where LTP occurred. However, when the PCA score plots of untouched control sample were compared to test pulse control samples, no obvious separation is observed, except the sp and sr of the CA3 in the PC3 axis.

To investigate specific changes of multiple compounds and identify compounds that changed significantly in different layers, OPLS as a supervised untargeted analysis

method was used. S-plot was used to find the compounds dominating the changes found in different layers (figure 4.2B).

S-plot indicates the difference of each compound in control versus LTP classes [23]. P[1] describes the magnitude of each compound change, and P(corr) represents the reliability of each compounds change. Thus, compound with high P[1] and P(corr) has a bigger influence on the separation of two classes, identifying the compound as the dominating difference between control and LTP. In accordance to previously published studies [24], we set $P[1] > 0.05$ and $P(corr) > 0.4$ as threshold. Compounds matching this threshold in different layers are listed in Table 4.1.

MS/MS spectra were obtained for these peaks to elucidate the precise structure including lipids side chains. Small alkaloids, amino acids and amino acid derivatives dominate the changes in the CA1. Changes in the CA2 and the CA3 are dominated by lipids such as phospholipids, ceramides, cholesterol and fatty acids.

We also compared the control and test pulse control classes. In the sp and sr layer of the CA3, which had obvious separation in PCA score plot, was used to do OPLS. Resulting s-plots show that among compounds listed in Table 4.1 only 5-HT, pyroglutamate and creatine have $p(corr) > 0.4$. Changes of these compounds were not

in the CA3 region for the LTP samples according the s-plot. Thus, compound changes identified in LTP samples are due to LTP induction instead of the test pulse.

Statistical analysis of biomarker changes after LTP induction

Ion images of compounds changed significantly after LTP induction in multiple regions and layers (Fig. 4.3). These include four alkaloids (creatine, creatinine, 5-hydroxyltryptophol and spermine), two amino acid derivatives (pyroglumtamic acid and GABA), four fatty acids (FA(20:4)/AA, FA(22:6)/DHA, FA(18:1) and FA (22:4)), one PC (PC(20:4/18:2)), three PEs (PE(20:4/20:3), PE(20:4/18:0) and PE(38:3)), cholesterol and one ceramide (Cer(d18:1/18:0)). The specific fold changes and p-values are listed in Table 4.1. Most of the alkaloids and amino acid derivatives increased in the CA1 cell layers, and most of the fatty acids and lipids increased in the CA2 or the CA3 cell layers, except PC(20:4/18:2) which decreased in the CA3 cell layers. Most of the mentioned compounds have previously been reported to be implicated in LTP, synaptic plasticity or neurotransmission processes. Details of the compounds and their functions are discussed in later sections.

For test pulse samples, the fold change and have no significant changes between control versus test pulse except for the increase of creatine in the sp and GABA in the slm of CA2, both of which were not observed in the LTP samples.

Correlating the change ratios with fEPSP magnitude

To investigate the correlation of the change ratios of above mentioned compounds with LTP magnitude, plot of change ratio versus corresponding LTP fEPSP of five replicate animals are constructed. All compounds investigated have linear correlation between change ratio and fEPSP magnitude, and all the correlation coefficients are higher than 0.75, with most near 0.9.

4.5 DISCUSSION

LTP process and its molecular mechanism

LTP is the long-lasting increase of synaptic strength induced by high-frequency stimulation. This phenomenon is an evidence for synaptic plasticity, which was proposed to be a foundational element in learning and memory. To this day LTP is believed to be one of the primary mechanisms giving rise to synaptic plasticity in the brain and remains an uncontested cellular model of learning and memory.

Elucidating the molecular mechanism of LTP is important for understanding learning and memory as well as treating neurodegenerative diseases. Majority of the published reports suggest the increase of synaptic strength following LTP is due to modification of the postsynapse [25,26].

As shown in Figure 4.5, depolarization of the postsynapse cause by HFS will displace the Mg^{2+} blockade of the NMDA receptor channel and cause Ca^{2+} influx [27,28]. Ca^{2+} influx activates a collection of enzymes and initiate several second messenger signaling pathways that proceed to modify the postsynapse. Here MSI of both small metabolites and lipids was used for the first time to observe the spatio-chemical changes associated with LTP induction, which may provide more information about the secondary signaling process. From literatures and also the hierarchical clustering results (Fig. 4.4A), chemical changes can be separated into different groups, and each group has similar spatial distribution changes during LTP (Fig. 4.4B). Creatine and creatinine are grouped as important energy shuttle for storing phosphate group (Fig. 4.5). Fatty acids and phospholipids are involved in hydrolysis reaction of phospholipases A2 which is activated by Ca^{2+} influx in the postsynapse. Spermine was separated into one class and is controlled by ornithine decarboxylase, whose activity is increased by Ca^{2+} influx. GABA and pyroglutamate, whose synthesis and metabolism are all closely related with glutamate, are grouped into one class. Another class includes cholesterol and ceramide, which are important component of lipid rafts, are grouped for discussion. Dipeptides are not previously reported to be involved in LTP, and some possible explanations of the changes are proposed.

Chemical changes

Creatine (Cr) is an important intracellular high-energy phosphate shuttle synthesized in the liver and the kidneys, which is transported to the brain to be stored in phosphate

form. When energy is needed for cellular activity, creatine phosphate (PCr) is dissociated into free Cr and phosphate for the regeneration of ATP through the Cr/PCr/creatine kinase pathway. In the meantime, creatinine as the breakdown product of Cr and PCr usually implies the total concentration of Cr and PCr.

Cr increased significantly in most of cell layers of the CA1 and especially in the so and sp layers (Fig. 4.3). Meanwhile, creatinine as the breakdown product of Cr and PCr decreased significantly in most of cell layers in the CA2. The increase of Cr may be the result of high energy demand of the postsynapses of Schaffer collateral-CA1 during LTP [29]. Since Cr has no significant changes in the CA2/3 regions, the decrease of creatinine in the CA2 may be caused by the decrease of PCr if the pH and temperature environment of the tissue did not change during LTP induction [30]. The decrease of PCr from the CA2 region may be explained by energy demands in presynaptic regions which dissociate PCr into Cr, but Cr level might be kept stable by the release from presynapse as a potential neurotransmitter. Previous report suggested that Cr can potentially function as a neurotransmitter, supported by data showing that Cr can be released from neurons in an action-potential dependent manner, while rat brain synaptosomes are able to uptake Cr [31,32]. However, postsynaptic Cr receptor is yet to be identified.

PC-FAs pathway

Depolarization-dependent Ca^{2+} influx through voltage-gated Ca^{2+} channels is the main cause of LTP induction. It has been demonstrated that direct Ca^{2+} entrance through voltage-dependent calcium channels activate phospholipase A2 (PLA2) to result in fatty acids release via phospholipid hydrolysis [6] (Fig. 4.5). Thus, Specific lipid messengers are cleaved from these reservoir phospholipids by phospholipases upon stimulation by neurotransmitters. It was reported that one such reservoir is the phospholipids that typically contain an alkyl-acyl chain in the C1 position and either arachidonate (20:4) or docosahexaenoate (22:6) in the C2 position of the glycerol backbone. The major PLA2 activated are cytoplasmic PLA2 which results in the release of arachidonic acid (AA), docosahexaenoic acid (DHA), and lyso-platelet-activating factor (PAF). Another PLA2 is secretary PLA2 which is co-released along with neurotransmitters, shown to promote active AA remodeling in cultured neurons and potentially promote DHA release [6].

PC containing C20:4 (PC(18:2/20:4)) decreased significantly in the sp layer of CA2 (Fig. 5.3). This can be the result of PLA2 activation which hydrolyzes PC(18:2/20:4). Also, FA(20:4)/(AA) increased in the same location. This is stronger proof that PC(20:4/18:2) was hydrolyzed by PLA2, and released its side chain.

Since FA(20:4) and FA(22:6) are all component at the C2 position on the glycerol backbone, the increase of them in the CA2/3 should be related to PC hydrolysis via PLA2. It was reported that DHA may act as a signaling molecule by binding to retinoid X receptor (RXR), a ligand-activated transcription factor, or it may be oxygenated to produce messenger molecules such as docosanoid in the postsynapse during LTP [6]. Thus, the lack of DHA increase in the CA1 may be due to sequestering of the oxygenated form by RXR, which balance the increased formation from PC hydrolysis. However, changes in FA(20:4)/AA is different from other fatty acids. AA increased significantly in the CA2/3, but decreased significantly in most of cell layers of the CA1. In addition to being a product of PLA2 activation modulated by Ca^{2+}, AA was also reported to be a retrograde messenger for LTP that diffuses from postsynapses to presynapses [33]. Thus, the increase in CA2/3 is not only due to PLA2 mediated hydrolysis, but also the result of retrograde diffusion. In the postsynapse, AA will then be degraded to eicosanoids for intercellular signaling. The decrease of AA in the CA1 region can be attributed to its degradation to eicosanoids and diffusion from post synaptic region to presynaptic region.

Other fatty acids such as FA(18:1) and FA(22:4) also increased in the CA2/3 regions, but they are seldom discussed in the LTP literature. FA(18:1)/oleic acid was reported to be released from the 2-acyl position of membrane phospholipids via cleavage by calcium-dependent PLA2 [34]. It is known that increase in oleic acid activates protein kinase C (PKC), and PKC activation is associated with synapse strengthening [35,36].

FA(22:4) is usually stored in the sn-2 position of phospholipids, and is the metabolic product of AA [37]. Thus, increase in FA(22:2) can be the consequence of either or both phospholipid hydrolysis via PLA2 or/and the increase of AA.

PE-FA pathway

Three PEs increased in the CA2/3 regions after LTP (Table 4.1). Among them, two 20:4 PEs significantly increased in the CA3 region, especially for the slm layer, while another PE (PE 38:3) increased largely in the CA2 region. It was reported that LPEAT2 is predominantly expressed in the brain, coinciding with the enrichment of PE in this tissue, and acts mainly to form Pes by acylating 1-acyl-lyso-PE [38]. It has been shown that LPEAT2 activity is not calcium-dependent. However, the increase in DHA or AA, which may be substrates of LPEAT2, can potentially be the reasons PEs increased after LTP [39].

Cholesterol and ceramide

Sphingolipids and cholesterols are major constituents of lipid rafts. Many previous works suggested that lipid rafts, especially the cholesterol within, facilitate nerve conduction and synaptic exocytosis/endocytosis [40,41]. Ceramides are generated when sphingomyelinase (SMase) hydrolyzes sphingophospholipids. Cer(d18:1/18:0) increase is observed in most of the cell layers of the CA2 after LTP (Fig. 5.3). Not much investigation has been done on the changes of ceramides in relation to LTP and

SMase is not directly modulated by Ca^{2+} influx. However, there are reports showing that the PLA2-FA(20:4) pathway mentioned above results in SMase activation [42]. Therefore the increase of ceramide after LTP induction might be the consequence of cPLA2-FA(20:4) pathway activation.

Cellular cholesterol levels fluctuate in response to strong neuronal activity, with implications in excitotoxicity and cellular stress [43]. However, it is not clear how changes in cholesterol levels relate to the regulation of synaptic strength during plasticity. A recent study demonstrated reduction of cholesterol from intracellular membranes of the CA1 pyramidal neurons during LTP induction, and this reduction required NMDAR activation [13]. We did not observe significant changes in cholesterol levels in the CA1 region, but saw significant increase in the CA2 region which contains mostly presynaptic axons (Fig. 4.3). Cholesterol levels detected by MSI are total tissue levels within target pixel indiscriminate of subcellular compartments or cell types. The reported reduction of intracellular cholesterol may be compensated by the reciprocal increases in other cellular compartments, and thus failed to show up in our analysis. The significant increase of cholesterol in the CA2 region remains puzzling with no good explanation.

Spermine

It has previously been shown that tissue levels of putrescine, spermine, spermidine, together with ornithine decarboxylase (ODC) activity, are transiently increased in excitable tissue by the activation of voltage- or receptor-gated calcium channels [44,45]. Thus, the increase of spermine in the CA2 region may be the result of HFS-induced NMDA receptor activation and subsequent Ca^{2+} influx (Fig. 4.3). Also, spermine has been reported to specifically facilitate LTP formation by potentiating the activation of NMDA receptors [46]. Our result of increased endogenous spermine after LTP agrees with the results of previous studies.

Dipeptides

From our previous work on DA-assisted TiO_2 LDI methodology, we found that the observed dipeptides may be photo-catalyzed fragments of proteins or longer peptides [19]. Thus, the significant increases of the two dipeptides may be the consequence of increased expression of certain proteins during LTP. However, since dipeptides are too small to trace back to the original protein, this result remains inconclusive.

GABA and pyroglutamatic acid

GABA and pyroglutamatic acid function directly in the neurotransmission process and are closely related to glutamate, which is the most abundant excitatory neurotransmitter in the vertebrate nervous system.

GABA increased significantly in the CA1 after LTP (Fig. 4.3). GABA is synthesized from glutamate by glutamate decarboxylase (GAD) with the cofactor pyridoxal phosphate [47,48]. Among GADs, GAD65 is only activated when GABA neurotransmission occurs, and is therefore regulated by the synaptic environment. GAD65 is activated by phosphorylation via PKC, which is in turn activated by increases in the concentrations of DAGs [3], AA, oleic acid [49] and calcium ions (Ca^{2+}) [50], all of which increased after LTP (Fig. 4.3). GABA is the major inhibitory neurotransmitter whose inhibitory effect is mainly mediated by the $GABA_A$ receptor. Activation of the $GABA_A$ receptor results in the decrease of membrane potential and usually induces hyperpolarization. LTP induction is enhanced by blocking $GABA_A$ receptors [51]. This enhancement is attributed to an increase in postsynaptic Ca^{2+} influx via NMDA receptors [52] since $GABA_A$ receptor blockade allows for greater postsynaptic depolarization that relieves the voltage-dependent blockade of NMDA receptors by Mg^{2+}. In our experiments, Picrotoxin was used as antagonist for $GABA_A$ receptors [53]. Thus, our detection of GABA increase in presynaptic regions demonstrate a decreased release of GABA from presynapses though its synthesis was enhanced by Ca^{2+} influx.

Though pyroglutamic acid itself is not a neurotransmitter, it has close relation with glutamate which activates AMPA and NMDA receptors. Pyroglutamic acid is derived from glutathione by γ-glutamyl cyclotransferase, which can then form glutamate via 5-oxoprolinase, which is the only enzyme known to act on pyroglutamic acid [54]. With

pyroglutamic acid easily converted into glutamate following hydrolysis, pyroglutamic acid can function potentially as a reservoir for glutamate. Pyroglutamic acid increased in the CA1 region after LTP, while glutamate levels did not change (Fig. 4.3). One possible explanation is that the high glutamate demand for neurotransmission during LTP induction largely increased the concentration of glutamate and pyroglutamic acid. However, glutamate is released quickly for neurotransmission during LTP, while pyroglutamic acid has increased concentration in the cell. The detailed molecular mechanism for this regulation is still unclear.

Conclusion

LTP is a remarkable form of brain plasticity and the best-studied animal model for learning and memory. Tracking the chemical changes during LTP is critical for unveiling the mechanisms underlying learning and memory as well as finding solutions to combat cognitive decline. In this work, we used DA-modified TiO_2-assisted LDI MSI to track the spatio-chemical changes in the hippocampus during LTP in the Schaffer collateral-CA1 synapses with focus on lipids and metabolites. From the PCA and the OPLS analysis, 20 compounds including amino acids, alkaloids, fatty acids, ceramides, diglycerides and phospholipids are identified to dominate the chemical changes in the hippocampus after LTP induction. The specific changes and spatial distributions of most of these compounds agreed with previous reports. This is the first time MSI is utilized to simultaneously visualize the reported signaling chemical changes, including the creatinine/Cr change related to energy shuttle, fatty

acids/PC/PE changes related to PUFA signaling, GABA change related to neurotransmission, spermine change related to NMDA receptor activation, and ceramides and cholesterol changes related to lipid rafts. Also, some changes such as cholesterol and pyroglutamic acid cannot be explained or are never reported according to known pathways. These results provided important new information for molecular substrates of brain plasticity which deserves further biological studies.

4.6 FIGURES AND TABLE

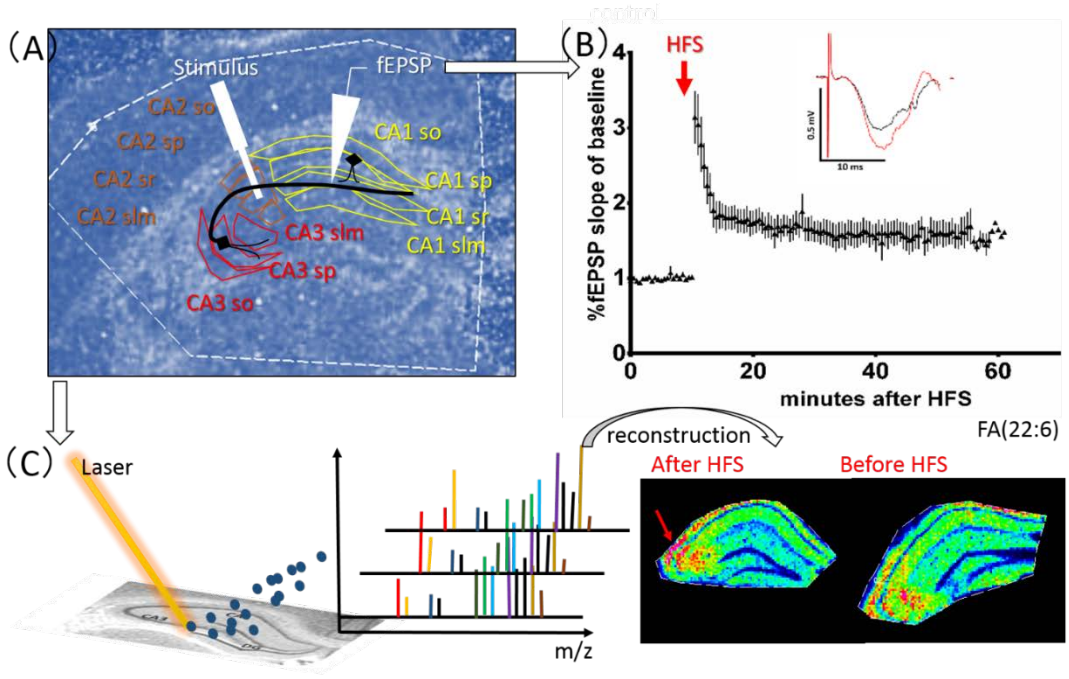

Figure 4.1. Illustrated overview of experimental scheme. (A) Schematic of mouse hippocampal region divisions for MSI analysis and electrode locations. (B) Mean %fEPSP slope to baseline (mean ± s.e.m.) versus time for mice hippocampal slices. High frequency stimulation HFS (3 x 100 Hz at test-pulse strength, 1000 ms duration, 15 s interval) is given at 10 min (n=5). Inset: sample fEPSP traces of baseline in black vs post-high frequency stimulation in red. HFS: high frequency stimulation. (C) Workflow of chemical change tracking after LTP with MSI.

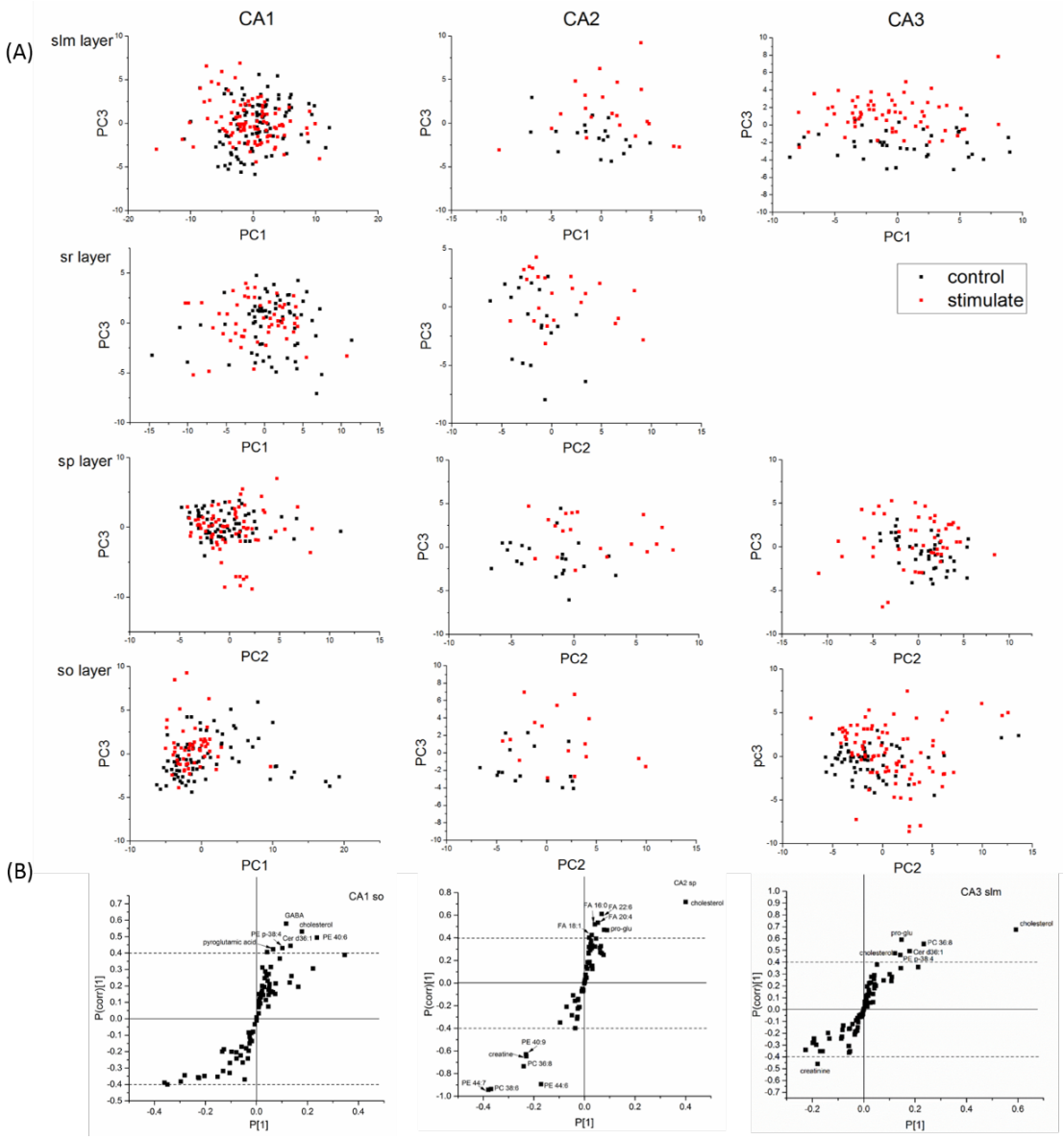

Figure 4.2. PCA and S-plot of individual cell layers before and after LTP. (A) PCA score plots of individual regions before and after LTP induction. (B) S-plot of representative cell layers of CA1, CA2 and CA3 by OPLS analysis. Compounds with P[1] > 0.05 and P[corr] > 0.4 are labeled in the plots.

Table 4.1. Statistic results of all the compounds dominating chemical changes after LTP

	CA1 SLM		*CA1 SO*		*CA1 SP*		*CA1 SR*		*CA2 SLM*		*CA2 SO*	
	fold	p	fold	p	fold	p	fold	p	fold	p	fold	p
GABA	1.2±0.2	0.01	1.5±0.4	0.03	1.3±0.3	0.0467	1.1±0.2	0.2	1.1±0.2	0.1	1.3±0.4	0.05
creatinine	1.1±0.3	0.3	1.1±0.5	0.3	1.0±0.3	0.3656	0.97±0.2	0.4	0.9±0.2	0.09	0.8±0.1	0.01
roglutamic acid	1.2±0.1	0.02	1.3±0.4	0.07	1.2±0.2	0.026	1.1±0.1	0.09	1.1±0.2	0.2	1.1±0.3	0.2
creatine	1.2±0.2	0.02	1.2±0.3	0.05	1.1±0.2	0.0674	1.1±0.1	0.08	0.97±0.2	0.4	0.9±0.1	0.09
spermine	1.1±0.1	0.02	1.3±0.4	0.09	1.1±0.1	0.0144	1.1±0.1	0.04	1.16±0.3	0.1	1.1±0.4	0.2
Glycyl-Tyrosine	1.0±0.2	0.2	0.7±0.2	0.03	0.9±0.7	0.3075	0.91±0.2	0.2	1.1±0.4	0.2	1.3±0.2	0.03
Pro Glu	1.2±0.4	0.2	1.0±0.4	0.4	1.1±0.3	0.2813	1.1±0.3	0.2	1.6±0.4	0.007	1.5±0.6	0.03
FA 18:1	0.9±0.3	0.4	1.2±0.3	0.06	1.1±0.4	0.3314	1.0±0.3	0.5	0.98±0.5	0.5	1.2±0.1	0.02
FA 20:4	0.8±0.2	0.07	1.1±0.3	0.3	0.8±0.3	0.1287	0.8±0.4	0.2	1.6±1.2	0.1	1.4±0.6	0.08
FA 22:6	0.9±0.2	0.2	1.2±0.5	0.2	0.9±0.2	0.2106	0.8±0.2	0.08	1.1±0.1	0.03	1.3±0.5	0.08
FA 22:4	1.1±0.8	0.4	1.5±0.6	0.05	1.1±1.3	0.4404	0.8±0.4	0.1	1.3±0.7	0.08	1.7±1.4	0.1
cholesterol	1.0±0.7	0.4255	1.1±0.5	0.2743	1.1±0.5	0.2756	1.0±0.5	0.426	1.3±0.4	0.0601	1.4±0.3	0.0132
Cer d36:1	1.3±0.6	0.2112	1.2±0.5	0.1852	1.3±0.5	0.1744	0.95±0.5	0.4145	1.6±1.0	0.1114	2.1±0.8	0.0581
PE 38:4	0.9±0.3	0.374	0.8±0.4	0.17	1.0±0.1	0.2989	1.1±0.3	0.3256	1.2±0.3	0.0892	1.2±0.3	0.2122
PE 38:3	0.9±0.2	0.2971	1.0±0.1	0.2028	1.0±0.2	0.4764	0.9±0.2	0.063	1.4±0.4	0.0131	1.5±0.3	0.0128
PE 40:7	1.0±0.2	0.3851	0.95±0.1	0.2576	1.0±0.1	0.4398	0.9±0.3	0.2898	1.2±0.2	0.0116	1.4±0.3	0.01
PC 38:6	1.1±0.3	0.2966	1.1±0.5	0.3318	1.0±0.4	0.4963	0.9±0.2	0.248	0.88±0.2	0.1278	1.0±0.4	0.4022

Table 4.1 (cont.).

	CA2 SP		*CA2 SR*		*CA3 SLM*		*CA3 SO*		*CA3 SP*	
	fold	p	fold	p	fold	p	fold	p	fold	p
GABA	1.4±0.2	0.006	1.3±0.2	0.004	1.0±0.4	0.5	0.9±0.4	0.3	1.1±0.4	0.3
creatinine	0.8±0.2	0.07	0.8±0.1	0.008	0.9±0.1	0.07	1.1±0.3	0.3	0.8±0.3	0.08
roglutamic acid	1.0±0.3	0.4	1.0±0.3	0.4	1.0±0.1	0.3	1.0±0.4	0.4	1.0±0.3	0.5
creatine	0.9±0.1	0.1	0.9±0.1	0.1	1.1±0.3	0.3	1.2±0.3	0.05	1.0±0.3	0.5
spermine	1.4±0.5	0.02	1.3±0.3	0.04	1.2±0.2	0.02	1.2±0.4	0.09	1.2±0.4	0.1
Glycyl-Tyrosine	1.3±0.4	0.1	1.0±0.3	0.4	1.2±0.7	0.2	1.2±0.2	0.06	1.1±0.4	0.4
Pro Glu	1.5±0.5	0.03	1.5±0.2	0.0008	1.4±0.6	0.07	1.1±0.3	0.2	1.1±0.4	0.3
FA 18:1	1.3±0.3	0.06	1.6±0.5	0.03	1.2±0.3	0.06	0.9±0.3	0.3	1.3±0.5	0.04
FA 20:4	1.4±0.8	0.09	2.0±1.3	0.06	1.2±0.4	0.2	0.8±0.2	0.05	1.2±0.5	0.2
FA 22:6	1.4±0.5	0.09	1.5±0.5	0.08	1.2±0.1	0.01	0.9±0.3	0.2	1.0±0.4	0.5
FA 22:4	1.3±0.4	0.04	1.7±1.5	0.03	1.5±0.7	0.04	0.9±0.6	0.3	1.2±0.7	0.3
cholesterol	1.3±0.4	0.0572	1.3±0.3	0.0152	1.3±0.2	0.0167	1.2±0.4	0.1482	1.3±0.4	0.0521
Cer d36:1	1.3±1.7	0.2212	1.2±0.6	0.2883	1.1±0.2	0.0601	0.8±0.7	0.31	0.96±0.5	0.4529
PE 38:4	1.1±0.4	0.2272	1.1±0.2	0.1127	1.2±0.1	0.0032	1.2±0.2	0.0342	1.2±0.2	0.047
PE 38:3	0.9±0.2	0.2717	1.0±0.2	0.4369	1.1±0.2	0.2012	0.97±0.2	0.39	1.0±0.2	0.3691
PE 40:7	1.1±0.2	0.1951	1.1±0.2	0.0553	1.3±0.2	0.0026	1.0±0.3	0.341	0.99±0.1	0.418
PC 38:6	0.7±0.2	0.0382	0.8±0.4	0.1793	0.8±0.2	0.1172	0.8±0.2	0.0827	0.8±0.2	0.0658

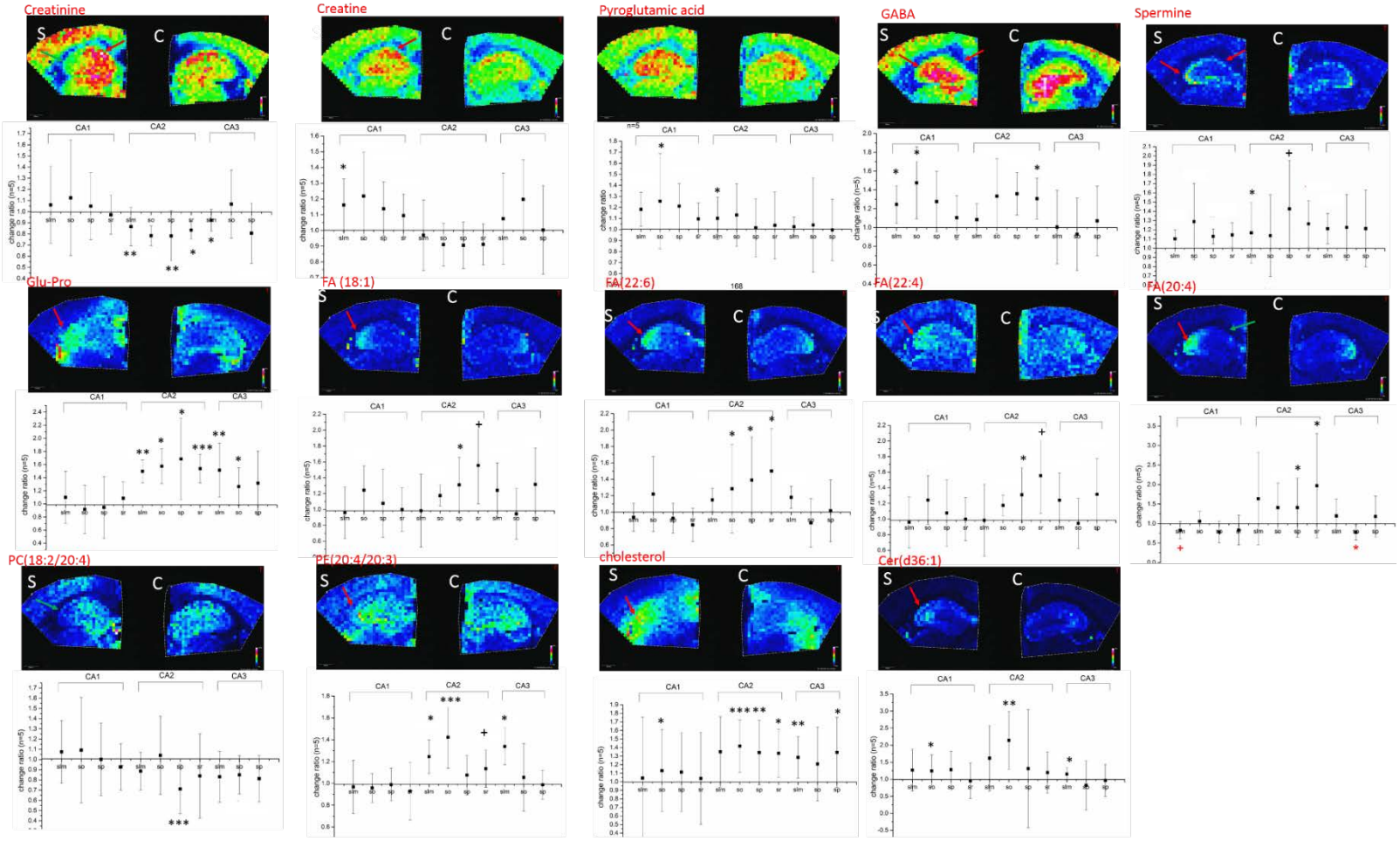

Figure 4.3. Ion images and average fold change of compounds in different cell layers of stimulated side after LTP (n=5). +, 0.4 > p(corr) > 0.3; *, 0.6 > p(corr) > 0.4; **, 0.8 > p(corr) > 0.6; ***, p(corr) > 0.8

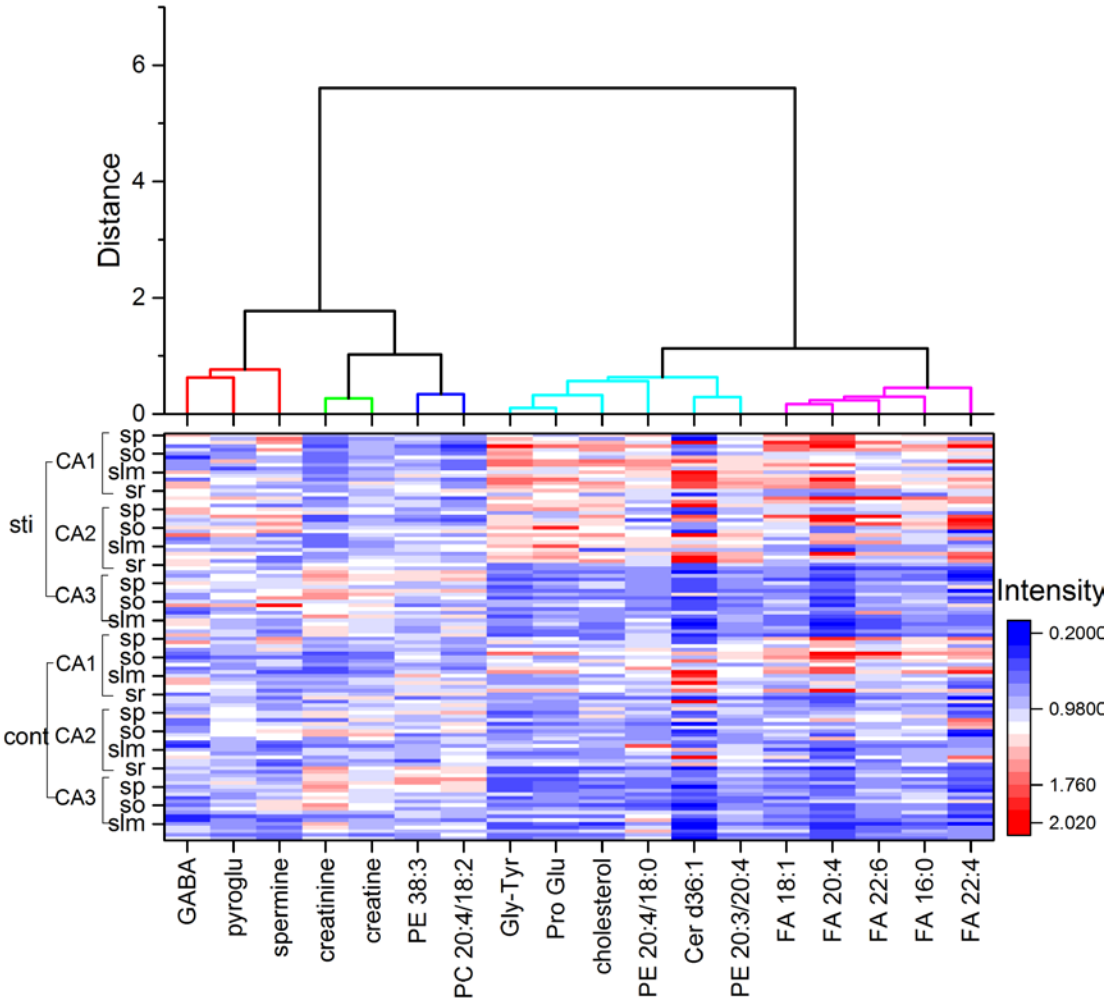

Figure 4.4. Hierarchical clustering of compounds and their region specific relative intensity heatmaps after LTP. (A) Hierarchical clustering of detected compounds. Each color indicates biologically closely related species. (B) Heat map of corresponding compounds in different regions. Sti: stimulated, Cont: Control.

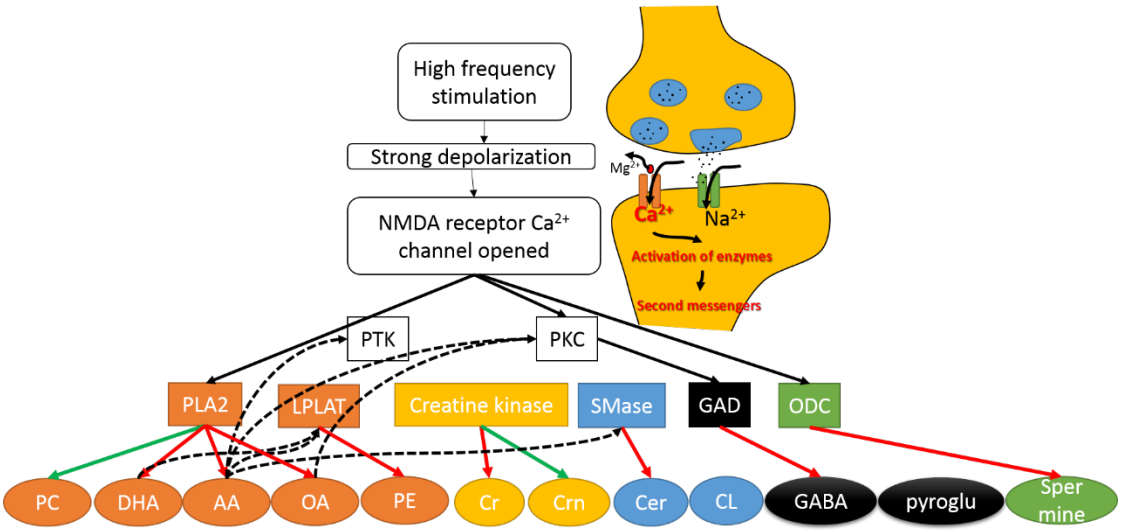

Figure 4.5. The reported mechanisms of LTP induced compound changes observed in MSI and their direction of change. Simplified mechanism of LTP formation is summarized in the illustration. Green arrows indicate decrease while red arrows indicate increase. Solid black arrows indicate activation of the enzymes via Ca^{2+} influx, and dashed black arrows indicate activation of the enzymes by increases in upstream signaling compounds.

4.7 REFERENCES

1. Bennett EL, Diamond MC, Krech D, Rosenzweig MR. Chemical and Anatomical Plasticity of Brain. Science (80-). 1964;146: 610–619.
2. Bliss T V, Collingridge GL. A synaptic model of memory: long-term potentiation in the hippocampus. Nature. 1993;361: 31–39.
3. Lynch MA. Age-related impairment in long-term potentiation in hippocampus: a role for the cytokine, interleukin-1 beta? Prog Neurobiol. 1998;56: 571–589.
4. Herring BE, Nicoll RA. Long-Term Potentiation: From CaMKII to AMPA Receptor Trafficking. Annu Rev Physiol. 2016;78: 351–365.
5. Piomelli D, Astarita G, Rapaka R. A neuroscientist's guide to lipidomics. Nat Rev Neurosci. 2007;8: 743–754.
6. Bazan NG. Synaptic lipid signaling: significance of polyunsaturated fatty acids and platelet-activating factor. J Lipid Res. 2003;44: 2221–2233.
7. Ostrowski SG, Van Bell CT, Winograd N, Ewing AG. Mass spectrometric imaging of highly curved membranes during Tetrahymena mating. Science (80-). 2004;305: 71–73.
8. Grassi S, Francescangeli E, Goracci G, Pettorossi VE. Role of Platelet-Activating-Factor in the Long-Term Potentiation of the Rat Medial Vestibular Nuclei. Eur J Neurosci. 1998;10: 15111.
9. Kiritoshi T, Ikeda H, Murase K. Long-term potentiation of neuronal excitation in the central nucleus of the rat amygdala revealed by imaging with a voltage-sensitive dye. Brain Res. Elsevier B.V.; 2010;1349: 32–40.
10. Padamsey Z, Emptage NJ. Imaging synaptic plasticity. Mol Brain. 2011;4: 1–10.
11. Ikeda H, Kusudo K, Murase K. Nitric oxide-dependent long-term potentiation revealed by real-time imaging of nitric oxide production and neuronal excitation in the dorsal horn of rat spinal cord slices. Eur J Neurosci. 2006;23: 1939–1943.
12. Mitani A, Kadoya F, Nakamura Y, Kataoka K. Visualization of hypoxia-induced glutamate release in gerbil hippocampal slice. Neurosci Lett. 1991;122: 167–170.
13. Brachet A, Norwood S, Brouwers JF, Palomer E, Helms JB, Dotti CG, et al. LTP-triggered cholesterol redistribution activates Cdc42 and drives AMPA receptor synaptic delivery. J Cell Biol. 2015;208: 791–806.

14. Pfefferbaum A, Adalsteinsson E, Spielman D, Sullivan E V., Lim KO. In vivo spectroscopic quantification of the N-acetyl moiety, creatine, and choline from large volumes of brain gray and white matter: Effects of normal aging. Magn Reson Med. 1999;41: 276–284.

15. Garrett TJ, Prieto-Conaway MC, Kovtoun V, Bui H, Izgarian N, Stafford G, et al. Imaging of small molecules in tissue sections with a new intermediate-pressure MALDI linear ion trap mass spectrometer. Int J Mass Spectrom. 2007;260: 166–176.

16. Liu H, Dai J, Zhou J, Huang H, Chen F, Liu Z. A hybrid ionic liquid–matrix material, [TiO2–Si–NH3+][CHC−], as a novel matrix for the analysis of small molecules by MALDI-TOF MS. Int J Mass Spectrom. Elsevier B.V.; 2015;376: 85–89.

17. Zemski Berry KA, Hankin JA, Barkley RM, Spraggins JM, Caprioli RM, Murphy RC. MALDI imaging of lipid biochemistry in tissues by mass spectrometry. Chem Rev. 2011;111: 6491–6512.

18. Goodwin RJA, Pennington SR, Pitt AR. Protein and peptides in pictures: Imaging with MALDI mass spectrometry. Proteomics. 2008;8: 3785–3800.

19. Wu Q, Chu JL, Rubakhin SS, Gillette MU, Sweedler J V. Dopamine-modified TiO_2 monolith-assisted LDI MS imaging for simultaneous localization of small metabolites and lipids in mouse brain tissue with enhanced detection selectivity and sensitivity. Chem Sci. Royal Society of Chemistry; 2017;0: 1–13.

20. Ting J, Daigle T, Chen Q, Feng G. Acute Brain Slice Methods for Adult and Aging Animals: Application of Targeted Patch Clamp Analysis and Optogenetics. Patch-Clamp Methods Protoc. 2014;1183: 221–242.

21. Shrivas K, Hayasaka T, Sugiura Y, Setou M. Method for Simultaneous Imaging of Endogenous Low Molecular Weight Metabolites in Mouse Brain Using TiO_2 Nanoparticles in Nanoparticle-Assisted Laser Desorption/Ionization-Imaging Mass Spectrometry. Anal Chem. 2011;83: 7283–7289.

22. Johnson WE, Li C, Rabinovic A. Adjusting batch effects in microarray expression data using empirical Bayes methods. Biostatistics. 2007;8: 118–127.

23. Wiklund S, Johansson E, Sjöström L, Mellerowicz EJ, Edlund U, Shockcor JP, et al. Visualization of GC/TOF-MS-based metabolomics data for identification of biochemically interesting compounds using OPLS class models. Anal Chem. 2008;80: 115–122.

24. Tajima Y, Ishikawa M, Maekawa K, Murayama M, Senoo Y, Nishimaki-mogami T, et al. Lipidomic analysis of brain tissues and plasma in a mouse model expressing mutated human amyloid precursor protein / tau for Alzheimer ' s disease. 2013; 1–14.

25. Kerchner GA, Nicoll RA. Silent synapses and the emergence of a postsynaptic mechanism for LTP. Nat Rev Neurosci. 2008;9: 813–825.

26. Giese KP. Long-term potentiation and memory. Philos Trans R Soc London - Ser B Biol Sci. 2003;358: 643–647.

27. Collingridge GL. Long term potentiation in the hippocampus: mechanisms of initiation and modulation by neurotransmitters. Trends Pharmacol Sci. 1985;6: 407–411.

28. Colino a, Malenka RC. Mechanisms underlying induction of long-term potentiation in rat medial and lateral perforant paths in vitro. J Neurophysiol. 1993;69: 1150–1159.

29. Rackayova V, Cudalbu C, Pouwels PJW, Braissant O. Creatine in the central nervous system: From magnetic resonance spectroscopy to creatine deficiencies. Anal Biochem. Elsevier Inc; 2016;8.

30. Wyss M, Kaddurah-Daouk R. Creatine and Creatinine Metabolism. Physiol Rev. 2000;80: 1107–1213.

31. Peral MJ, Vázquez-Carretero MD, Ilundain AA. Na+/Cl-/creatine transporter activity and expression in rat brain synaptosomes. Neuroscience. Elsevier Inc.; 2010;165: 53–60.

32. Almeida LS, Salomons GS, Hogenboom F, Jakobs C SA. Exocytotic Release of Creatine in Rat Brain. Synapse. 2006;60: 118–123.

33. Williams JH, Errington ML, Lynch M a, Bliss T V. Arachidonic acid induces a long-term activity-dependent enhancement of synaptic transmission in the hippocampus. Nature. 1989;341: 739–742.

34. Saitoh T, Dobkins KR. Protein kinase C in human brain and its inhibition by calmodulin. Brain Res. 1986;379: 196–199.

35. Akers RF, Routtenberg A. Protein kinase C phosphorylates a 47 Mr protein (F1) directly related to synaptic plasticity. Brain Res. 1985;334: 147–151.

36. Routtenberg A. Protein kinase C activation leading to proteins F1 phophorylation may regulate synaptic plasticity by presynaptic terminal growth. Behav& Neural Biol. 1985;44: 186–200.

37. Guijas C, Astudillo AM, Gil-De-Gómez L, Rubio JM, Balboa MA, Balsinde J. Phospholipid sources for adrenic acid mobilization in RAW 264.7 macrophages. Comparison with arachidonic acid. Biochim Biophys Acta - Mol Cell Biol Lipids. Elsevier B.V.; 2012;1821: 1386–1393.

38. Cao J, Shan D, Revett T, Li D, Wu L, Liu W, et al. Molecular identification of a novel mammalian brain isoform of acyl-CoA:Lysophospholipid acyltransferase with prominent ethanolamine lysophospholipid acylating activity, LPEAT2. J Biol Chem. 2008;283: 19049–19057.

39. Su HM. Mechanisms of n-3 fatty acid-mediated development and maintenance of learning memory performance. J Nutr Biochem. Elsevier Inc.; 2010;21: 364–373.

40. Petrov A, Kudryashova K, Odnoshivkina YG, Zefirov A. Cholesterol and Lipid Rafts in the Plasma Membrane of Nerve Terminal and Membrane of Synaptic Vesicles. Neurochem J. 2011;5: 13–19.

41. Wasser CR, Ertunc M, Liu X, Kavalali ET. Cholesterol-dependent balance between evoked and spontaneous synaptic vesicle recycling. J Physiol. 2007;579: 413–429.

42. Malaplate-Armand C, Florent-Béchard S, Youssef I, Koziel V, Sponne I, Kriem B, et al. Soluble oligomers of amyloid-β peptide induce neuronal apoptosis by activating a cPLA2-dependent sphingomyelinase-ceramide pathway. Neurobiol Dis. 2006;23: 178–189.

43. Brachet A, Norwood S, Brouwers JF, Palomer E, Helms JB, Dotti CG, et al. LTP-triggered cholesterol redistribution activates Cdc42 and drives AMPA receptor synaptic delivery. J Cell Biol. 2015;208: 791–806.

44. Koenig H, Goldstone A, Lu CY. Polyamines regulate calcium fluxes in a rapid plasma membrane response. Nature. 1983;305: 530–534.

45. Iqbal Z, Koenig H. Polyamines appear to be second messengers in mediating Ca2+ fluxes and neurotransmitter release in potassium-depolarized synaptosomes. Biochem Biophys Res Commun. 1985;133: 563–573.

46. Chida N, Saito H, Abe K. Spermine facilitates the generation of long-term potentiation of evoked potential in the dentate gyrus of anesthetized rats. Brain Res. 1992;593: 57–62.

47. Petroff OAC. Book Review: GABA and Glutamate in the Human Brain. Neurosci. 2002;8: 562–573.

48. Schousboe A, Waagepetersen HS. GABA: Homeostatic and pharmacological aspects. Prog Brain Res. 2007;160: 9–19.

49. Linden DJ, Murakami K, Routtenberg A. A newly discovered protein kinase C activator (oleic acid) enhances long-term potentiation in the intact hippocampus. Brain Res. 1986;379: 358–363.

50. Wilson CH, Ali ES, Scrimgeour N, Martin AM, Hua J, Tallis GA, et al. Steatosis inhibits liver cell store-operated Ca2+ entry and reduces ER Ca2+ through a protein kinase C-dependent mechanism. Biochem J. 2015;466: 379–390.

51. Wigström H, Gustafsson B. Large long-lasting potentiation in the dentate gyrus in vitro during blockade of inhibition. Brain Res. 1983;275: 153–158.

52. Wigstrom H, Gustafsson B. Facilitation of hippocampal long-lasting potentiation by GABA antagonists. Acta Physiologica Scandinavica. 1985. pp. 159–172.

53. Ramakrishnan L, Hess GP. Picrotoxin inhibition mechanism of a gamma-aminobutyric acid A receptor investigated by a laser-pulse photolysis technique. Biochemistry. 2005;44: 8523–8532.

54. Kumar A, Bachhawat AK. Pyroglutamic acid: Throwing light on a lightly studied metabolite. Curr Sci. 2012;102: 288–297.

CHAPTER FIVE: METABOLOMIC AND LIPIDOMIC CHANGES IN THE HIPPOCAMPUS OF DIETARY MODIFIED AGED MICE BEFORE AND AFTER LONG TERM POTENTIATION, REVEALED BY MASS SPECTROMETRY IMAGING[1]

5.1 INTRODUCTION

When the brain ages, it is believed that the composition of the brain changes and the connections in the brain become fixed, which eventually lead to neurodegeneration and impairment in learning and memory [1]. It has been reported that aging of the brain and a number of neurodegenerative diseases are correlated to neuro-inflammation [2], neuronal apoptosis [3], breakdown of the blood–brain barrier (BBB) [4], decrease in cell membrane fluidity and increase in oxidative stress [5]. Dietary intervention is widely studied as a potential method to improve the learning and memory of aged animals. For example, diet containing antioxidants was used to combat oxidative stress [6] and diet containing key signaling compounds was used to control neuro-inflammation [7]. Fish oil, which is rich in n-3 polyunsaturated fatty

[1] This work was done in collaboration with Qian Wu Ph.D. from the lab of Prof. Jonathan Sweedler of analytical chemistry at the University of Illinois at Urbana-Champaign. This work was supported by the Center for Nutrition, Learning and Memory (CNLM) with funding from Abbott's Nutrition Business. Qian Wu assembled the initial manuscript, and James Chu edited the manuscript extensively in preparation for submission for publication. James Chu performed the LTP recordings and analyzed the electrophysiological data. Qian Wu performed the MSI experiments and analyzed analytical chemistry data. Ann Benefiel and Mia Yu Ph.D. provided animal care and managed the diet modifications. Jennifer Mitchell Ph.D., Stas Rubakhin Ph.D., Prof. Martha Gillette and Prof. Jonathan Sweedler provided guidance for experiments and manuscript assembly.

acid (PUFA), is widely studied as an efficient dietary supplement to improve cognitive functions [8,9]. However, the mechanisms behind these beneficiary effects of fish oil are not well understood. Previous studies suggest it is related to the metabolic products of n-3 PUFA, which have anti-inflammatory effects [10]. Recently cocoa powder is suggested as another dietary supplement capable of improving cognitive function [3,11]. It was observed that flavonoids in cocoa powder function as neuro-protective antioxidants, capable of enhancing neuronal function and stimulating regeneration possibly via intracellular signaling pathways controlling neuronal survival and differentiation. However, the proposed mechanisms remain hypothetical and have not been experimentally confirmed.

Mass spectrometry imaging (MSI) is a sensitive and multiplexed approach for the characterization and localization of a wide range of small metabolites [12,13], lipids [14], peptides, and proteins [15], making it a suitable method for visualizing important lipid-related compounds while simultaneously discovering key substrates in signaling processes. For example, time-of-flight secondary-ion mass spectrometry (TOF-SIMS) had been used to obtain high-resolution images of the microscopic changes in lipid composition that occurred at fusion sites between two mating cells of the protozoon Tetrahymena thermophile [16]. Indeed, the goal of profiling large-scale changes in lipid composition or determining the topographical distributions of individual lipid species is no longer beyond reach after MSI techniques are developed. However, it is still a less exploited field [17].

Recently, we developed a new surface assisted laser desorption/ionization (MALDI) MSI method with dopamine (DA)-modified TiO_2 monolith. With this method, small amino acids, alkaloids, fatty acids together with larger lipids including diglycerides, ceramides, phosphoethanolamine (PE) and phosphatidylcholine (PC) can be localized simultaneously in brain tissue at 20 μm spatial resolution [18]. In this work, our improved MSI method was used to track the lipidomic and metabolomic changes induced by diet modifications and determine the most important signaling molecules dominating the changes among the compounds. To unveil more information on the effects of fish oil (FO) and/or cocoa powder (CP), we tracked the changes in the compounds of interest induced by different diet modifications in aged mice. We examined Schaffer collateral CA3 – CA1 hippocampal long term potentiation (LTP) in these diet modified aged mice. Finally, we investigated how the same compounds changed in the diet modified aged animals before and after LTP induction.

5.2 MATERIALS AND METHODS

Chemicals and Materials

The following chemicals were purchased from Sigma-Aldrich (St. Louis, MO): n-methyl-D-glucamine, potassium chloride, sodium phosphate monobasic, (+)-sodium L-ascorbate, thiourea, sodium pyruvate, magnesium sulfate anhydrous, picrotoxin, titanium(IV) n-butoxide, dopamine hydrochloride (>98%). Concentrated phosphoric acid (analytical grade), sodium bicarbonate, HEPES, calcium chloride, D-glucose,

sodium chloride, acetonitrile, ethanol, and water (liquid chromatography (LC)/MS grade) were purchased from Fisher Scientific (Pittsburgh, PA).

Animal Experiments

Inbred C57BL/6 mice of both genders between the ages of 20 - 24 months were used. Animals were housed under a 12h:12h light-dark cycle at 18–26 °C, 30–70% humidity. Food and water were accessible ab libitum. All animal-related procedures, including euthanasia by cervical dislocation, were performed in compliance with local and federal regulations and according to animal use protocols approved by the University of Illinois Institutional Animal Care and Use Committee.

Diet Modifications

Starting at 16 month, aged mice were fed modified diet ab libitum for at least 4 month until used for experiment. Mice body weight were monitored weekly with no drastic changes or differences between diets. Experiments were performed without knowledge of specific modified diet. The composition of the modified diet is listed in Table 5.1.

Mouse of the correct age was cervically dislocated, decapitated and the brain quickly extracted. The brain was chilled in NMDG-artificial cerebral spinal fluid (ACSF) slicing solution at 4 °C containing (in mM) NMDG 93, KCl 2.5, NAH_2PO_4, 1.2,

$NaHCO_3$ 30, HEPES 20, glucose 25, sodium ascorbate 5, thiourea 2, sodium pyruvate 3, $MgSO_4$ 10 and $CaCl_2$ 0.5, bubbled continuously with 95% O_2/ 5% CO_2. Coronal hippocampal slices, 400 µm thick, were obtained with a Leica vibratome.

LTP Induction

The brain slices were allowed to recover for 10 min in NMDG-ACSF at 30 °C, then transferred to a submerged chamber perfused with ACSF solution 2 ml/min containing (in mM) NaCl 124, KCl 2.5, NaH_2PO_4 1.2, $NaHCO_3$ 24, HEPES 5, glucose 12.5, $MgSO_4$ 2, $CaCl_2$ 2 and Picrotoxin 50, bubbled continuously with 95% O_2/ 5% CO_2 at 30 °C and recover for 1 h before LTP recording. At this point, half of the brain slices were placed on glass slides covered with Parafilm and flash frozen over dry ice for MSI analysis on the effects of diet modifications on the hippocampus.

Stimulations were performed with a concentric bipolar electrode (FHC) placed at the Schaffer collateral between the CA3 and the CA1, recordings were performed with a tungsten electrode (FHC) placed at the striatum radiatum at CA1. Field excitatory postsynaptic potential (fEPSP) was monitored until stable and input-output curves were obtained. Slices were given test-pulses (0.033 Hz) at ~ 40% maximum fEPSP throughout the recording. After a minimum of 20 min stable baseline recording, LTP was induced by 3 trains of 100 Hz, 1000 ms duration, 15 s interval high frequency stimulations (HFS) at test-pulse strength. For signal acquisition, amplifier gain was set

to 1000 and filtered between 1 Hz to 3 kHz. Signals were recorded and processed with pClamp 10 software. To control for the effect of electrode insertions and electrical stimulations on mass spec analysis, control slices were generated from the same brains and only subjected to test-pulses without HFS LTP induction.

After LTP recording brain slices were transferred to glass slides covered with Parafilm and flash frozen over dry ice for further cryo-sectioning and MSI analysis on the effects of LTP induction on the diet modified hippocampus.

Synthesis of TiO2 Monolith and Sample Preparation for MSI

TiO_2 nanoparticles were prepared using the same protocol described in the previous chapter. Sample preparation for MSI analysis is described in detail in the previous chapter.

Data Processing and Statistical Analysis

The molecular ion distribution images of tissue sections were visualized using flexImaging. Different cell layers in different regions were manually defined according to both the optical images and the ion images. The spectra in regions of interest (ROI) were exported and imported into ClinProTools (Bruker) with automatic baseline subtraction and total ion count normalization. Peaks were selected with a signal/noise

threshold greater than 3 on average spectra and matrix-related peaks were removed. Selected peaks were exported as m/z value-peak intensity tables. For five repeated slides with aged diet mice samples, combat method [19] was used for normalization to remove batch effect of different slides using online tool (metaboanalysis 3.0, http://www.metaboanalyst.ca/faces/Secure/utils/BatchUpload.xhtml).

After normalization, data from five replicates were combined for multivariate analysis. Principal component analysis (PCA)) was performed with OriginPro 8.5 (OriginLab Corporation, Northampton, MA), and Orthogonal partial least squares (OPLS) was done in SIMCA 14.1. For comparisons of averaged peak intensities for signals acquired from different brain regions in pairs, a two-sample t-test was calculated using OriginPro 8.5 in triplicates. For comparison of mean LTP fEPSP magnitudes, 2-way ANOVA with Bonferroni's multiple comparison test was done in GraphPad Prism6.

5.3 RESULTS

Effect of Diet modification of old mice on LTP and chemical change

Combinations of cocoa polyphenol and/or fish oil were used as diet supplements for aged mice to investigate their effects on hippocampal chemistry and plasticity (Table. 5.1). The aged mice are fed with different diets from 16-month old for at least 4 months before the hippocampus was examined with MSI and/or electrophysiology. Above established model for investigating spatio-chemical changes analysis with MSI

was used to unveil the chemical changes between different diet mice and the difference of their chemical changes during synaptic plasticity process.

Chemical difference between aged mice fed with different diets

PCA was performed on hippocampal slices from the aged mice supplemented with the four different diets. It is apparent that the CP + FO diet can be distinguished from the other diets in the CA3 region of the PC1 axis, especially when compared to either the CP or the FO diet. In the PC3 axis, the FO diet can be distinguished from the CP and the CP + FO in most of the cell layers of the CA2 and the CA3 regions. In the CA1 layers no obvious separations are observed between diets along either the PC1 or the PC3 axis. From the loading plots, compounds dominating the changes in the PC1 and the PC3 axis are of interest.

From the PCA analysis, the peak area of the compounds of interest in the diet modified aged mice were used to construct a hierarchical clustering that categorize the compounds into different classes. Five major classes were clustered (Fig. 5.2A). Amongst them, small metabolites were divided into three classes; GABA and pyroglutamate in one, creatine and creatinine in another, while spermine and PC 36:6 are each in their own class. All the lipids including the fatty acids, cholesterol, ceramides and diglycerides are in one class. The lipids are further categorized into sub groups based on their structural differences.

The change fold and p-value of all 20 compounds between the diet modified aged animals are listed in the supplementary information. Only molecules smaller than 700 Da had significant differences between the different dietary supplemented groups. Representative compounds with significant changes are shown in Figure 5.3.

GABA, pyroglutamate, creatine and creatinine had similar changing trends in different diets, with the FO diet having significantly lower levels in the CA1 region compared to the CP and the CP + FO diet (Fig. 5.3). In the CA2 and CA3 regions, Cholesterol, DAG (34:1), Cer (d36:1) and DHA (FA 22:6) had similar changing trends between diets, with the CP + FO diet having the highest levels. The differences between the CP diet and the CP + FO diet were significant.

Compared to the control and the FO diet, the CP diet significantly increased the GABA content in the CA1 region (Fig 5.2B, 5.3). The FO diet significantly decreased creatine level in the aged hippocampus (Fig. 5.3). The CP and the CP + FO diets did not change creatine level compared to the control brain.

Cholesterol have been reported to have a moderate loss in brain with age [20]. However, other evidences support that there is not an age-dependent change in the absolute amount of cholesterol in the hippocampus [21]. It was also shown that cholesterol synthesis is decreased in the human hippocampus, while absolute

cholesterol content remains stable [22]. These reported results relatively support our results that no significant changes of cholesterol have been found between young animals and old animals. The CP + FO diet significantly increased the cholesterol levels in the CA3 and the CA2 regions compared to the other diets.

Comparison of chemical changes during LTP for four diet samples

CA3 – CA1 LTP was induced in the hippocampal slices of the diet modified animals. MSI was then performed on the slices to measure LTP-induced compound changes under different diet modifications. Although not statistically significant, the CP + FO diet animal had the highest LTP induction (Fig. 5.4). The FO diet animals meanwhile had significantly lower LTP induction compared to the other two diets and the control. The CP diet had the most significant compound changes after LTP induction (Fig. 5.5). The control diet had much less change after LTP, and the FO diet samples had the least change. Interestingly, the CP + FO diet had significant decreases in several PEs, while the CP diet had significant increases in the same PEs in addition to cholesterol, DHA, AA and Cer (d36:1).

5.4 DISCUSSION

Energy shuttle

Creatine is an important intracellular high-energy phosphate shuttle synthesized in the liver and the kidneys, which is transported to the brain to be stored in phosphate form.

When energy is needed for cellular activity, creatine phosphate is dissociated into free creatine and phosphate for the regeneration of ATP through the Cr/phosphocreatine/creatine kinase (Cr/PCr/CK) pathway. In the meantime, creatinine as the breakdown product of creatine and creatine phosphate usually implies the total concentration of creatine and creatine phosphate.

It has been shown that aging significantly increases the creatine content in the brain [23,24]. However, the FO diet significantly decreased the creatine and creatinine level in aged animals (Fig. 5.3). Previous studies showed that creatine can modulate GABAergic neurons by acting as partial agonists of the post-synaptic $GABA_A$ receptor ($GABA_AR$) [25,26]. Moreover, creatine showed neuroprotective effects against oxidative stress and prevents neurodegeneration, while creatine supplementation can significantly improve LTP [27]. Thus, the lower creatine level in the FO diet hippocampus may explain the lower LTP induction observed (Fig. 5.4).

Lipid signaling

PC-FAs pathway

It has been demonstrated that direct Ca^{2+} entrance through voltage-dependent calcium channels activate phospholipase A2(PLA2), which releases fatty acids via phospholipid hydrolysis [28] (Fig. 5.6). PLA2 cleaves synaptic membrane phospholipid reservoirs and releases biologically active lipid messengers. It was

reported that one such reservoir is the phospholipids that typically contain an alkyl-acyl chain in the C1 position and either an arachidonate (20:4) or a docosahexaenoate (22:6) in the C2 position of the glycerol backbone. Activation of the cytoplasmic PLA2 leads to the release of arachidonic acid (AA or FA 20:4), docosahexaenoic acid (DHA or FA 22:6), and lyso-platelet-activating factor (PAF). PLA2 can also be co-released along with neurotransmitters to promote active AA remodeling in cultured neurons and possibly promote DHA release [28].

DHA and AA are well studied PUFAs which are reported to decrease with age due to lipid peroxidation [29]. Age-related decrease of DHA and AA have been linked to a decrease in membrane fluidity, which leads to impaired LTP formation. When we compared the fatty acids levels between different diets, only DHA was significantly higher in the CP + FO diet. Since DHA influences membrane fluidity and is an important signaling lipid during LTP formation, its increase in the CP + FO diet may be one of reasons for the higher LTP induction (Fig. 5.4). However, it is interesting that the FO diet containing high amount of DHA had no significant impact on the of DHA content in the hippocampus. This result echoes the reported decrease in n-3 PUFA levels in aged brains as a consequence of decreased transport of dietary fatty acids across the BBB [30].

Other contributing factors to decreased n-3 PUFAs in the aged brain includes reduced dietary intake, undefined impediments to uptake and utilization, or impeded shuttling of DHA from the liver to the brain [31]. Increased reactive oxygen species in the hippocampus [32,33] also leads to increased lipid peroxidation of the PUFAs [5]. Thus, even with elevated intake of DHA with the FO diet, difficulties still exist for the DHA to get to the brain. Cocoa polyphenols containing flavonoids on the other hand are reported to have anti-inflammatory and antioxidative effects. This perhaps explains the ability of the CP + FO diet to significantly increase PUFA contents in the hippocampus possibly by decreasing reactive oxygen species.

20:4-DAG

DAG is an important family of signaling lipids produced from the hydrolysis of phosphatidylinositol (PI) and phosphatidylcholine (PC) that can activate downstream phosphokinase C (PKC) that contributes to LTP formation [28]. From Figure 5.3, the CP + FO diet significantly increased DAG contents in the aged hippocampus, which may contribute to the establishment of LTP and possibly explain the higher LTP induction compared to other diet modifications (Fig. 5.4).

Cholesterol and ceramide

Sphingolipids and cholesterols are major constituents of lipid rafts. Many previous works suggested that lipid rafts, especially the cholesterol component, facilitates nerve

conduction and exocytosis/ endocytosis at the synapse [34,35]. Ceramide is generated by the hydrolysis of sphingophospholipids by sphingomyelinase (SMase).

It is now well established that the generation of ceramide through the sphingomyelin pathway has functions in signal transduction and the regulations of cell growth, differentiation and apoptosis. However, it was also reported that generation of ceramide contributes to the loss of mitochondrial membrane integrity, disrupting the mitochondrial respiratory chain and stimulate the increase in mitochondria-derived reactive oxygen species. When comparing ceramide levels between different diets, the CP + FO diet had the highest ceramide level, perhaps contributing to the higher LTP induction observed.

Cholesterol levels are regulated in response to strong neuronal activity, linked to excitotoxicity and cellular stress. However, it is not clear what the molecular mechanisms are that link changes in cholesterol to the regulation of synaptic strength during plasticity. Recent research has demonstrated the decrease of cholesterol from the intracellular membranes in CA1 neurons during LTP induction by a mechanism involving NMDAR activation [36].

During aging, moderate loss of brain cholesterol by increased expression of choleseterol-24-hydroxylase been described [37]. The reduction of cholesterol triggers

phospho-Akt accumulation, which in turn perturbs the normal cellular and molecular responses induced by long term depression (LTD), such as impaired AMPA receptor internalization and its reduced lateral diffusion, and these cause memory impairment [38] and poor cognition [39]. The CP + FO diet largely increased the cholesterol level in the aged hippocampus, which may contribute to the observed highest LTP induction (Fig. 5.4). The FO diet exhibited the lowest LTP induction (Fig. 5.4) and coincidently had the lowest hippocampal cholesterol levels. How the combination of CP and FO but not FO alone led to higher hippocampal cholesterol requires further investigations.

Spermine

It has been reported that the tissue levels of putrescine, spermine, spermidine, and the activity of ornithine decarboxylase are transiently increased in excitable tissue by the activation of voltage- or receptor-operated calcium channels [40,41].

It is now presumed that polyamines allosterically regulate the NMDA receptor channel complex by acting at a novel binding site distinct from the recognition sites for glutamate or glycine. Furthermore, several electrophysiological studies have shown that spermine and spermidine potentiate the NMDA induced currents in cultured neurons or in Xenopus oocytes transfected to express NMDA receptors. These observations are of great interest, implying novel roles of spermine and spermidine as neuromodulators in the brain [42]. Also, It has been reported that spermine can

facilitate the formation of LTP [42]. This might explain why the CP + FO diet, which had the highest spermine levels, had the highest LTP induction (Fig. 5.4). Interestingly, spermine was decreased after LTP in the CP + FO diet, suggest utilization of the compound in the formation of LTP.

GABA and pyroglutamatic acid

GABA and pyroglutamatic acid are directly involved in neurotransmission and are closely related to glutamate, which is the most abundant excitatory neurotransmitter in the vertebrate nervous system. GABA is the major inhibitory neurotransmitter that exerts its effects through the $GABA_A$ receptor. Activation of the $GABA_A$ receptor leads to hyperpolarization and the inhibition of neuronal firing. GABAergic neurons have GABA as their main output and are the primary inhibitory neurons in the vertebrate nervous system.

Not surprisingly, GABA has been shown before to exert an inhibitory effect on the induction of long-term potentiation. $GABA_A$ receptor antagonist Picrotoxin was used in our experiments to negate this inhibitory effect, which appears to be more pronounced in aged hippocampus. On the other hand, number of studies reported decrease of GABA levels during aging [43], which is linked to age-related memory loss [44]. These suggested the importance of GABA in synaptic plasticity. One possibility is that the higher GABA levels of the CP + FO diet had positive effects on

synaptic plasticity when the inhibitory effect is suppressed. This might explain the high LTP induction, while the FO diet with the lowest level of GABA had the lowest LTP induction.

Though pyroglutamic acid itself is not a neurotransmitter, it can easily be converted into glutamate, which can activate NMDAR and AMPAR. Pyroglutamic acid is derived from glutathione through the action of γ-glutamyl cyclotransferase. Pyroglutamic acid can be converted into glutamate by 5-Oxoprolinase, the only enzyme known to act on pyroglutamic acid (5-oxoproline) [45]. Since pyroglutamic acid is easily converted into glutamate with hydrolysis, one of its functions could be a reservoir for glutamate.

Pyroglutamic acid level in the hippocampus was reported to decrease with age. In the FO diet, pyroglutamic acid level was significantly lower than the other diets. Since pyroglutamic acid was reported to improve age-associated memory impairment [46], the low pyroglutamic acid level in the FO diet might contribute to the low LTP induction (Fig. 5.6).

Conclusion

Aging leads to deficits in brain plasticity and decline in learning and memory. FO has long been studied as an efficient diet supplementation to improve learning and

memory. CP is another recently widely studied antioxidant for improving memory and learning. In this work, we used DA-modified TiO2-assisted laser desorption/ionization (LDI)-mass spectrometry imaging (MSI) to track the spatio-chemical changes in diet modified aged hippocampus before and after CA3-CA1 LTP induction.

Aged mice were fed with the FO diet, the CP diet or the combination of both from 16-month old, and were compared with 24-month aged mice on control diet. LTP results showed that aged mice receiving the combination of CP and FO had the highest fEPSP, while FO alone gave rise to the lowest fEPSP. Among 20 compounds, the levels of around 10 compounds significantly changed between the control diet versus the modified diets (n=5). In the energy shuttle pathway, creatine was significantly lower in the FO diet mice in CA1 region; in signaling lipid pathways, DHA had significantly lower level in FO diet, cholesterol and ceramide have significantly lower level in the CP diet. However, the CP + FO diet had significantly higher levels of DHA, DAG, cholesterol and ceramide among four aged mice. In the neurotransmitter pathways, pyroglutamate have significantly lower level in the FO diet, GABA had significantly higher levels in both the CP diet and the CP + FO diet. These results show possible underlying mechanisms leading to higher LTP induction in combination diets while fish oil alone had even lower LTP inductions than the control diet.

5.5 FIGURES AND TABLE

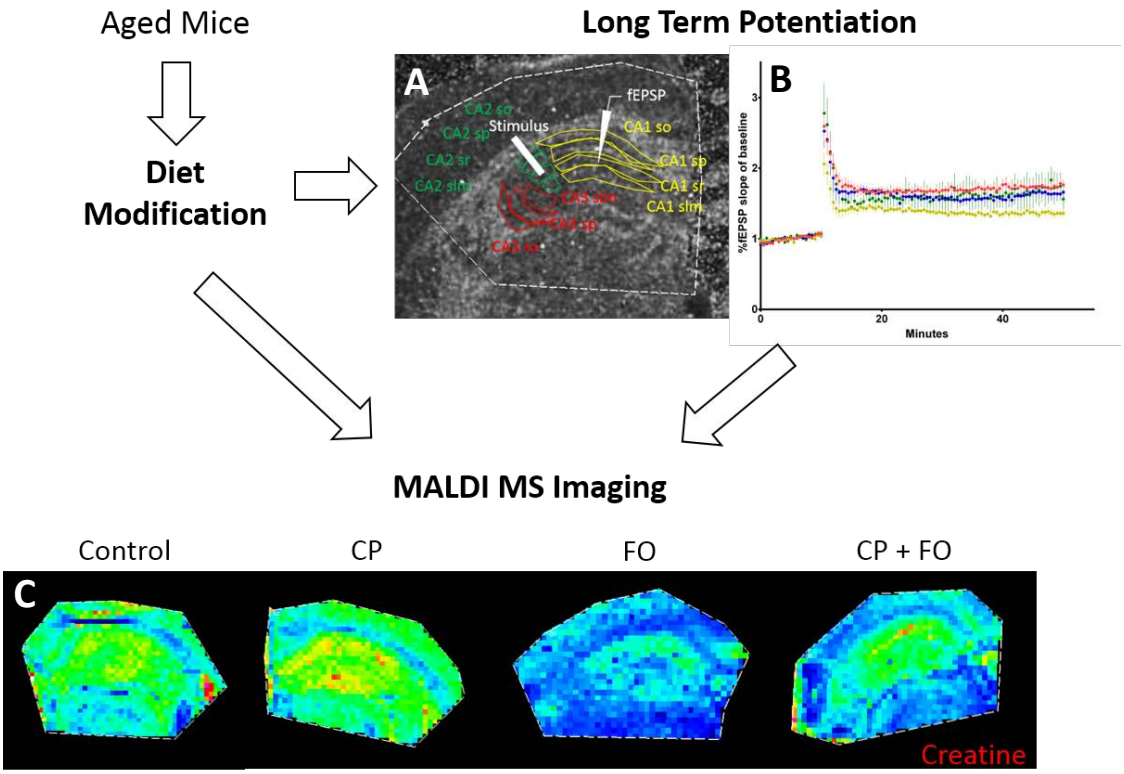

Figure 5.1. Illustrated overview of experimental scheme. Aged mice (20 month of age) were given modified diets for 4 months, then subjected to either long term potentiation recording or directly for MSI measurements. (A) Microscope image with schematic of mouse hippocampal region divisions for MSI analysis and electrode placements. (B) Mean %fEPSP slope to baseline (mean ± s.e.m.) versus time for different diet modified mouse hippocampal slices. High frequency stimulation (3 x 100Hz at test-pulse strength, 1000 ms duration, 15 s interval) is given at 10 min (n=6 per diet). Blue: control, Yellow: fish oil, Green: cocoa powder, Red: cocoa powder + fish oil. (C) Example ion map for creatine levels measured with MSI. CP: cocoa powder, FO: fish oil.

Table 5.1. Composition of the designed diets

Dietary supplement (g/kg)	Control	Cocoa Powder (CP)	Fish Oil (FO)	Cocoa Powder + Fish Oil (CP + FO)
Theobromine	0.209		0.209	0.209
Caffeine	0.024		0.024	0.024
Cocoa Powder		8.617		8.617
Fish Oil (3:1 DHA to EPA)			1.764	1.764

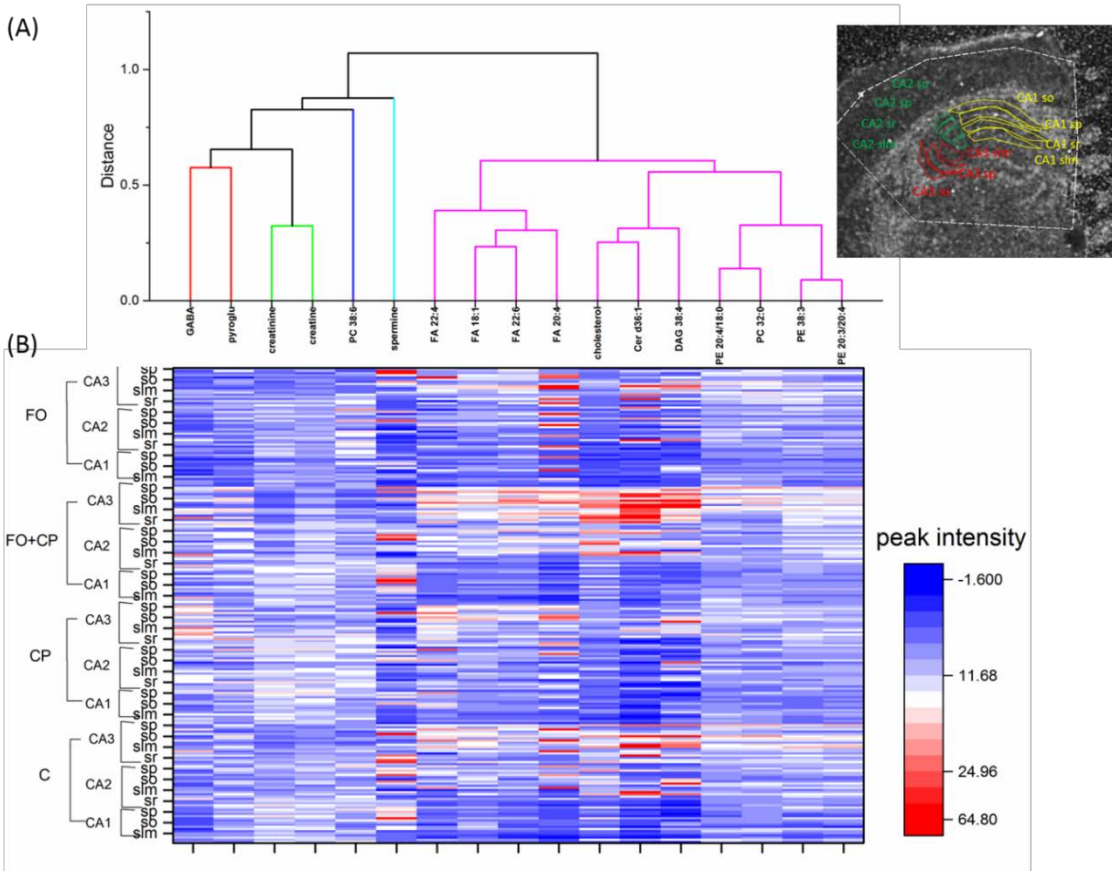

Figure 5.2. Hierarchical clustering of the compounds and their region specific relative intensity heatmaps in diet modified animals before LTP. (A) Hierarchical clustering of detected compounds. Each color indicates biologically closely related species. (B) Heat map of corresponding compounds in different regions. C: control, CP: cocoa powder, FO: fish oil.

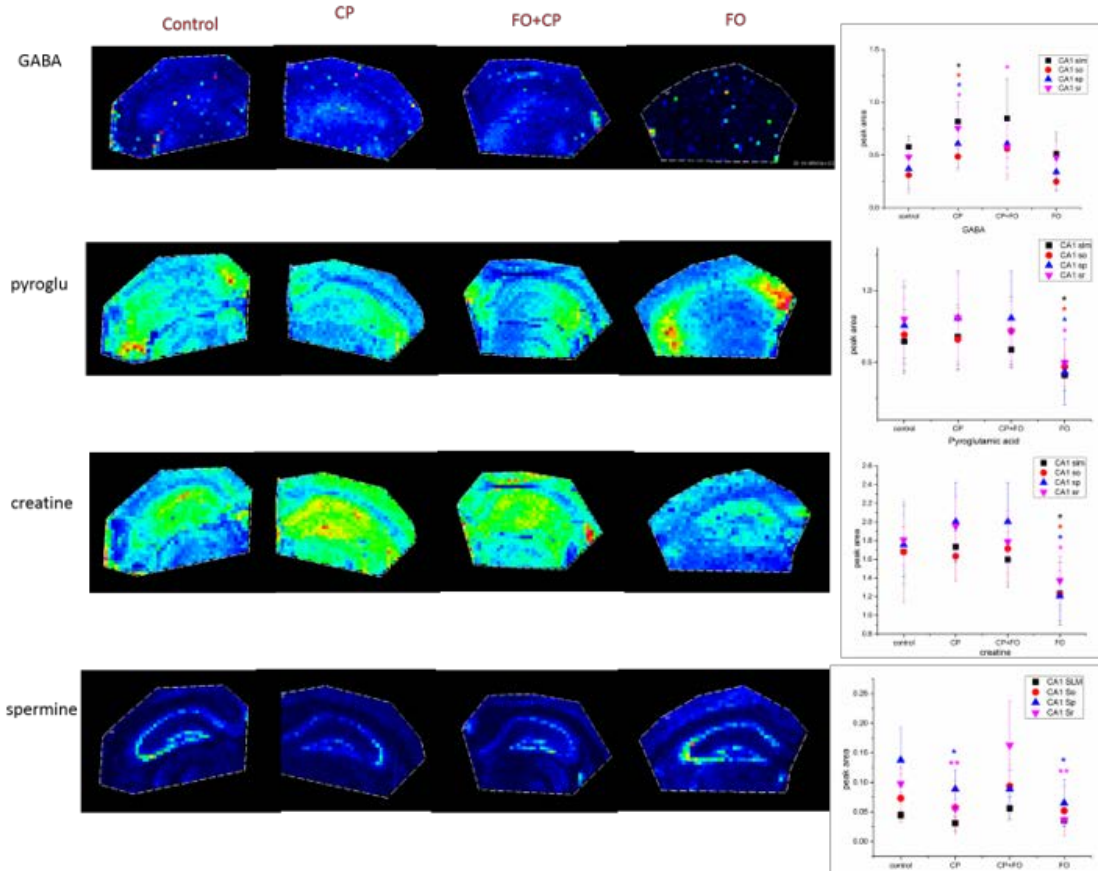

Figure 5.3. Ion images and average fold change of compounds in different cell layers of diet modified animals before LTP. Each ion image consists of one contralateral hippocampus cryosectioned from the freshly prepared slices. (n=5 per diet). *, $p < 0.05$; **, $p < 0.01$. CO: cocoa powder, FO: fish oil.

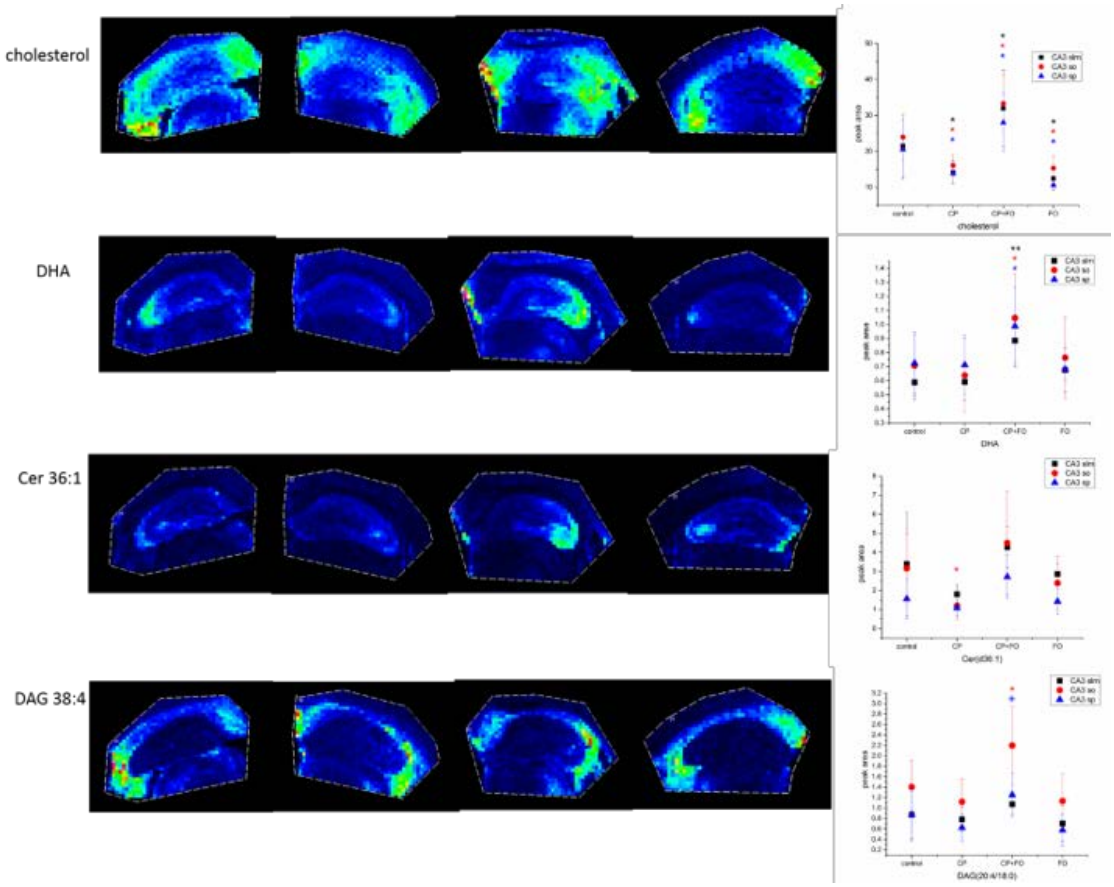

Figure 5.3 (cont.).

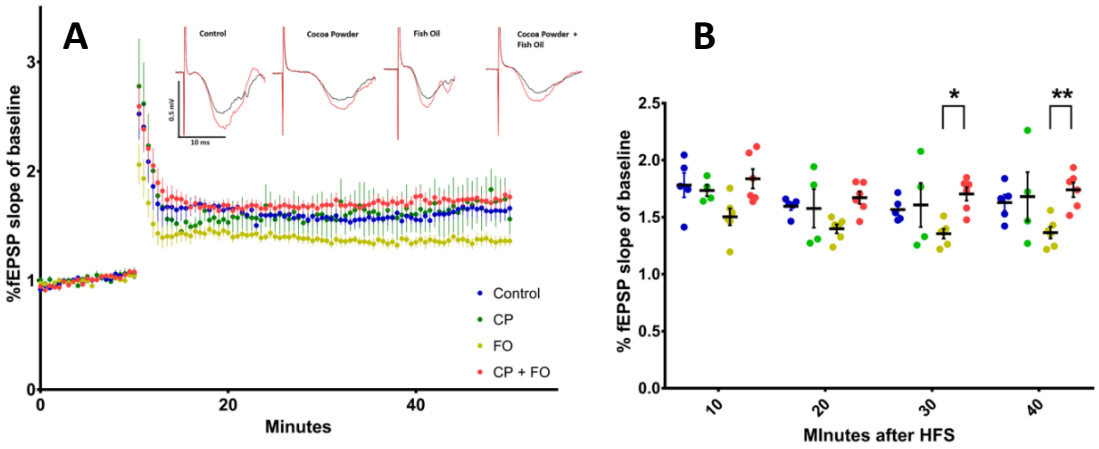

Figure 5.4. Long term potentiation results of different diet modified aged mice. (A) Mean %fEPSP slope to baseline (mean ± s.e.m.) versus time for old mice with different diets after high frequency stimulation (3 x 100 Hz at test-pulse strength, 1000 ms duration, 15 s interval) at after 10 minutes of stable baseline fEPSP (n=4 for CP, CP + FO and FO, and n=5 for Control). Sample fEPSP traces of baseline in black and post-HFS in red. (B) 10 minutes binned %fEPSP slope to baseline (individual slices and mean ± s.e.m.) versus time for old mice with different diets after high frequency stimulation. (2-way ANOVA with Bonferroni's multiple comparisons test. * $p < 0.05$, ** $P < 0.01$). fEPSP of fish oil diet versus cocoa powder + fish oil diet were significantly different at final 20 minutes of recording. CP: cocoa powder, FO: fish oil.

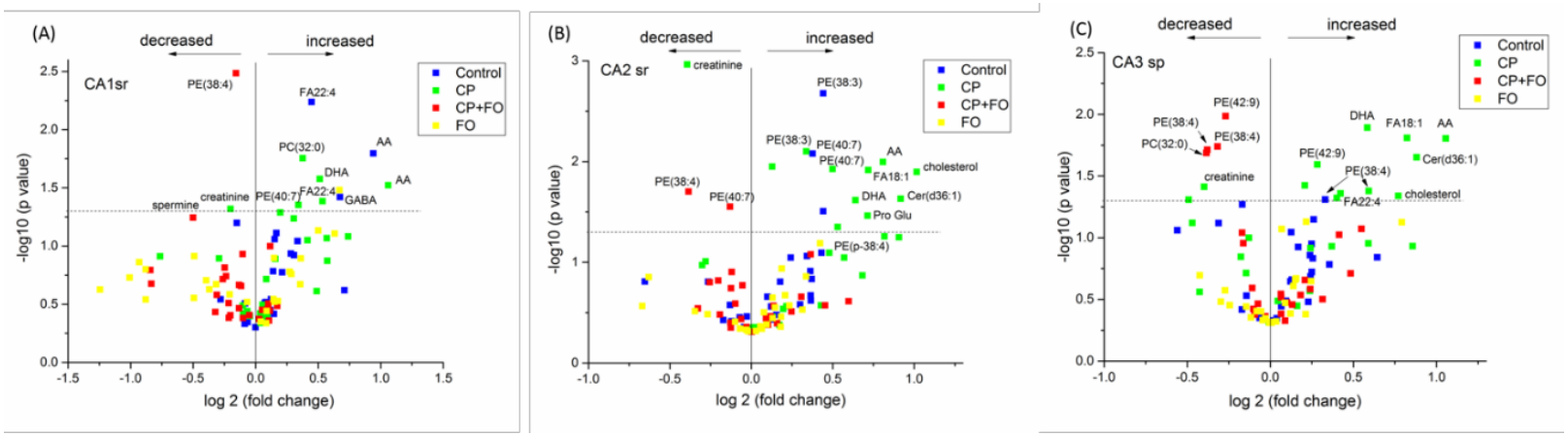

Figure 5.5. Volcano plot for representative cell layers of CA1, CA2 and CA3 of hippocampus for diet modified animals. (A) CA1 region sr cell layer. (B) CA2 region sr cell layer. (C) CA3 region sp cell layer. Labeled compounds have p-value < 0.05. (n=4 for CP, FO and CP +FO, n=5 for control). CP: cocoa powder, FO: fish oil.

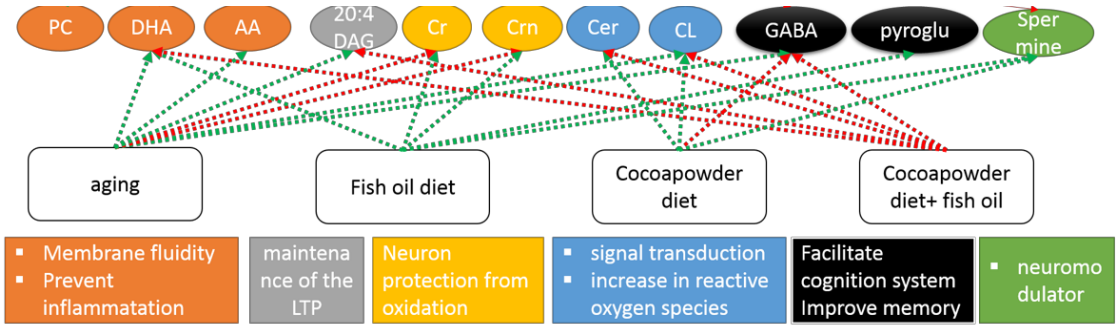

Figure 5.6. Schematic summarized the known functions of the compounds of interest and how they changed in different diet modifications. Green arrows indicate decrease of compound after diet modification, while red arrows indicate increase after diet modification.

5.6 REFERENCES

1. Wyss-Coray T. Ageing, neurodegeneration and brain rejuvenation. Nature. 2016;539: 180–186.

2. Yin F, Sancheti H, Patil I, Cadenas E. Energy metabolism and inflammation in brain aging and Alzheimer's disease. Free Radic Biol Med. Elsevier; 2016;100: 108–122.

3. Pollack M, Phaneuf S, Dirks A. The role of apoptosis in the normal aging brain, skeletal muscle, and heart. Ann NY Acad Sci. 2002;959: 93–107.

4. Gorlé N, Van Cauwenberghe C, Libert C, Vandenbroucke RE. The effect of aging on brain barriers and the consequences for Alzheimer's disease development. Mamm Genome. 2016;27: 407–420.

5. Lynch MA. Age-related impairment in long-term potentiation in hippocampus: a role for the cytokine, interleukin-1 beta? Prog Neurobiol. 1998;56: 571–589.

6. Spencer JPE. The impact of fruit flavonoids on memory and cognition. Br J Nutr. 2010;104: S40–S47.

7. Belkouch M, Hachem M, Elgot A, Van A Lo, Picq M, Guichardant M, et al. The pleiotropic effects of omega-3 docosahexaenoic acid on the hallmarks of Alzheimer's disease. J Nutr Biochem. Elsevier Inc.; 2016;38: 1–11.

8. Avraham Y, Saidian M, Burston JJ, Mevorach R, Vorobiev L, Magen I, et al. Fish oil promotes survival and protects against cognitive decline in severely undernourished mice by normalizing satiety signals. J Nutr Biochem. Elsevier Inc.; 2011;22: 766–776.

9. Rachetti ALF, Arida RM, Patti CL, Zanin KA, Fernades-Santos L, Frussa-Filho R, et al. Fish oil supplementation and physical exercise program: Distinct effects on different memory tasks. Behav Brain Res. Elsevier B.V.; 2013;237: 283–289.

10. Denis I, Potier B, Vancassel S, Heberden C, Lavialle M. Omega-3 fatty acids and brain resistance to ageing and stress: Body of evidence and possible mechanisms. Ageing Res Rev. Elsevier B.V.; 2013;12: 579–594.

11. Neshatdoust S, Saunders C, Castle SM, Vauzour D, Williams C, Butler L, et al. High-flavonoid intake induces cognitive improvements linked to changes in serum brain-derived neurotrophic factor: Two randomised, controlled trials. Nutr Heal Aging. 2016;4: 81–93.

12. Garrett TJ, Prieto-Conaway MC, Kovtoun V, Bui H, Izgarian N, Stafford G, et al. Imaging of small molecules in tissue sections with a new intermediate-pressure MALDI linear ion trap mass spectrometer. Int J Mass Spectrom. 2007;260: 166–176.

13. Liu H, Dai J, Zhou J, Huang H, Chen F, Liu Z. A hybrid ionic liquid–matrix material, [TiO2–Si–NH3+][CHC−], as a novel matrix for the analysis of small molecules by MALDI-TOF MS. Int J Mass Spectrom. Elsevier B.V.; 2015;376: 85–89.

14. Zemski Berry KA, Hankin JA, Barkley RM, Spraggins JM, Caprioli RM, Murphy RC. MALDI imaging of lipid biochemistry in tissues by mass spectrometry. Chem Rev. 2011;111: 6491–6512.

15. Goodwin RJA, Pennington SR, Pitt AR. Protein and peptides in pictures: Imaging with MALDI mass spectrometry. Proteomics. 2008;8: 3785–3800.

16. Ostrowski SG, Van Bell CT, Winograd N, Ewing AG. Mass spectrometric imaging of highly curved membranes during Tetrahymena mating. Science (80-). 2004;305: 71–73.

17. Goodwin RJA, Dungworth JC, Cobb SR, Pitt AR. Time-dependent evolution of tissue markers by MALDI-MS imaging. Proteomics. 2008;8: 3801–3808.

18. Wu Q, Chu JL, Rubakhin SS, Gillette MU, Sweedler J V. Dopamine-modified TiO_2 monolith-assisted LDI MS imaging for simultaneous localization of small metabolites and lipids in mouse brain tissue with enhanced detection selectivity and sensitivity. Chem Sci. Royal Society of Chemistry; 2017;0: 1–13.

19. Johnson WE, Li C, Rabinovic A. Adjusting batch effects in microarray expression data using empirical Bayes methods. Biostatistics. 2007;8: 118–127.

20. Svennerholm L, Gottfries C -G. Membrane Lipids, Selectively Diminished in Alzheimer Brains, Suggest Synapse Loss as a Primary Event in Early-Onset Form (Type I) and Demyelination in Late-Onset Form (Type II). J Neurochem. 1994;62: 1039–1047.

21. Söderberg M, Edlund C, Kristensson K, Dallner G. Lipid Compositions of Different Regions of the Human Brain During Aging. J Neurochem. 1990;54: 415–423.

22. Thelen KM, Rentsch KM, Gutteck U, Heverin M, Olin M, Andersson U, et al. Brain Cholesterol Synthesis in Mice Is Affected by High Dose of Simvastatin but Not of Pravastatin. J Pharmacol Exp Ther. 2006;316: 1146–1152.

23. Kuzyk A, Kastyak M, Agrawal V, Gallant M, Sivakumar G, Rak M, et al. Association among amyloid plaque, lipid, and creatine in hippocampus of TgCRND8 mouse model for Alzheimer disease. J Biol Chem. 2010;285: 31202–31207.

24. Pfefferbaum A, Adalsteinsson E, Spielman D, Sullivan E V., Lim KO. In vivo spectroscopic quantification of the N-acetyl moiety, creatine, and choline from large volumes of brain gray and white matter: Effects of normal aging. Magn Reson Med. 1999;41: 276–284.

25. Koga Y, Takahashi H, Oikawa D, Tachibana T, Denbow DM, Furuse M. Brain creatine functions to attenuate acute stress responses through GABAnergic system in chicks. Neuroscience. 2005;132: 65–71.

26. Neu A, Neuhoff H, Trube G, Fehr S, Ullrich K, Roeper J, et al. Activation of GABA(A) receptors by guanidinoacetate: a novel pathophysiological mechanism. Neurobiol Dis. 2002;11: 298–307.

27. Sartini S, Lattanzi D, Ambrogini P, Di Palma M, Galati C, Savelli D, et al. Maternal creatine supplementation affects the morpho-functional development of hippocampal neurons in rat offspring. Neuroscience. IBRO; 2016;312: 120–129.

28. Bazan NG. Synaptic lipid signaling: significance of polyunsaturated fatty acids and platelet-activating factor. J Lipid Res. 2003;44: 2221–2233.

29. Urano S, Sato Y, Otonari T, Makabe S, Suzuki S, Ogata M, et al. Aging and oxidative stress in neurodegeneration. Biofactors. 1998;7: 103–112.

30. Björkhem I, Lütjohann D, Diczfalusy U, Ståhle L, Ahlborg G, Wahren J. Cholesterol homeostasis in human brain: turnover of 24S-hydroxycholesterol and evidence for a cerebral origin of most of this oxysterol in the circulation. J Lipid Res. 1998;39: 1594–1600.

31. Abad-Rodriguez J, Ledesma MD, Craessaerts K, Perga S, Medina M, Delacourte A, et al. Neuronal membrane cholesterol loss enhances amyloid peptide generation. J Cell Biol. 2004;167: 953–960.

32. Murray CA, Lynch MA. Dietary supplementation with vitamin E reverses the age-related deficit in long term potentiation in dentate gyrus. J Biol Chem. 1998;273: 12161–8.

33. O'Donnell E, Lynch MA. Dietary antioxidant supplementation reverses age-related neuronal changes. Neurobiol Aging. 1998;19: 461–467.

34. Petrov A, Kudryashova K, Odnoshivkina YG, Zefirov A. Cholesterol and Lipid Rafts in the Plasma Membrane of Nerve Terminal and Membrane of Synaptic Vesicles. Neurochem J. 2011;5: 13–19.

35. Wasser CR, Ertunc M, Liu X, Kavalali ET. Cholesterol-dependent balance between evoked and spontaneous synaptic vesicle recycling. J Physiol. 2007;579: 413–429.

36. Brachet A, Norwood S, Brouwers JF, Palomer E, Helms JB, Dotti CG, et al. LTP-triggered cholesterol redistribution activates Cdc42 and drives AMPA receptor synaptic delivery. J Cell Biol. 2015;208: 791–806.

37. Martin MG, Perga S, ` LT, Rasola A, Holm P, Rantama T, et al. Cholesterol Loss Enhances TrkB Signaling in Hippocampal Neurons Aging in Vitro. Mol Biol Cell. 2008;19: 2101–2112.

38. Petrov AM, Kasimov MR, Zefirov AL. Brain cholesterol metabolism and its defects: Linkage to neurodegenerative diseases and synaptic dysfunction. Acta Naturae. 2016;8: 58–73.

39. Martin MG, Ahmed T, Korovaichuk A, Venero C, Menchon SA, Salas I, et al. Constitutive hippocampal cholesterol loss underlies poor cognition in old rodents. EMBO Mol Med. 2014;6: 902–917.

40. Koenig H, Goldstone A, Lu CY. Polyamines regulate calcium fluxes in a rapid plasma membrane response. Nature. 1983;305: 530–534.

41. Iqbal Z, Koenig H. Polyamines appear to be second messengers in mediating Ca2+ fluxes and neurotransmitter release in potassium-depolarized synaptosomes. Biochem Biophys Res Commun. 1985;133: 563–573.

42. Chida N, Saito H, Abe K. Spermine facilitates the generation of long-term potentiation of evoked potential in the dentate gyrus of anesthetized rats. Brain Res. 1992;593: 57–62.

43. He X, Koo B-B, Killiany RJ. Edited magnetic resonance spectroscopy detects an age-related decline in nonhuman primate brain GABA levels. Biomed Res Int. 2016;2016.

44. Riese F, Gietl A, Zölch N, Henning A, O'Gorman R, Kälin AM, et al. Posterior cingulate γ-aminobutyric acid and glutamate/glutamine are reduced in amnestic mild cognitive impairment and are unrelated to amyloid deposition and apolipoprotein E genotype. Neurobiol Aging. Elsevier Ltd; 2015;36: 53–59.

45. Kumar A, Bachhawat AK. Pyroglutamic acid: Throwing light on a lightly studied metabolite. Curr Sci. 2012;102: 288–297.

46. Grioli S, Lomeo C, Quattropani M, Spignoli G, Villardita C. Pyroglutamic acid improves the age associated memory impairment. Fundam Clin Pharmacol. 1990;4: 169–173.

CHAPTER SIX: CONCLUSION & DISCUSSION

6.1 CONCLUSION & DISCUSSION

With the advance in mass spectrometry technology, high throughput screens of the small peptides in various regions of the central nervous system became achievable [1–3]. The suprachiasmatic nucleus (SCN), the mammalian center of control for circadian rhythm was discovered to contain a rich collection of small peptides [4–6]. One small peptide previously unknown to be associated with the SCN is cerebellin-short, a C-terminus one amino acid truncated form of the 16 amino acid cerebellin peptide highly enriched in the cerebellum [7–10]. Originally discovered in 1987, cerebellin peptide was speculated to perform important functions in the Purkinje cells [11]. It was later discovered that the precursor of cerebellin, Cbln1, is critical for the formation of parallel fiber-Purkinje cell synapses in the cerebellum [12,13]. The mechanism of Cbln1 function in the cerebellum was reviewed in the first chapter. The study of cerebellin peptide on the other hand, remains scarce. Several studies reported that synthetic cerebellin peptide can induce the secretion of catecholamine and norepinephrine from the adrenal gland in human and rats respectively through indirect mechanisms [14,15]. One study reported that intracerebroventricular injection of synthetic cerebellin peptide induced feeding behavior in rats possibly by increasing the secretion of neuropeptide Y (NPY) from the arcuate nucleus (ARC) [16]. Another study reported mechanical hypersensitivity in mice when the synthetic N-terminal one amino acid truncated form of cerebellin was intrathecally injected [1]. To the extent of

our knowledge no receptor has been identified for the cerebellin peptides, and the mechanism of cerebellin functions remain a mystery.

Cbln1 and cerebellin presents the interesting case where both the precursor and the processed peptide are biologically functional. In cerebellum, granule cells secret both Cbln1 and cerebellin peptides, making the control between precursor vs peptide levels and the mechanism of their secretions intriguing questions. Cbln1 contains a signal peptide and is likely secreted through the traditional protein export pathway at the synapse [17–19]. Cerebellin peptides are known to be present at the synapse and undergo Ca^{2+} and electrical activity mediated secretion [20]. However, signaling molecule secretions are not limited to the synapses. Serotonin for example, can be secreted from exons and dendrites away from the synapses [21,22]. Arginine vasopressin (AVP) and oxytocin in the supraoptic nucleus (SON) are released from dendrites through dense core vesicles (DCV) [23]. Cerebellin-short is released from the SCN in circadian fashion [4], and we showed that the cleavage product of Cbln1 is enriched in the synaptosomes prepared from SCN tissue.

The dramatic difference in size (Cbln1 193 aa vs cerebellin 15 or 16 aa) and the lack of functional domains in cerebellin peptides suggest they have different mechanisms of action [17]. The idea has been proposed that some peptides produced from functional proteins can bind and modulate protein function by either disrupting the multimeric

stoichiometry or by covering important binding surfaces [3]. Cerebellin however, was shown by yeast two-hybrid assays to have no interaction with Cbln1, an unsurprising result due to cerebellin's lack of the complete C1q domain critical for Cbln1 multimerization [17]. The C-terminus C1q domain of Cbln1 was also shown to be critical for binding to its two known receptors, glutamate receptors delta 1 and 2 (GluRD1 & GluRD2) [24–26]. The N-terminus of Cbln1 interacts with a subset of neurexins, which is also cleaved off in the formation of cerebellin [17,26,27]. It is therefore unlikely that cerebellin exerts its function through known Cbln1 binding partners. One likely possibility is that cerebellin peptides bind to G protein-coupled receptors (GPCRs), since virtually all known neuropeptides exert their effects through GPCRs [28]. The SCN expresses a number of orphan GPCRs, and a method for systematically screening GPCRs in the SCN was recently described and used to discover a new GPCR relevant to circadian regulation [29]. The same method could be combined with reporter cell lines expressing candidate GPCRs and screening them for activation by the cerebellin peptides. Discerning the receptor for cerebellin peptides in the SCN will no doubt be a pivotal step in understanding its mechanism and function in circadian time keeping.

Cbln1 in the SCN is under circadian modulation at multiple levels in terms of gene/protein expression and peptide processing.

RT-PCR experiments of CBLN1 in the SCN suggests that the level of CBLN1 mRNA changes around the day and peaks at ZT 20. However, the level of the translated

product Cbln1 did not vary significantly around the day. Mismatch in the two profiles suggests that Cbln1 translation is under circadian modulation. The level of the 15 kDa cleavage product in the SCN peaks at ZT 8, which is 12 h after the peak in mRNA. After which cerebellin-short release from the SCN peaks later at ZT 16, 4 h after the peak in the 15 kDa intermediate. This substantial lag between peak mRNA level and peptide release is different from other peptides in the SCN. For instance, AVP and VIP mRNA levels in the mouse SCN peak around ZT 9 and ZT 15 respectively, while the peptide levels of AVP and VIP peak around 2 h after the mRNA [30,31]. Since Cbln1 and cerebellin peptides are both biologically active, one possibility is that a portion of the Cbln1 produced in the SCN is transported to other regions in the hypothalamus. The remaining Cbln1 is then processed into cerebellin-short to be released locally for circadian modulation. Fibrous staining of Cbln1 observed immediately dorsal to the SCN along the 3rd ventricle supports the hypothesis that Cbln1 is transported either to or from the SCN. Alternatively, the 4 h window resolution in sampling the SCN tissue did not capture the true peak of Cbln1 protein.

Cbln1 and cerebellin intermediate do not seem to display region specific localizations in the SCN

Unlike well-studied peptides such as AVP, VIP, and GRP among others [30,32,33], cerebellin-short did not localize to a distinct region in the SCN. Instead, cerebellin-short immunoreactivity (IR) co-localized with both AVP and VIP positive cells and was generally diffused throughout the SCN. Regional division of the SCN is tied to

their functional roles in circadian time keeping. For instance, the ventral VIP and GRP regions are responsible for receiving and integrating input signals that can be relayed to the dorsomedial AVP region via innervations and peptide secretions [31,34,35]. The AVP region then generates and maintains a cohesive rhythm that can be communicated to the rest of the brain [36–38]. Being present throughout the SCN suggests that cerebellin-short might be secreted from multiple populations of neurons and serves to maintain the overall synchrony of the SCN.

On the other hand, the majority of Cbln1 seems to be present outside of the SCN in other hypothalamic nuclei. High levels of Cbln1 IR observed in the SON, the PVN and the ARC suggest that Cbln1 itself is functional in the hypothalamus. Whether this is related to the circadian modulatory function of cerebellin-short in the SCN is unknown. It is interesting to note that another member of the C1q family, Cbln2, was recently reported to be preferentially expressed in the ventral region of the SCN [39]. Cbln2 has high sequence homology to Cbln1 and can cross interact with Cbln1 to form heterohexomers that also binds neurexins and GluRD2 [27,40,41]. Previous study showed that ectopic expression of Cbln2 in Purkinje cells could rescue the cerebellar synaptic deficits of Cbln1-KO mice [40,41]. The possibility that Cbln1 & 2 interact in the SCN for synaptic functions is intriguing.

Cerebellin-short peptide can phase-advance the SCN firing rhythm both in the day and the early night. Most likely not downstream of the light GLU pathway

Rhythm of the SCN is manifested in oscillations of multiple measurable cellular properties. In addition to the molecular transcription translation feedback loop (TTFL), the SCN is rhythmic in spontaneous neuronal activities and membrane potentials [42,43]. Ca^{2+} and redox states of the SCN also undergo daily cycles [44–47]. Rhythms in spontaneous firing and membrane potentials are coupled and synchronized throughout the SCN, whereas the TTFL and the Ca^{2+} rhythm are offset in phase across the SCN [46]. Cerebellin-short phase advances the SCN spontaneous firing rhythm during the day and in the early night. Light and glutamate (GLU) have no effect during the day and phase delay the SCN during the early night [48–50]. This suggests that cerebellin-short does not function to change the phase of the SCN through the GLU/light pathway. Pituitary adenylyl cyclase-activating peptide (PACAP) phase advances the SCN during the day by stimulating the cAMP/cAMP-dependent protein kinase (PKA) pathway and has no effects in the night [50–52]. On the other hand, activation of the cholinergic pathway phase advances the SCN during the night by stimulating the cGMP/cGMP-dependent protein kinase (PKG) pathway [53,54].

It is possible that cerebellin-short phase advances the SCN during the day by elevating the SCN cAMP level through activating an unidentified G protein-coupled receptor. During the early night cerebellin-short might induce phase advance by activating the cGMP/PKG pathway. The release of cerebellin-short from the SCN peaked in the early

night at ZT 16 [4], so exogenous cerebellin-short administered at CT 14 perhaps elicited phase advance by prematurely activating the intended responses for the rise in endogenous cerebellin-short level. Interestingly, cerebellin-short did not phase shift the SCN during the late night, a time during which the induction of the cGMP will also phase advance the SCN [50,54]. Perhaps the activation of cGMP by cerebellin-short in the SCN is gated and restricted to the early night window.

What is known so far from past literature and our investigation is summarized in the hypothetical bifurcated processing and secretions of Cbln1 versus cerebellin peptides in the cerebellum and the SCN (Fig. 6.1).

6.2 REMAINING QUESTIONS AND FUTURE DIRECTIONS

We showed that cerebellin-short can phase-shift the spontaneous firing rhythm in the SCN. Spontaneous firing rhythm of the SCN has been hypothesized to be a synchronous output of the SCN. It is related, but not coupled to the TTFL, which is responsible for generating and maintaining rhythms in individual SCN cells [46,55]. The rhythm in expression of the core clock protein period 2 (Per2) can be monitored through bioluminescence imaging of the SCN of the PER2::LUCIFERASE transgenic mice [56]. PER2::LUC imaging allows for high throughput monitoring of the dose and phase responses in the SCN TTFL at the cellular level [46]. Knowledge on how

cerebellin-short influences the TTFL of the SCN could provide insights to its mechanism of action and its role in circadian time keeping.

There are more than 14 orphan GPCRs whose function and ligands are unidentified [29,57]. A number of these orphan GPCRs were identified to be present in the SCN [29], a result not surprising considering the rich collection of peptides expressed by the SCN [4,5]. Screening these orphan GPCRs against cerebellin-short can potentially identify the receptor and further the understanding of the function and the phase shifting mechanism of cerebellin-short.

One method to investigate the physiological effects of cerebellin-short on circadian rhythm is to monitor the wheel-running activity of the commercially available Cbln1-KO mouse. Cbln1 exerts its synaptic formation and maintenance functions in the cerebellum through interaction with the glutamate receptor delta 2 (GluRD2). Previous study on GluRD2 mutant mice showed that they maintained rhythmic wheel-running behavior in D:D despite ataxic phenotype [58]. This suggests that the known Cbln1-GluRD2 synaptic mechanism is not necessary for maintaining behavior rhythms. If Cbln1-KO mice lose rhythmic wheel-running behavior in D:D, it suggest that cerebellin-short is important for maintaining rhythm. Alternatively, Cbln1 is important for rhythm independent of the Cbln1-GluRD2 mechanism. Rescuing free running rhythm via intra-SCN cannulation and injection of cerebellin-short in arrhythmic

Cbln1-KO mice would distinguish between these two possibilities. If Cbln1-KO mice maintain free running rhythm, then it would suggest that cerebellin-short functions to modulate circadian rhythm and is not critical for the maintenance of rhythm.

Finally, by identifying the endopeptidases responsible for the processing of Cbln1 to cerebellin peptides, we would gain insights into how the process is circadianlly regulated and what pathways are related to the circadian function of cerebellin-short.

6.4 FIGURE

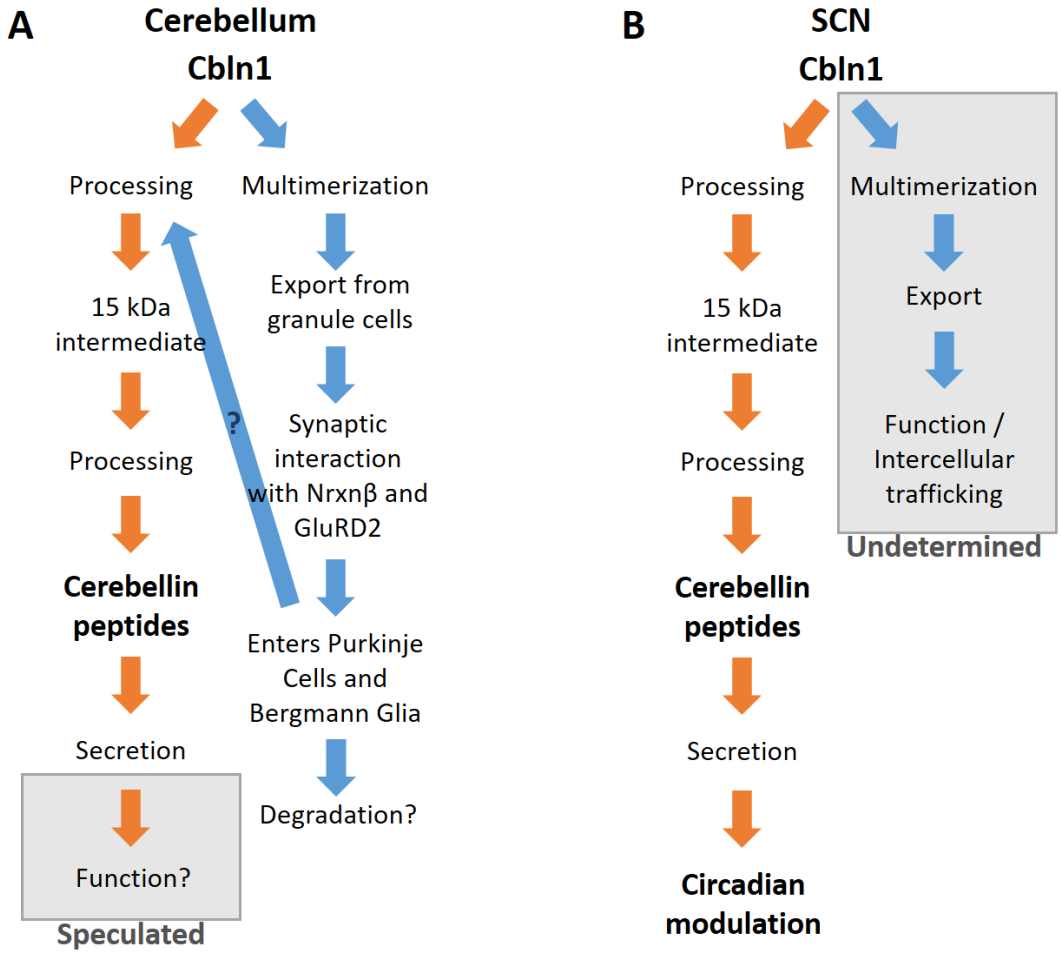

Figure 6.1. The hypothetical bifurcated pathways of Cbln1 versus cerebellin peptides secretion in the cerebellum and the SCN. (A) In the cerebellum, Cbln1 is translated in the granule cells and transported to the parallel fiber-Purkinje cell synapse after multimerizing into hexamers. Cbln1 hexamer interacts with presynaptic Nrxnβ and postsynaptic GluRD2 to confer synaptic scaffolding function. At the synapse a portion of Cbln1 hexamer is internalized by the Purkinje cells or the Bergmann glia through the endo-lysosomal pathway and transported to the respected cell soma for reasons yet unknown. Somewhere alone this pathway, Cbln1 is also processed through multiple steps into the cerebellin peptides. The cerebellin peptides are then secreted to perform functions in the cerebellum that are not yet elucidated. (B) In the SCN, Cbln1 is expressed in neurons and processed through multiple steps into the cerebellin peptides. The cerebellin peptides then undergo circadian release to modulate circadian function in the SCN through unknown mechanisms. It is unclear whether the full length Cbln1 is also released in the SCN and has any function in this part of the brain.

6.4 REFERENCES

1. Su J, Sandor K, Sköld K, Hökfelt T, Svensson CI, Kultima K. Identification and quantification of neuropeptides in naïve mouse spinal cord using mass spectrometry reveals [des-Ser1]-cerebellin as a novel modulator of nociception. J Neurochem. 2014;130: 199–214.

2. Fricker LD, Lim J, Pan H, Che F-Y. Peptidomics: identification and quantification of endogenous peptides in neuroendocrine tissues. Mass Spectrom Rev. 2006;25: 327–44.

3. Fricker LD. Analysis of mouse brain peptides using mass spectrometry-based peptidomics: implications for novel functions ranging from non-classical neuropeptides to microproteins. Mol Biosyst. 2010;6: 1355.

4. Hatcher NG, Atkins Jr. N, Annangudi SP, Forbes AJ, Kelleher NL, Gillette MU, et al. Mass spectrometry-based discovery of circadian peptides. Proc Natl Acad Sci U S A. United States; 2008;105: 12527–12532.

5. Lee JE, Atkins Jr. N, Hatcher NG, Zamdborg L, Gillette MU, Sweedler J V, et al. Endogenous peptide discovery of the rat circadian clock: a focused study of the suprachiasmatic nucleus by ultrahigh performance tandem mass spectrometry. Mol Cell Proteomics. United States; 2010;9: 285–297.

6. Lee JE, Zamdborg L, Southey BR, Atkins N, Mitchell JW, Li M, et al. Quantitative peptidomics for discovery of circadian-related peptides from the rat suprachiasmatic nucleus. J Proteome Res. 2013;12: 585–93.

7. Yiangou Y, Burnet P, Nikou G, Chrysanthou BJ, Bloom SR. Purification and characterisation of cerebellins from human and porcine cerebellum. J Neurochem. UNITED STATES; 1989;53: 886–889.

8. Morgan JI, Slemmon JR, Danho W, Hempstead J, Berrebi a S, Mugnaini E. Cerebellin and related postsynaptic peptides in the brain of normal and neurodevelopmentally mutant vertebrates. Synapse. 1988;2: 117–24.

9. Slemmon JR, Blacher R, Danho W, Hempstead JL, Morgan JI. Isolation and sequencing of two cerebellum-specific peptides. Proc Natl Acad Sci U S A. 1984;81: 6866–70.

10. Academy N, Academy N, States U. The Neuropeptide Cerebellin is a Marker for Two Similar Neuronal Circuits in Rat Brain. Proc Natl Acad Sci. 1987;84: 8692–8696.

11. Mugnaini E, Dahl AL, Morgan JI. Cerebellin is a postsynaptic neuropeptide. Synapse. 1988;2: 125–38.

12. Matsuda K, Miura E, Miyazaki T, Kakegawa W, Emi K, Narumi S, et al. Cbln1 is a ligand for an orphan glutamate receptor delta2, a bidirectional synapse organizer. Science. United States; 2010;328: 363–368.

13. Uemura T, Lee SJ, Yasumura M, Takeuchi T, Yoshida T, Ra M, et al. Trans-synaptic interaction of GluRdelta2 and Neurexin through Cbln1 mediates synapse formation in the cerebellum. Cell. United States: Elsevier Inc; 2010;141: 1068–1079.

14. Mazzocchi G, Andreis PG, De Caro R, Aragona F, Gottardo L, Nussdorfer GG. Cerebellin enhances in vitro secretory activity of human adrenal gland. J Clin Endocrinol Metab. 1999;84: 632–5.

15. Albertin G, Malendowicz LK, Macchi C, Markowska A, Nussdorfer GG. Cerebellin stimulates the secretory activity of the rat adrenal gland: in vitro and in vivo studies. Neuropeptides. 2000;34: 7–11.

16. Gardiner J V, Beale KE, Roy D, Boughton CK, Bataveljic A, Campbell DC, et al. Cerebellin1 is a novel orexigenic peptide. Diabetes Obes Metab. England: Blackwell Publishing Ltd; 2010;12: 883–890.

17. Bao D, Pang Z, Morgan JI. The structure and proteolytic processing of Cbln1 complexes. J Neurochem. England; 2005;95: 618–629.

18. Wei P, Rong Y, Li L, Bao D, Morgan JI. Characterization of trans-neuronal trafficking of Cbln1. Mol Cell Neurosci. Elsevier Inc.; 2009;41: 258–73.

19. Yuzaki M. Synapse formation and maintenance by C1q family proteins: a new class of secreted synapse organizers. Eur J Neurosci. France:). Journal Compilation (c) Federation of European Neuroscience Societies and Blackwell Publishing Ltd; 2010;32: 191–197.

20. Burnet PW, Bretherton-Watt D, Ghatei MA, Bloom SR. Cerebellin-like peptide: tissue distribution in rat and guinea-pig and its release from rat cerebellum, hypothalamus and cerebellar synaptosomes in vitro. Neuroscience. ENGLAND; 1988;25: 605–612.

21. Nurrish S. Dense core vesicle release: Controlling the where as well as the when. Genetics. 2014;196: 601–604.

22. De-Miguel FF, Trueta C. Synaptic and extrasynaptic secretion of serotonin. Cell Mol Neurobiol. 2005;25: 297–312.

23. Ludwig M, Stern J. Multiple signalling modalities mediated by dendritic exocytosis of oxytocin and vasopressin: Figure 1. Philos Trans R Soc B Biol Sci. 2015;370: 20140182.

24. Kuroyanagi T, Hirano T. Flap loop of GluD2 binds to Cbln1 and induces presynaptic differentiation. Biochem Biophys Res Commun. United States: Elsevier Inc; 2010;398: 537–541.

25. Elegheert J, Kakegawa W, Clay JE, Shanks NF, Behiels E, Matsuda K, et al. Structural basis for integration of GluD receptors within synaptic organizer complexes. 2016;353.

26. Cheng S, Seven AB, Wang J, Skiniotis G, Özkan E. Conformational Plasticity in the Transsynaptic Neurexin-Cerebellin-Glutamate Receptor Adhesion Complex. Structure. 2016;24: 2163–2173.

27. Joo JY, Lee SJ, Uemura T, Yoshida T, Yasumura M, Watanabe M, et al. Differential interactions of cerebellin precursor protein (Cbln) subtypes and neurexin variants for synapse formation of cortical neurons. Biochem Biophys Res Commun. 2011/03/02. 2011;406: 627–632.

28. van den Pol AN. Neuropeptide Transmission in Brain Circuits. Neuron. Elsevier Inc.; 2012;76: 98–115.

29. Doi M, Murai I, Kunisue S, Setsu G, Uchio N, Tanaka R, et al. Gpr176 is a Gz-linked orphan G-protein-coupled Receptor That Sets the Pace of Circadian Behaviour. Nat Commun. Nature Publishing Group; 2016;7: 1–13.

30. Dardente H, Menet JS, Challet E, Tournier BB, Pevet P, Masson-Pevet M. Daily and circadian expression of neuropeptides in the suprachiasmatic nuclei of nocturnal and diurnal rodents. Brain Res Mol Brain Res. 2004/05/12. 2004;124: 143–151.

31. Moore RY, Speh JC, Leak RK. Suprachiasmatic nucleus organization. Cell Tissue Res. 2002;309: 89–98.

32. Romijn H, Sluiter A, Pool C. Differences in colocalization between Fos and PHI, GRP, VIP and VP in neurons of the rat suprachiasmatic nucleus after a light stimulus during the phase delay versus. J Comp Neurol. 1996;372: 1–8.

33. Atkins Jr. N, Mitchell JW, Romanova E V, Morgan DJ, Cominski TP, Ecker JL, et al. Circadian integration of glutamatergic signals by little SAAS in novel suprachiasmatic circuits. PLoS One. United States; 2010;5: e12612.

34. Moga MM, Moore RY. Organization of neural inputs to the suprachiasmatic nucleus in the rat. J Comp Neurol. 1997;389: 508–34.

35. Antle MC, Silver R. Orchestrating time: arrangements of the brain circadian clock. Trends Neurosci. 2005;28: 145–151.

36. Campos LMG, Cruz-Rizzolo RJ, Watanabe IS, Pinato L, Nogueira MI. Efferent projections of the suprachiasmatic nucleus based on the distribution of vasoactive intestinal peptide (VIP) and arginine vasopressin (AVP) immunoreactive fibers in the hypothalamus of Sapajus apella. J Chem Neuroanat. Elsevier B.V.; 2014;57–58: 42–53.

37. Dai J, Swaab DF, Buijs RM. Distribution of vasopressin and vasoactive intestinal polypeptide (VIP) fibers in the human hypothalamus with special emphasis on suprachiasmatic nucleus efferent projections. J Comp Neurol. 1997;383: 397–414.

38. Vrang N, Larsen PJ, Moller M, Mikkelsen JD. Topographical organization of the rat suprachiasmatic-paraventriocular projection. J Comp Neurol. 1995;353: 585–603.

39. Seigneur E. Cerebellins are differentially expressed in selective subsets of neurons throughout the brain. 2017;

40. Rong Y, Wei P, Parris J, Guo H, Pattarini R, Correia K, et al. Comparison of Cbln1 and Cbln2 functions using transgenic and knockout mice. J Neurochem. 2011/11/29. 2012;120: 528–540.

41. Wei P, Pattarini R, Rong Y, Guo H, Bansal PK, Kusnoor S V, et al. The Cbln Family of Proteins Interact with Multiple Signaling Pathways. J Neurochem. 2012/01/10. 2012;

42. Schaap J, Bos NPA, De Jeu MTG, Geurtsen AMS, Meijer JH, Pennartz CMA. Neurons of the rat suprachiasmatic nucleus show a circadian rhythm in membrane properties that is lost during prolonged whole-cell recording. Brain Res. 1999;815: 154–166.

43. Medanic M, Gillette MU. Serotonin regulates the phase of the rat suprachiasmatic circadian pacemaker in vitro only during the subjective day. J Physiol. 1992;450: 629–42.

44. Koizumi K, Nishino H. Circadian and other rhythmic activity of neurones in the ventromedial nuclei and lateral hypothalamic area. J Physiol. Physiological Soc; 1976;263: 331.

45. Green DJ, Gillette R. Circadian rhythm of firing rate recorded from single cells in the rat suprachiasmatic brain slice. Brain Res. 1982;245: 198–200.

46. Enoki R, Oda Y, Mieda M, Ono D, Honma S, Honma K. Synchronous circadian voltage rhythms with asynchronous calcium rhythms in the suprachiasmatic nucleus. Proc Natl Acad Sci. 2017;114: E2476–E2485.

47. Enoki R, Ono D, Kuroda S, Honma S, Honma K. Dual origins of the intracellular circadian calcium rhythm in the suprachiasmatic nucleus. Sci Rep. Nature Publishing Group; 2017;7: 41733.

48. Ding JM, Buchanan GF, Tischkau S a, Chen D, Kuriashkina L, Faiman LE, et al. A neuronal ryanodine receptor mediates light-induced phase delays of the circadian clock. Nature. 1998;394: 381–384.

49. Ebling FJP. The role of glutamate in the photic regulation of the suprachiasmatic nucleus. Prog Neurobiol. 1996;50: 109–132.

50. Gillette MU, Mitchell JW. Signaling in the suprachiasmatic nucleus: Selectively responsive and integrative. Cell Tissue Res. 2002;309: 99–107.

51. Harmar AJ, Marston HM, Shen S, Spratt C, West KM, Sheward WJ, et al. The VPAC2 receptor is essential for circadian function in the mouse suprachiasmatic nuclei. Cell. 2002;109: 497–508.

52. Gillette MU, Prosser R a. Circadian rhythm of the rat suprachiasmatic brain slice is rapidly reset by daytime application of cAMP analogs. Brain Res. 1988;474: 348–52.

53. Tischkau S a, Mitchell JW, Pace L a, Barnes JW, Barnes J a, Gillette MU. Protein kinase G type II is required for night-to-day progression of the mammalian circadian clock. Neuron. 2004;43: 539–49.

54. Prosser RA, McArthur AJ, Gillette MU. cGMP induces phase shifts of a mammalian circadian pacemaker at night, in antiphase to cAMP effects. Proc Natl Acad Sci. National Acad Sciences; 1989;86: 6812.

55. Mohawk JA, Takahashi JS. Cell autonomy and synchrony of suprachiasmatic nucleus circadian oscillators. Trends Neurosci. 2011/06/15. 2011;

56. Yoo SH, Yamazaki S, Lowrey PL, Shimomura K, Ko CH, Buhr ED, et al. PERIOD2::LUCIFERASE real-time reporting of circadian dynamics reveals persistent circadian oscillations in mouse peripheral tissues. Proc Natl Acad Sci U S A. United States; 2004;101: 5339–5346.

57. Vassilatis DK, Hohmann JG, Zeng H, Li F, Ranchalis JE, Mortrud MT, et al. The G protein-coupled receptor repertoires of human and mouse. Proc Natl Acad Sci U S A. 2003;100: 4903–8.

58. Mendoza J, Pevet P, Felder-Schmittbuhl MP, Bailly Y, Challet E. The cerebellum harbors a circadian oscillator involved in food anticipation. J Neurosci. United States; 2010;30: 1894–1904.